

1 **Comparative cofactor screens show the influence of transactivation**  
2 **domains and core promoters on the mechanisms of transcription**

3

4 Charles C. Bell<sup>1,2,3\*</sup>, Jesse J. Balic<sup>1,2#</sup>, Laure Talarmain<sup>1,2#</sup>, Andrea Gillespie<sup>1</sup>, Laura  
5 Scolamiero<sup>1,2</sup>, Enid Y.N. Lam<sup>1</sup>, Ching-Seng Ang<sup>4</sup>, Geoffrey J. Faulkner<sup>3,5</sup>, Omer Gilan<sup>1,6</sup>,  
6 Mark A. Dawson<sup>1,2,7,8\*</sup>

7

8 <sup>1</sup>Cancer Research Division, Peter MacCallum Cancer Centre, Melbourne, VIC, Australia

9 <sup>2</sup>Sir Peter MacCallum Department of Oncology, University of Melbourne, VIC, Australia

10 <sup>3</sup>Mater Research Institute, University of Queensland, TRI Building, Woolloongabba, QLD, Australia

11 <sup>4</sup>Bio21 Mass Spectrometry and Proteomics Facility, The University of Melbourne, Parkville, VIC,  
12 Australia

13 <sup>5</sup>Queensland Brain Institute, University of Queensland, Brisbane, QLD, Australia

14 <sup>6</sup>Australian Centre for Blood Diseases, Monash University, VIC, Australia

15 <sup>7</sup>Department of Haematology, Peter MacCallum Cancer Centre, Melbourne, VIC, Australia

16 <sup>8</sup>Centre for Cancer Research, University of Melbourne, VIC, Australia

17 \* Corresponding authors

18 # Equal contribution

19 **Correspondence:**

20 Professor Mark A. Dawson

21 Peter MacCallum Cancer Centre,

22 305 Grattan Street, Melbourne, VIC 3000, Australia

23 Email: [mark.dawson@petermac.org](mailto:mark.dawson@petermac.org)

24

25 Dr Charles Bell

26 Peter MacCallum Cancer Centre,

27 305 Grattan Street, Melbourne, VIC 3000, Australia

28 Email: [charles.bell@petermac.org](mailto:charles.bell@petermac.org)

29

30 *This research was funded in whole or part by the National Health and Medical Research Council*  
31 *[Grant number 1196749]. For the purposes of open access, the author has applied a CC BY public*  
32 *copyright licence to any Author Accepted Manuscript version arising from this submission.*

33 **Abstract**

34 Eukaryotic transcription factors (TFs) activate gene expression by recruiting cofactors to  
35 promoters. However, the relationships between TFs, promoters and their associated cofactors  
36 remain poorly understood. Here, we combine GAL4-transactivation assays with comparative  
37 CRISPR-Cas9 screens to identify the cofactors used by nine different TFs and core promoters  
38 in human cells. Using this dataset, we associate TFs with cofactors, classify cofactors as  
39 ubiquitous or specific, and discover transcriptional co-dependencies. Through a reductionistic,  
40 comparative approach, we demonstrate that TFs do not display discrete mechanisms of  
41 activation. Instead, each TF depends on a unique combination of cofactors, which influences  
42 distinct steps in transcription. In contrast, the influence of core promoters appears relatively  
43 discrete. Different promoter classes are constrained by either initiation or pause-release, which  
44 influences their dynamic range and compatibility with cofactors. Overall, our comparative  
45 cofactor screens characterize the interplay between TFs, cofactors, and core promoters,  
46 identifying general principles by which they influence transcription.

## 47 **Introduction**

48 Regulation of gene expression allows different cell states to arise from a single genome. This  
49 process is coordinated by transcription factors (TFs), which use DNA binding domains to  
50 recognise DNA sequences, and specialised activation domains (ADs) to recruit the  
51 transcriptional cofactors (cofactors) required for gene regulation<sup>1,2</sup>. The recruited cofactors can  
52 remodel chromatin, modify histones or act as multi-subunit protein complexes that link with  
53 the transcriptional machinery<sup>3</sup>. Importantly, cofactors do not demonstrate DNA sequence  
54 specificity and are generally recruited to specific loci by TFs.

55

56 Despite decades of research, our understanding of why certain cofactors are needed by different  
57 TFs remains incomplete<sup>1,4,5</sup>. Structural approaches, which have been critical in characterising  
58 the DNA binding domains of TFs, have been unable to provide insights into function of ADs  
59 as they are often unstructured<sup>5,6</sup>. Moreover, since transcription is such a complex process,  
60 traditional functional approaches are generally unable to deconvolute how each of the various  
61 regulatory inputs (such as the activating TF, collaborating TFs, core promoter or cellular  
62 context) influences which cofactors are used. Thus, exploring how TFs and core promoters  
63 influence the mechanisms of transcription requires a reductionist approach, where ADs and  
64 promoters can be isolated and studied independently of other variables.

65

66 In recent years, such systematic, synthetic approaches have provided important insights<sup>7-11</sup>.  
67 For example, a recent study assessed the requirement for individual cofactors across thousands  
68 of promoters and enhancers, identifying widespread variation in cofactor requirements<sup>8</sup>.  
69 However, the reciprocal approach, to define the entire range of cofactors needed by individual  
70 TFs or promoters, has yet to be performed<sup>1,12</sup>. Consequently, a number of key questions about  
71 cofactor specificity and cofactor-promoter compatibility remain unanswered<sup>1,5,12-18</sup>.

72

## 73 **Results**

### 74 *Establishing a transcription factor-based screening system*

75 To address this challenge, we developed a screening system consisting of (i) a GAL4-DNA  
76 binding domain fused to a transactivation domain of interest and (ii) a reporter containing  
77 GAL4 binding motifs upstream of a mCMV promoter driving a fluorescent reporter (Extended  
78 Data Fig.1A-B). This reductionistic design controls the promoter and DNA-binding element to  
79 isolate how the activation domain alters the cofactors used for transcription. To enable  
80 investigation of all transcriptional regulators, including those required for cell survival, our

81 reporter construct contains an unstable GFP<sup>19</sup>. Using this reporter, we observed a dramatic  
82 reduction of fluorescent signal within 24 hours (hrs) of transcription inhibition, prior to cell  
83 death (Extended Data Fig.1C-D) and detected complete loss of expression upon knockout (KO)  
84 of the catalytic subunit of RNA polymerase II (*POLR2A*) (Extended Data Fig.1E),  
85 demonstrating our ability to identify common-essential proteins necessary for transcription.

86

87 We decided to investigate the cofactors needed by a representative set of nine transcription  
88 factors with diverse and important functions in synthetic biology, development and disease.  
89 These include VP64, c-MYB (MYB), EWSR1 (EWS), p65 (NF- $\kappa$ B), p53, IRF1, PU.1,  
90 NOTCH and glucocorticoid receptor (GR). The AD regions used were largely unstructured,  
91 enriched for acidic, proline and glutamine residues, and previously shown to have activation  
92 potential (Extended Data Fig.1B and Supplementary Table 1,2).

93

94 To perform genetic screens using these ADs, we developed an isogenic, constant reporter line  
95 by lentiviral integration of the reporter construct at high multiplicity of infection (MOI) into a  
96 Cas9-K562 clone. Polyclonal, high MOI integration enabled detection of the unstable GFP,  
97 while also reducing the potential for technical artefacts associated with a single integration site.  
98 To illustrate the robustness of our approach, firstly, we introduced our reporter into the  
99 endogenous *AAVS* safe-harbour locus and validated hits identified from our screens (Extended  
100 Data Fig.2A). Secondly, we developed an independent reporter line through a separate viral  
101 transduction, which is unlikely to share the same integration sites. We observed a very high  
102 correlation ( $r=0.918$ , Pearson) between screens performed on lines derived from separate  
103 transductions (Extended Data Fig. 2B). Lastly, we replicated the screen using an insulated  
104 reporter introduced via piggyBac integration. In this setting, the AD is fused to an artificial  
105 zinc-finger protein (ZFP), rather than GAL4, and recruited to an alternative DNA binding  
106 sequence (Extended Data Fig.2C). Despite differences in the DNA binding domain and DNA  
107 context, the results were highly correlated ( $r=0.830$ , Pearson) (Extended Data Fig.2C).

108

109 The nine GAL4-AD constructs were introduced into this constant reporter line, after which we  
110 confirmed that GFP signal was completely GAL4 dependent (Extended Data Fig.2D). Some  
111 TFs, such as VP64 and MYB, are known to be particularly dependent on certain cofactors. To  
112 validate that we could capture this specificity, we confirmed that these ADs were

113 disproportionately affected by loss of MED25 and p300 respectively<sup>20-23</sup> (Extended Data  
114 Fig.1E).

115

116 Having established the validity and reproducibility of our platform, we used the nine GAL4-  
117 AD reporter lines to perform comparative CRISPR-Cas9 screens with a bespoke guide RNA  
118 (gRNA) library targeting 1137 transcriptional regulators and chromatin-associated proteins  
119 (Supplementary Table 3). To minimise technical variation, the screens were performed in  
120 parallel, and cells with a reduction in transcription (as measured by GFP signal) were harvested  
121 at three timepoints (Day 5, Day 6, Day 7 post guide library infection). Isolating at multiple  
122 timepoints enabled robust quantitative comparisons of the effects of different cofactors on AD  
123 activity (Extended Data Fig.3A, Supplementary Note 1). Altogether, we identified 239 genes  
124 in the library as significantly enriched for at least one of the nine ADs (Supplementary Table  
125 4). As expected, hits clustered together by STRING analysis, with enrichment for RNA  
126 polymerase initiation and elongation, Mediator complex, SWI/SNF components and  
127 SET/COMPASS family members (Extended Data Fig.3B-C).

128

129 To confirm that we could separate transcriptional effects from effects on viability, we  
130 intersected the screen hits with dropout data from matched samples. Approximately 30% of  
131 genes required for cell growth were not significantly enriched in any AD screen (Extended  
132 Data Fig.3D). Similarly, integration with DEPMAP, identified that many common-essential  
133 cofactors were not enriched for any AD (Extended Data Fig.3E). We also confirmed that there  
134 was not substantial dropout of essential genes at the screen timepoints (Extended Data Fig.3F-  
135 G), and essential genes did not display more variability relative to non-essential genes  
136 (Extended Data Fig.3H). Together this demonstrates that our screens can identify essential  
137 transcriptional regulators, divorcing their contribution to transactivation from their requirement  
138 for cell viability.

139

#### 140 ***Overview of the specificity of TF-cofactor interactions***

141 To represent this large dataset, we developed a spoke and wheel plot to provide an overview  
142 of dependence on key transcriptional regulators across the 9 ADs (Fig. 1). As expected, the  
143 entire RNA polymerase II (RNA Pol II) complex is necessary for all of the ADs (90/90 possible  
144 enrichments). As are components of the preinitiation complex, such as TFIIA, TFIIB, TFIIE,  
145 TFIIIF, TFIIH, the FACT complex and DSIF components. Beyond these core transcriptional  
146 proteins, other coactivator complexes, such as Mediator, SET/COMPASS, Integrator,

147 chromatin remodellers and transcriptional elongation components display more interesting  
148 patterns.

149

150 Reassuringly, our approach identified several previously reported interactions between TFs and  
151 cofactors, including MYB-p300<sup>20,24</sup>, MYB-TAF12<sup>25</sup>, VP64-MED25<sup>21-23</sup>, p53-CDK8<sup>26</sup> and  
152 NOTCH-WDR5<sup>27</sup> (Fig.1). In addition to these known interactions, several novel TF-cofactor  
153 associations were observed. One that was particularly striking was a submodule of Integrator  
154 containing INTS5, INTS2 and INTS8<sup>28</sup>, which is especially important for NF- $\kappa$ B activity  
155 (Fig.1, Extended Data Fig.4A). To confirm that INTS5 is preferentially needed for the  
156 endogenous activity of NF- $\kappa$ B, we treated K562 cells with TNF- $\alpha$  and assessed the effects in  
157 control and INTS5 KO cells. By cell surface and ChIP-seq analyses, we also confirmed that  
158 INTS5 KO has an impact on endogenous NF- $\kappa$ B activity (Extended Data Fig.4), illustrating  
159 that our method was able to identify endogenous cofactor dependencies for specific TFs.

160

### 161 *Exploring cofactor specificity across activation domains*

162 Our comparative screens not only serve as an important resource, but also provide the  
163 opportunity to obtain systematic insights into the transactivation process. To begin with, we  
164 explored the relationship between cofactor specificity and quantitative contribution to  
165 transcription. In general, we observed that cofactors that contribute broadly to activation by  
166 most ADs, tend to display higher enrichment (Fig.2A). Interestingly, we observed very few  
167 examples of cofactors with potent and highly selective requirement, with the notable exception  
168 of NCOA1, which is a major dependency for Glucocorticoid Receptor-mediated  
169 transactivation. This suggests that, in general, TFs do not to have highly specific, dedicated  
170 cofactors that contribute strongly to transcription.

171

172 A lack of potent, selective cofactors does not necessarily imply generic mechanisms of  
173 transactivation. Instead, our data suggests that rather than using dedicated cofactors, ADs may  
174 achieve specificity by using unique combinations of cofactors (Fig.1). To explore this  
175 possibility, we first identified heterogeneously enriched cofactors across the 9 screens,  
176 anchoring the analysis on cofactors that are not expected to be variable (i.e. RNA Pol II). This  
177 analysis identified ~100 cofactors that display heterogeneity in their requirement, some of  
178 which were enriched for a large number of ADs, such as p300 or CHD1, and others that are  
179 enriched for few ADs, such as SETD1B or NCOA1 (Fig.2B).

180 To identify patterns in our data, we performed Pearson-based hierarchical clustering of the top  
181 50 heterogeneous cofactors. The data was bi-clustered to identify ADs with similar patterns of  
182 cofactor dependency and cofactors with similar patterns of enrichment across ADs (Fig.2C).  
183 Clustering of ADs demonstrates, that for the most part, ADs do not separate into a small number  
184 of discrete groups. Interestingly, Glucocorticoid Receptor clustered away from the other ADs,  
185 perhaps due to its structured AD (Fig.2C, Extended Data Fig.1B). Similarly, clustering of the  
186 cofactors was relatively indiscrete, with no clear co-dependency relationships identified  
187 between distinct cofactor complexes. The few co-dependent clusters identified were within  
188 large multi-subunit complexes, such as MED16, MED24 and MED25 (Mediator), and INTS2,  
189 INTS5 and INTS8 (Integrator) (Fig.2C). Together, this suggests that, while certain ADs utilise  
190 submodules of multi-subunit complexes, each AD is dependent upon a different combination  
191 of cofactors.

192

193 To provide further confidence in these results, we selected eleven heterogeneous cofactors, and  
194 independently quantified their contribution to transactivation by each AD. Overall, with some  
195 minor exceptions, we observed a high degree of concordance between the enrichment scores  
196 reported by the screen and the reduction in GFP signal in each respective AD line,  
197 demonstrating that the heterogeneity is genuine and reinforcing the quantitative nature of the  
198 screens (Fig.2D, Extended Data Fig.5). Importantly, the heterogeneity was reproduced using  
199 rapid protein degradation and specific inhibitors at a much earlier timepoint (Extended Data  
200 Fig. 6). We also confirmed that transcriptional regulation of the GAL4-ADs (Extended Data  
201 Fig.7A-C), GAL4-AD protein levels and stability (Extended Data Fig.7D), or GAL4-AD  
202 chromatin occupancy (Extended Data Fig.7E), are unlikely to be major contributors to the  
203 cofactor heterogeneity observed.

204

205 Taken together, our screen and validation data illustrate that cofactor dependence across  
206 different ADs does not conform to simple patterns. Instead, our data suggests that each AD  
207 uses a unique set of cofactors to activate transcription (Fig.1, Fig.2C-D).

208

### 209 ***Co-dependency between Mediator tail 2 and the kinase module***

210 While cofactors from distinct chromatin complexes did not show clear co-dependencies, our  
211 Pearson-based clustering identified highly correlated, co-dependent cofactors within multi-  
212 subunit complexes (Fig.1, Fig.2C). Clustering of all ~100 heterogeneous cofactors identified  
213 strong correlations within tail 2 of the Mediator complex (MED16, MED23, MED24, MED25),

214 CDK12 and its associated cyclin CCNK, subunits of the Integrator complex (INTS2, INTS5,  
215 INTS8) and PAF1/WDR61 (Extended Data Fig.8A-B).

216

217 Due to its key role in transcription, we were particularly interested in co-dependencies observed  
218 within the Mediator complex. Mammalian Mediator is organised into 5 major modules – head,  
219 middle, tail 1 (upper tail), tail 2 (lower tail) and sub-stoichiometric kinase module<sup>29,30</sup> (Fig.3A).  
220 Whilst structural composition has been well-characterised, functional relationships within the  
221 complex remain poorly understood. Our data suggests that the head, middle and tail 1 modules  
222 are ubiquitously enriched (Fig.3A), with most of the functional heterogeneity observed in the  
223 tail 2 module, kinase module and MED1, which is structurally positioned proximal to tail 2  
224 (Fig.3A).

225

226 We noted that enrichment of tail 2 subunits is strongly correlated, and that they correlate with  
227 the sub-stoichiometric kinase module (Fig.2C-D, Fig.3A, Extended Data Fig.8B). VP64, EWS,  
228 NF-κB and p53 are highly dependent on tail 2 and the kinase module, while MYB and  
229 Glucocorticoid Receptor are largely tail 2 independent and show minimal requirement for  
230 kinase module subunits (Fig.2C-D, Fig.3A, Extended Data Fig.6A). To test whether this co-  
231 dependency extends beyond our screening system, we performed RNA Pol II ChIP-seq upon  
232 genetic deletion of tail 2 subunits (MED16, MED24, MED25), the kinase module (CDK8,  
233 MED12, CCNC) and a core structural subunit (MED14) and assessed whether the effects were  
234 correlated at endogenous genes. As expected<sup>29,31</sup>, loss of the core subunit (MED14) led to a  
235 marked, relatively uniform decrease in RNA Pol II levels (Fig.3B). In contrast, loss of tail 2  
236 subunits (MED16, MED24, MED25) or the kinase module (CDK8, MED12, CCNC) resulted  
237 in disproportionate effects on particular subsets of genes (Fig.3B)<sup>32</sup>. Importantly, the effects of  
238 disrupting individual tail 2 and kinase subunits were highly correlated, with clear concordance  
239 between the rank order of genes effected by MED16, MED24, MED25, MED12, CDK8 and  
240 CCNC loss (Fig.3B-C). Consistent with our screens, correlation is strongest within tail 2, with  
241 a minority of tail 2 dependent genes, not dependent on CDK8 and CCNC (Fig.3B-C).  
242 Importantly, the co-dependency is highly specific to tail 2 and the kinase module, as there was  
243 minimal correlation with disruption of the core (MED14 KO) (Fig.3B-C).

244

245 To confirm these results are likely due to direct functional interplay between these submodules,  
246 we developed dTAG lines<sup>33</sup> to rapidly degrade MED12, MED14 and MED25 (Fig.3D,

247 Extended Data Fig.8C). Using these degron lines and a CDK8 inhibitor, we monitored RNA  
248 Pol II chromatin occupancy upon rapid perturbation of these subunits (Fig.3E and Extended  
249 Data Fig.8D-F). Consistent with our CRISPR KO results, we confirmed a high correlation  
250 between perturbations of tail 2 and kinase module subunits (MED12, MED25 and CDK8,  
251  $r=0.6-0.73$ , Pearson), with markedly less correlation with loss of the core (MED14,  $r=0.33-$   
252  $0.45$ , Pearson) (Fig.3E). Taken together, our comparative screens uncover a previously  
253 uncharacterised functional association within tail 2, and between tail 2 and the kinase module  
254 of the Mediator complex.

255

### 256 *TFs and cofactors influence different steps in transcription*

257 As transcription is a multistep process that involves promoter opening, initiation, pausing,  
258 elongation and termination, we hypothesised that TFs may recruit diverse cofactors to influence  
259 different steps in transcription. To explore this hypothesis, we used ChIP-nexus<sup>34</sup> to precisely  
260 map RNA Pol II on the reporter construct in each of the GAL4-AD cell lines. Remarkably,  
261 when the reporter is activated by different ADs, we observed differences in the ratio of RNA  
262 Pol II within the gene body, relative to the amount adjacent to the TSS (Fig.4A), suggesting  
263 that TFs have different capacities to facilitate RNA Pol II initiation and elongation.

264

265 Importantly, the degree of elongating RNA Pol II was associated with enrichment of cofactors  
266 involved in RNA Pol II pause-release (Fig.4A). Notably, the two ADs with the highest  
267 elongation ratios, VP64 and NF- $\kappa$ B, were most dependent on major pause-release regulators,  
268 NELF and Integrator (Fig.4A). Interestingly, each of these ADs were most dependent on  
269 different regulators of pausing (Fig.4A), supporting the prospect of multiple, independent  
270 pause-release checkpoints<sup>35</sup>. We also observed that other regulators of elongation, such as  
271 CDK8, CCNC, CDK9, CDK12, ELL1, PAF1 and CDC73, displayed a general correlation  
272 between screen enrichment and the proportion of elongating RNA Pol II (Fig.4A).

273

274 While no cofactor alone is predictive of elongation potential, we were struck by the association  
275 between the proportion of elongating RNA Pol II and dependence on Mediator kinase (CDK8)  
276 and its associated cyclin (CCNC) (Extended Data Fig.9A-B). Based on the co-dependency  
277 between CDK8 kinase module and tail 2 of Mediator (Fig.2, 3), we considered the prospect  
278 that some TFs, such as VP64, interact with subunits in tail 2 to engage the kinase module to  
279 potentiate elongation<sup>21</sup>. To test this idea, we assessed RNA Pol II in the VP64 cell line treated

280 with CDK8 inhibitor. Here, CDK8 inhibition reduced the ability of the VP64-AD to potentiate  
281 elongation (Fig.4B) whereas elongation was unperturbed by CDK8 inhibition in cells  
282 expressing MYB-AD (Fig.4B), which is not reliant on CDK8 or tail 2 for transactivation  
283 (Fig.2C-D, Fig.3A). Together these findings suggest that these submodules of Mediator are  
284 preferentially used by certain TFs to facilitate transcriptional elongation<sup>36</sup>.

285

### 286 *Exploring the influence of core promoters on transcription*

287 Transactivation requires cofactors to converge onto a promoter where RNA Pol II is loaded.  
288 Our screens suggest that TFs recruit diverse sets of cofactors to potentiate different steps in  
289 transcription. However, it remains unclear how the core promoter influences which cofactors  
290 are needed. To address this, we adapted our screening system to vary the core promoter while  
291 maintaining a constant activation domain (Nf-KB) (Extended Data Fig.10A). We chose to  
292 study promoters containing different well-characterised core promoter elements: (i) TATA  
293 box, (ii) TATA-like element with reduced affinity for TBP<sup>37-39</sup>, (iii) Initiator sequence (Inr)  
294 and/or (iv) polypyrimidine Initiator (TCT) sequence (Extended Data Fig.10B). These core  
295 motifs are associated with different classes of genes, suggesting that they influence how their  
296 associated genes are regulated<sup>40</sup>. Many genes containing a TATA box have focussed promoters  
297 that are tissue specific, have a large dynamic range and can be rapidly induced<sup>41-45</sup>. In contrast,  
298 the TCT element is present in housekeeping genes, primarily ribosomal proteins<sup>46</sup>, which are  
299 often widely expressed across tissues and have a narrow dynamic range in gene expression<sup>41</sup>.  
300 Interestingly, previous reports indicate that these promoter classes are differentially responsive  
301 to NF-kB<sup>7</sup>, suggesting inherently different mechanisms of regulation; an observation we  
302 confirmed using our transactivation system (Extended Data Fig.10C)

303

304 We hypothesised that our comparative cofactor screens could demonstrate how different core  
305 promoters influence cofactor requirements, while also providing mechanistic insights into  
306 cofactor-promoter compatibility<sup>7</sup>. To this end, we created nine independent promoter lines and  
307 performed the screens using the same experimental design described earlier (Extended Data  
308 Fig.3A and Methods). The results of these screens are summarised with another spoke and  
309 wheel chart, which provides a global overview of how core promoters influence the  
310 mechanisms of transcription (Fig.5A, Supplementary Table 5).

311

312 Using the same approach as the AD screens, we began by isolating the most heterogeneously  
313 enriched cofactors across 9 core promoters and performed Pearson-based hierarchical

314 clustering to unbiasedly identify patterns in the data. Interestingly, this analysis separated the  
315 highly responsive TATA/TATA-like promoters from less responsive TCT promoters,  
316 suggesting that differential cofactor use underpins differences in compatibility (Fig.5B). In  
317 stark contrast with the AD screens (Fig.2C), cofactor clustering across core promoters was  
318 discrete (Fig.5B). Promoters containing similar core motifs displayed relatively similar  
319 cofactor requirements, with cofactors clustering primarily based on their degree of dependence  
320 at TATA/TATA-like or TCT promoters (Fig.5B).

321

322 Amongst the cofactors with differential enrichment between promoter classes were various  
323 components of the TFIID complex. As expected, TBP was identified as a major requirement  
324 for promoters with a TATA box (Fig.5A). Consistent with recent structural studies, in which  
325 TAF11 and TAF13 form a bridge linking TBP to TFIID<sup>47</sup>, we identified that these two subunits  
326 are also needed together with TBP. Notably, components of this submodule of TFIID were  
327 largely not necessary for activation at TCT-containing core promoters (Fig.5A-C). At TCT-  
328 containing promoters, we instead identified an increased dependence on TAF1, TAF2, TAF7  
329 and TAF8, which are structurally co-located and interact with promoter elements in a manner  
330 distinct from TBP (Fig.5A-C)<sup>47-50</sup>. Our data suggests TFIID-mediated assembly of the pre-  
331 initiation complex is required across all of these core promoters, however promoters lacking a  
332 TATA box are more dependent on the TAF2/7/8 submodule for TFIID assembly.

333

334 We also observed that TATA/TATA-like and TCT promoters were differentially dependent on  
335 submodules of Mediator (Fig.3), Integrator (Extended Data Fig.4) and several other cofactors  
336 implicated in pause-release and elongation (Fig.1, Fig4A, Fig.5A-C). Interestingly, these  
337 cofactors were generally much less enriched at TCT promoters, which are less responsive to  
338 NF- $\kappa$ B-AD (Fig.5A-C). The inability for pause-release cofactors to contribute to transcription  
339 at TCT promoters suggests that their reduced responsiveness may be due to differences in the  
340 rate-limiting step for activation. To test this hypothesis, we performed RNA Pol II ChIP-nexus  
341 on our reporter constructs containing the responsive (TATA) and unresponsive (TCT)  
342 promoters activated by the NF- $\kappa$ B-AD. TATA promoters displayed clear evidence of RNA Pol  
343 II accumulation at the pause site, suggesting that pausing is the rate-limiting step (Fig.6A). In  
344 contrast, both unresponsive TCT promoters display a ~10-fold lower in accumulation of RNA  
345 Pol II around the TSS and no discernible pausing of RNA Pol II (Fig.6A). This suggests that  
346 output from these TCT promoters is constrained by the rate of RNA Pol II initiation rather than

347 pause-release. Based on these findings, we hypothesize that cofactor/promoter incompatibility  
348 occurs when TFs recruit cofactors to promoters which do not activate the appropriate rate-  
349 limiting step for transcription.

350

351 To provide further support for this hypothesis, we swapped promoter elements from the  
352 responsive and unresponsive promoters in an attempt to alter the rate-limiting step and  
353 therefore influence cofactor-promoter compatibility (Fig.6B). Replacing the TCT motif with  
354 an Initiator motif from TATA or TATA-like promoters did not influence responsiveness,  
355 demonstrating that Initiator motifs alone do not have a dominant influence on cofactor-  
356 promoter compatibility (Fig.6B). However, adding a TATA or TATA-like element and an  
357 Initiator motif into the unresponsive RPL30 promoter, completely restored responsiveness,  
358 markedly increasing the dynamic range of gene expression (Fig.6B). Importantly, these  
359 changes induced dependency on the pause-release cofactor, CDK8, suggesting that pause-  
360 release and elongation became the rate-limiting step (Fig.6B).

361

362 TATA boxes increase the rate of transcriptional initiation by enabling efficient assembly of the  
363 pre-initiation complex<sup>51,52</sup> and our screens, and prior work<sup>53,54</sup> suggest that the incompatible  
364 TCT promoters are more dependent on a submodule of TFIID that is TBP-independent (Fig.5).  
365 This suggests that by adding a TATA box to this unresponsive promoter, we increased the  
366 initiation rate, changing the rate-limiting step from initiation to elongation, restoring cofactor-  
367 promoter compatibility and increasing the dynamic range of gene expression. Overall, our data  
368 supports a model of cofactor-promoter compatibility dictated by core promoter motifs that  
369 result in different rate-limiting steps in transcription (Fig.6C).

## 370 **Discussion**

371 Using a synthetic, reductionistic screening system, we have provided key insights into how  
372 TFs and core promoters influence the cofactors required for transcription. Our comparative  
373 screens across 9 different ADs suggest that TFs rarely have highly specific, dedicated cofactors  
374 with a dominant contribution to transactivation. In contrast, each AD appears to use unique  
375 combinations of cofactors. Even when cofactors contribute to transactivation by many TFs (i.e.,  
376 p300), they can still display variable contributions to transcription. Consequently, there are  
377 likely to be a large number of distinct mechanisms by which genes can be activated. Due to our  
378 reductionistic design, it is likely that cofactor preference is conferred by AD sequence, however  
379 precisely how these intrinsically disordered domains achieve this specificity remains unclear.

380

381 Exactly why each AD requires a unique combination of cofactors also remains unclear. One  
382 possibility is that this type of combinatorial specificity enables TFs to integrate a large amount  
383 of information about cellular state when activating their targets<sup>55-57</sup>. Another possibility is that  
384 cofactor specificity enables TFs to regulate distinct steps in transcription. While previous  
385 reports have suggested that different TFs can activate different steps<sup>58-60</sup>, here we demonstrate  
386 that these differences are associated with differences in cofactor use, providing important  
387 mechanistic insights into this process. This ability for different TFs to activate different steps  
388 in transcription provides the capacity for kinetic synergy<sup>61,62</sup>. Kinetic synergy creates an AND  
389 logic, where only in the context of complementary TFs does transcription proceed at maximum  
390 efficiency. Therefore, TFs may use different sets of cofactors, to enable more complex logic  
391 downstream of DNA binding, or enable different kinetic behaviours, that would not be possible  
392 if each TF used the same set of cofactors<sup>5,45,59,63</sup>.

393

394 We also extended our screens to address how core promoters influence cofactors use. In stark  
395 contrast to ADs, the influence of core promoters appears to be discrete. Core promoters with  
396 highly divergent sequences, from distinct origins (synthetic, viral or endogenous), but sharing  
397 similar promoter motifs, displayed similar cofactor requirements. This suggests that the logic  
398 of core promoters is relatively simple, an observation supported by recent deep learning and  
399 mutational approaches<sup>64-66</sup>. Despite similarities within promoter classes, distinct classes  
400 displayed dramatic differences for cofactors involved in transcriptional initiation and  
401 elongation. Importantly, these differences were associated with responsiveness to the NF- $\kappa$ B-  
402 AD, leading us to propose a rate-limiting step model of cofactor-promoter compatibility (Fig.

403 5C). TCT promoters, which often regulate genes with a narrow range of gene expression,  
404 appear to be constrained by initiation rate, restricting their ability to respond to NF- $\kappa$ B-AD. In  
405 contrast, TATA gene promoters, which often regulate dynamically expressed genes, appear to  
406 be constrained by pause-release, enabling greater responsiveness and a higher dynamic range  
407 in gene expression<sup>67</sup>. This raises the prospect that the pause-release checkpoint evolved to  
408 enable a higher dynamic range for genes with promoter elements that efficiently assemble RNA  
409 Pol II. Overall, our comparative cofactor screens support a model of transactivation in which  
410 promoters establish different rate-limiting steps, that are activated by specific TFs, in order to  
411 achieve effective regulation of ubiquitous or inducible gene expression.

412

413 Our comparative screens required a genetic approach and a reductionistic design. Whilst our  
414 experiments using rapid protein degradation and transcriptional inhibitors suggest that our  
415 major findings result from direct effects, future work assessing other candidates should also  
416 employ methods with rapid kinetics. Further work will also be needed to consider how other  
417 variables, such as different TF domains, chromatin context, regulation from distal enhancers,  
418 and combinations of TFs, interact to regulate endogenous gene expression.

419 **Acknowledgements**

420 The authors would like to acknowledge all members of the Dawson Lab for their support and  
421 intellectual input throughout the project. We would also like to acknowledge the Peter  
422 MacCallum Cancer Centre Flow Cytometry and Genomics core facilities for their assistance  
423 with the research. **Funding:** This research was supported by Cancer Council Victoria  
424 Postdoctoral fellowship (C.C.B), NHMRC Investigator Grant (1196749) (M.A.D), Cancer  
425 Council Victoria Dunlop Fellowship (M.A.D), Howard Hughes Medical Institute international  
426 research scholarship (55008729) (M.A.D) and ARC project grant (DP220103927) (M.A.D).

427

428 **Author Contributions**

429 C.C.B, O.G and M.A.D designed the research and interpreted data. M.A.D supervised the  
430 research, with assistance from C.C.B. C.C.B and M.A.D wrote the manuscript with helpful  
431 input from all the authors. C.C.B performed the experiments with assistance from J.J.B, L.S,  
432 C-S.A and O.G. G. J. F provided critical research support and input. L.T performed the  
433 bioinformatic analysis with assistance from A.G and E.Y.N.L and input from C.C.B and  
434 M.A.D.

435

436 **Competing Interests**

437 M.A.D. has been a member of advisory boards for GSK, CTX CRC, Storm Therapeutics,  
438 Celgene, and Cambridge Epigenetix and receives research funding from Pfizer. The remaining  
439 authors declare no competing interests.

440 **Main figure legends**

441 **Figure 1) Comparative CRISPR screens identify the cofactors needed by nine different**  
442 **ADs**

443 Spoke and wheel plot demonstrating the enrichment of key cofactors in each of the 9 AD  
444 screens. The colour in each wedge reflects the average fold enrichment for each AD. Cofactors  
445 are organised into particular complexes based on their known complex associations or  
446 molecular functions. Components of this figure were created with biorender.com.

447

448

449 **Figure 2) Transcription factors display a diverse range of activation mechanisms**

450 **(A)** Violin plot of maximum fold enrichment for each cofactor in the library across the 9 AD  
451 screens. The number of genes in each category is displayed. **(B)** Violin plot of the coefficient  
452 of variation for each gene across the 9 screens. Selected variable genes are listed. Genes that  
453 were validated by independent KO experiments are highlighted in bold. **(C)** (Left) Heatmap  
454 showing the enrichment of the top 50 most heterogeneously used cofactors across the 9 AD  
455 screens. Heatmap is bi-clustered by Pearson correlation distance. Pearson correlation matrices  
456 are displayed alongside the heatmap to enable visualisation of which cofactors (right) and ADs  
457 (bottom) display correlated patterns of enrichment. **(D)** Heatmap comparing fold enrichment  
458 in the screens (left) with fold change in GFP upon knockout of various candidate,  
459 heterogeneous cofactors (right). Fold reduction in GFP calculated by dividing the average  
460 fluorescence signal (M.F.I) in perturbed cells by the M.F.I in cells containing the safe guide  
461 control at D5 after sgRNA infection. Fold reduction in GFP calculated based on at least two  
462 sgRNAs per gene.

463

464 **Figure 3) A direct co-dependent relationship between the tail 2 and kinase modules of the**  
465 **Mediator complex**

466 **(A)** Spoke and wheel plot of the fold enrichment of Mediator complex subunits across the nine  
467 ADs. **(B)** Waterfall plots showing the change in RNA pol II levels at Mediator dependent genes  
468 after individual subunit KO. Mediator dependent genes defined as genes with at least 30%  
469 reduction in RNA pol II signal upon MED14 KO. Each sample is compared to a safe guide  
470 control to calculate a change in RNA pol II ChIP-seq signal. The genes are ordered based on  
471 the degree of reduction in each KO sample enabling direct comparison of whether the same  
472 genes are affected by removal of different subunits. Spearman rank order correlation is  
473 displayed on each waterfall plot. The colour of each sample reflects which submodule it

474 belongs to. Orange = middle/core, blue = tail 2 and purple = kinase module. (C) Correlation  
475 matrix of the Spearman rank order correlation coefficient upon KO of various components of  
476 the Mediator complex. (D) Western blot for HA-dTAG-tagged MED12, MED14 and MED25  
477 after 4hrs of dTAGV<sup>-1</sup> or CDK8i treatment. Alpha-Tubulin displayed as loading control.  
478 Representative blot of two biological replicates. Blot performed on matched samples from  
479 ChIP-seq and SLAM-seq experiments. (E) Scatter plots demonstrating the correlation between  
480 the change in RNA pol II ChIP-seq signal upon MED12, MED14, MED25 degradation (4hrs  
481 dTAGV<sup>-1</sup>) and CDK8i treatment (4hrs). Fold change calculated by comparing each sample to  
482 matched DMSO treated control. Red line and r value reflect Pearson correlation.

483

484 **Figure 4) Transcription factors use different cofactors to regulate different steps in**  
485 **transcription**

486 (A) (Left) RNA pol II ChIP-nexus coverage across the reporter construct in each of the GAL4-  
487 AD cell lines. Blue signal reflects reads from the sense strand, red signal reflects reads from  
488 the anti-sense strand and shaded blue signal reflects cumulative signal between both strands.  
489 Elongation index is the inverse of the pausing index i.e., total gene body signal divided by the  
490 total promoter signal. (Right) Heatmap displaying fold enrichment of various key regulators of  
491 pause-release and transcriptional elongation in each AD screen. (B) RNA pol II ChIP-nexus  
492 coverage across the reporter construct in the GAL4-VP64 and GAL4-MYB cell lines treated  
493 for 1hr with DMSO or CDK8i. Blue and red lines reflect cumulative ChIP-nexus signal in  
494 DMSO and CDK8i treatment respectively. Quantification of the change in GFP upon CDK8i,  
495 CDK8 KO and CCNC KO in these two cell lines is also shown. For GFP quantification, n = 3  
496 biological replicates, error bars = S.E.M.

497

498 **Figure 5) Comparative screens shows discrete cofactor preferences dictated by core**  
499 **promoter elements**

500 (A) Spoke and wheel plot demonstrating the enrichment of key cofactors in each of the 9 core  
501 promoter screens. The colour in each wedge reflects the average fold enrichment for each AD.  
502 Cofactors are organised into particular complexes based on their known complex associations  
503 or molecular functions. For ease of comparison, the same cofactors are displayed as Fig. 1. (B)  
504 (Left) Heatmap showing the enrichment of the top 50 most heterogeneously used cofactors  
505 across the 9 core promoter screens. Heatmap is bi-clustered by Pearson correlation distance.  
506 Pearson correlation matrices are displayed alongside the heatmap to enable visualisation of  
507 which cofactors (right) and core promoters (bottom) display correlated patterns of enrichment.

508 Display is consistent with Fig. 2C to enable direct comparison of the clustering across different  
509 ADs and core promoters. **(C)** Validation of screen data through quantification change in GFP  
510 signal upon individual cofactor KO. Relative GFP signal is calculated by dividing the average  
511 fluorescence signal (M.F.I) cells containing the safe guide control by the M.F.I in perturbed  
512 cells at D5 after sgRNA infection. n = 2 sgRNAs per gene, error bars = S.E.M. Components of  
513 this figure were created with biorender.com.

514

515 **Figure 6) Cofactor-promoter compatibility is influenced by the rate limiting step in**  
516 **transcription**

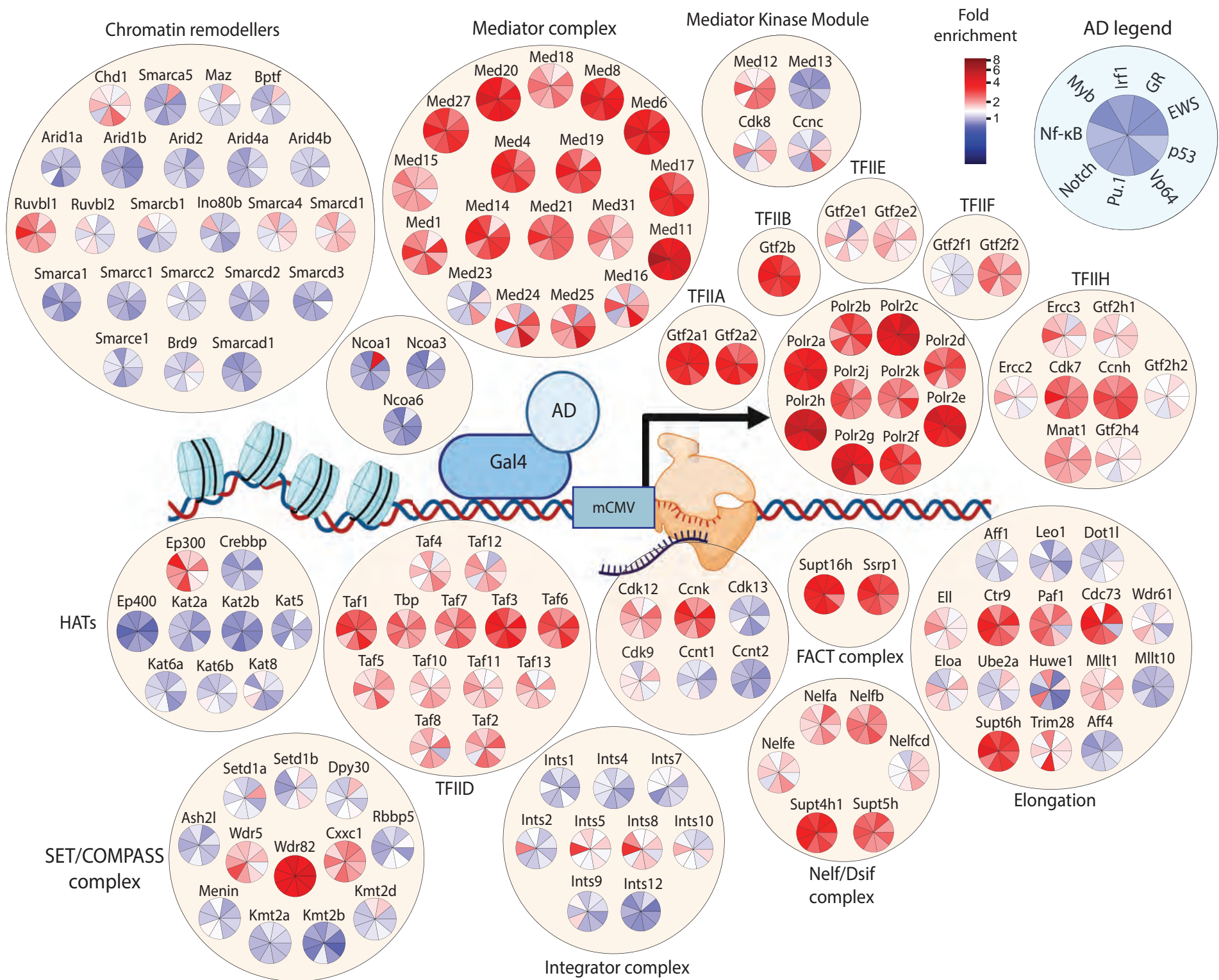
517 **(A)** RNA pol II ChIP-nexus coverage across the reporter construct in responsive and  
518 unresponsive promoter lines activated by GAL4-NF- $\kappa$ B. Blue signal reflects reads from the  
519 sense strand, red signal reflects reads from the anti-sense strand and shaded blue signal reflects  
520 cumulative signal between both strands. The top number adjacent to the graph reflects the  
521 cumulative normalised read counts from both strands. The bottom two numbers reflect the  
522 normalised read counts from each strand respectively. **(B)** Luciferase assays performed with  
523 different promoter constructs with or without GAL4-NF- $\kappa$ B demonstrating that adding of a  
524 TATA box restores responsiveness and cofactor-promoter compatibility. CDK8i was dosed for  
525 12hrs prior to luciferase assay. n=3 technical replicates. Error bars = S.E.M. Data is  
526 representative of two independent biological replicates. **(C)** Rate limiting step model of  
527 cofactor-promoter compatibility. Pause-release cofactors have limited ability to activate  
528 promoters where initiation is the rate-limiting step. + symbols do not directly correspond to  
529 any quantitatively information, instead reflecting a conceptual model.

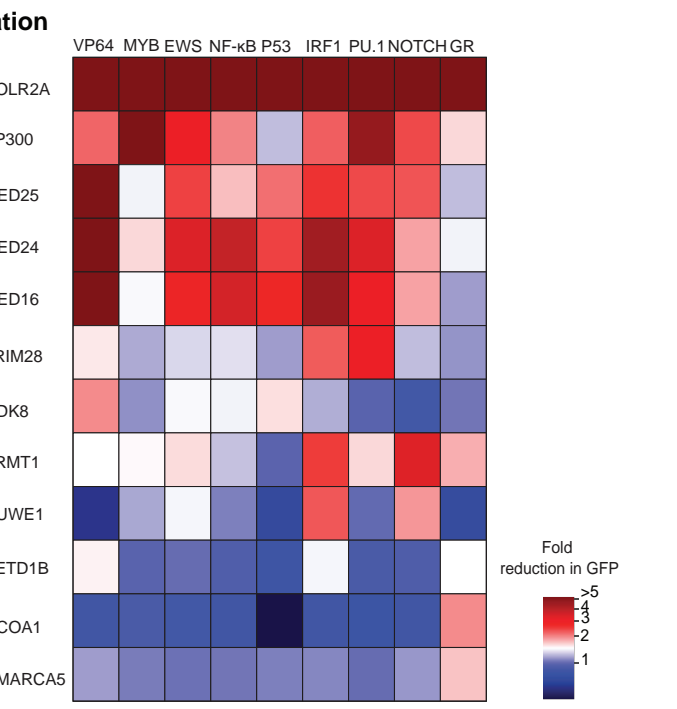
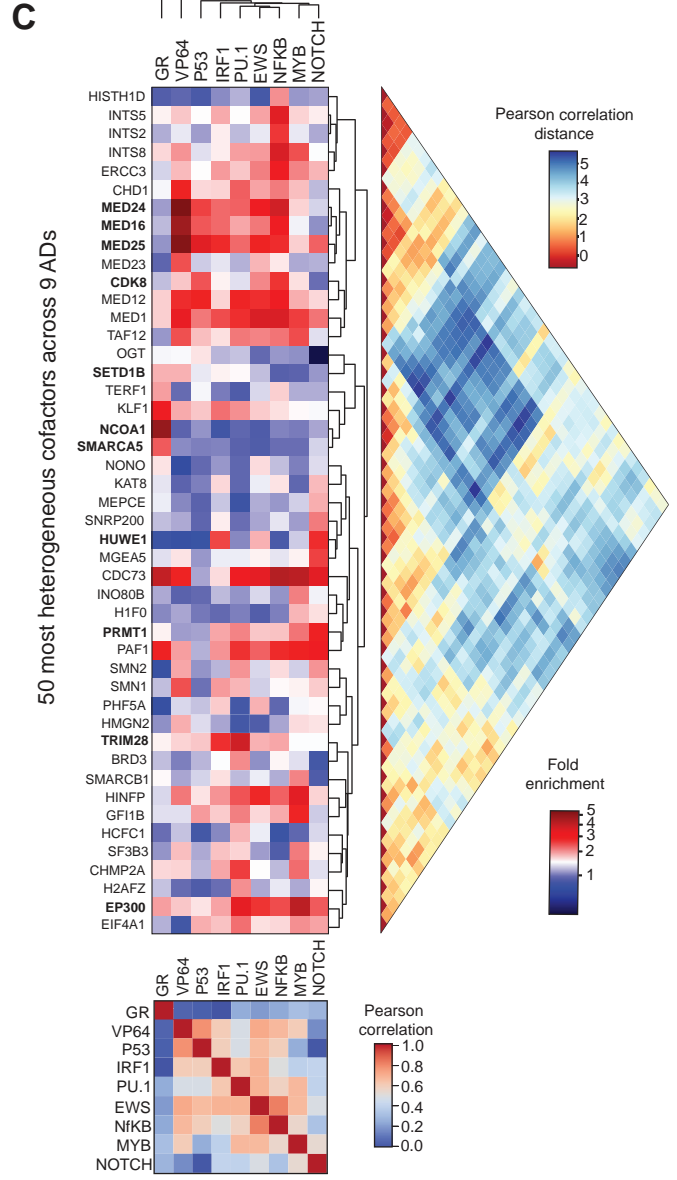
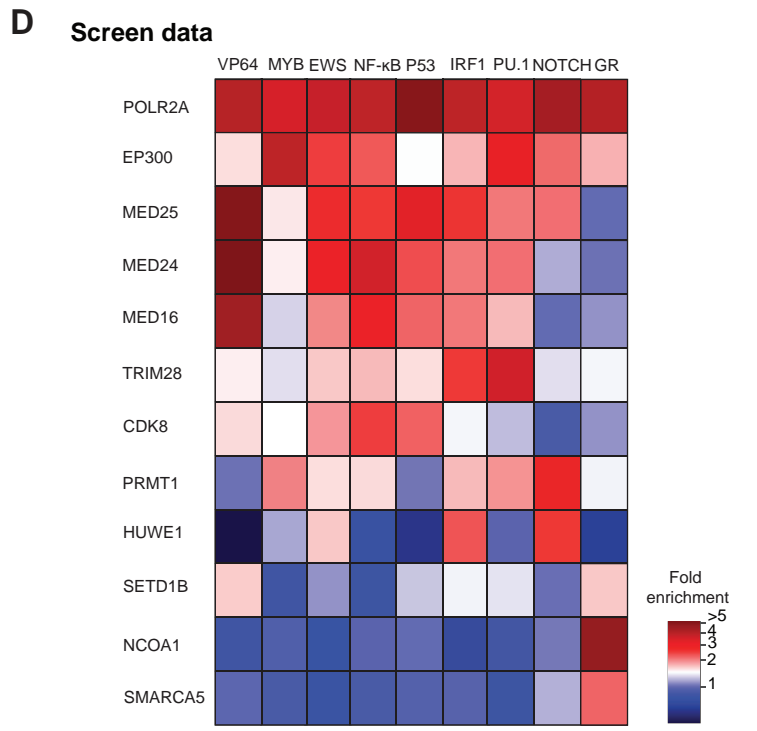
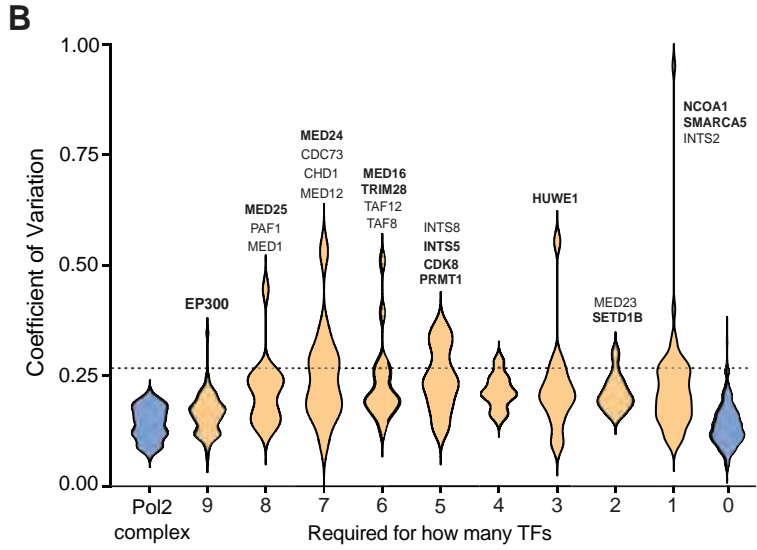
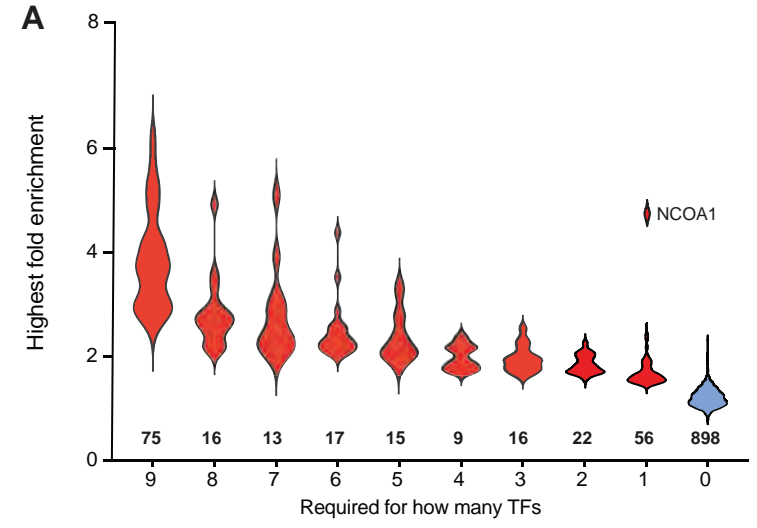
530

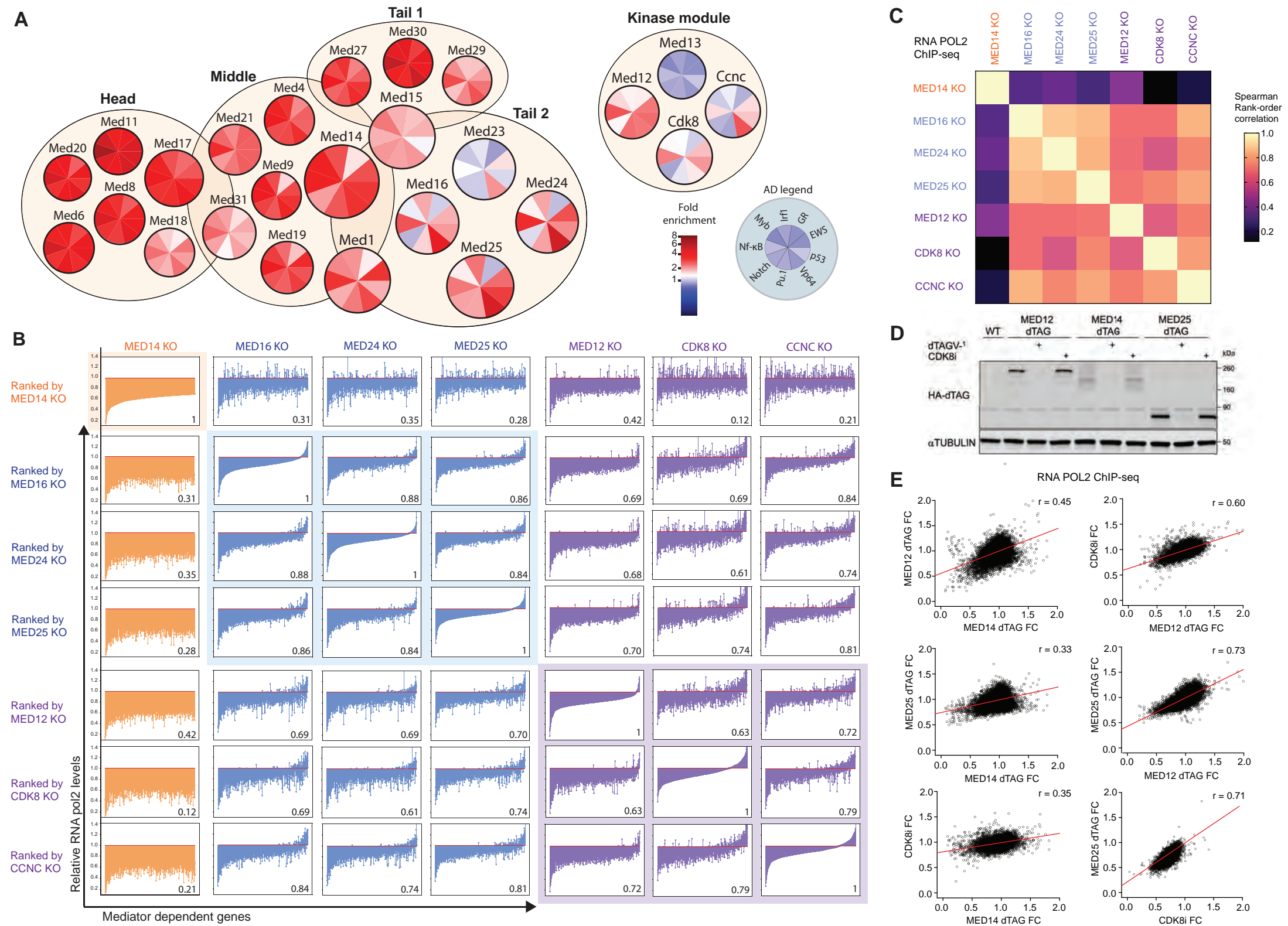
531 **Figure – Representative FACS gating**

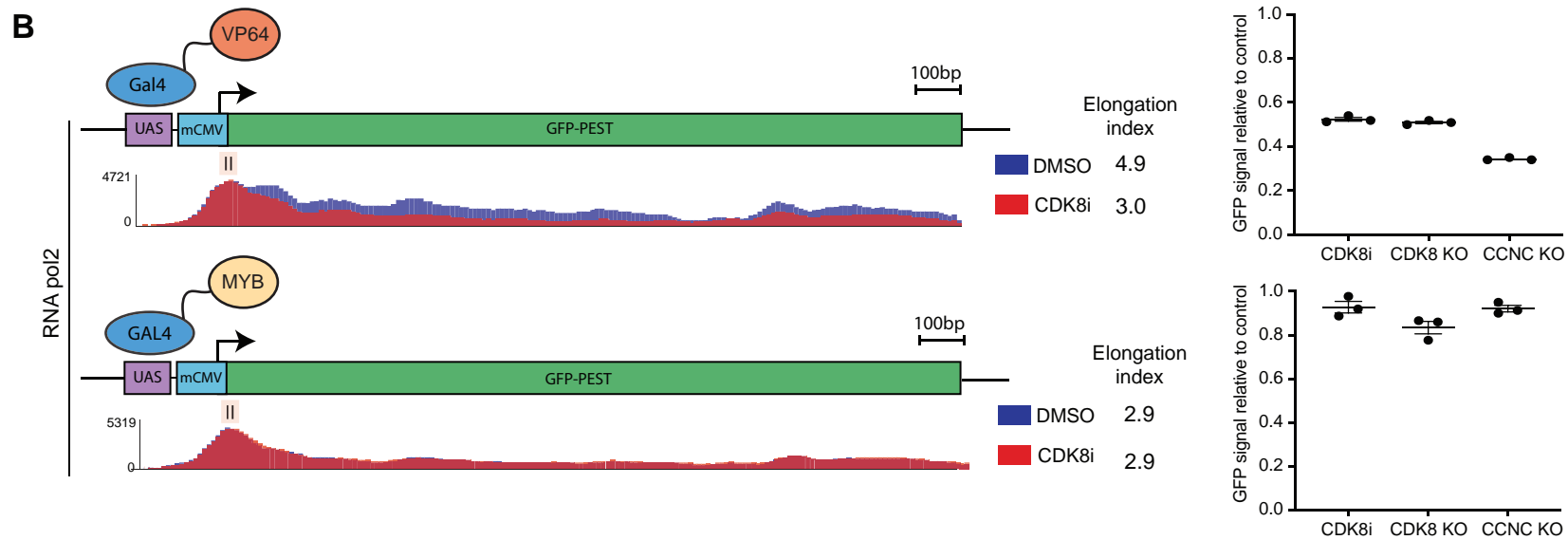
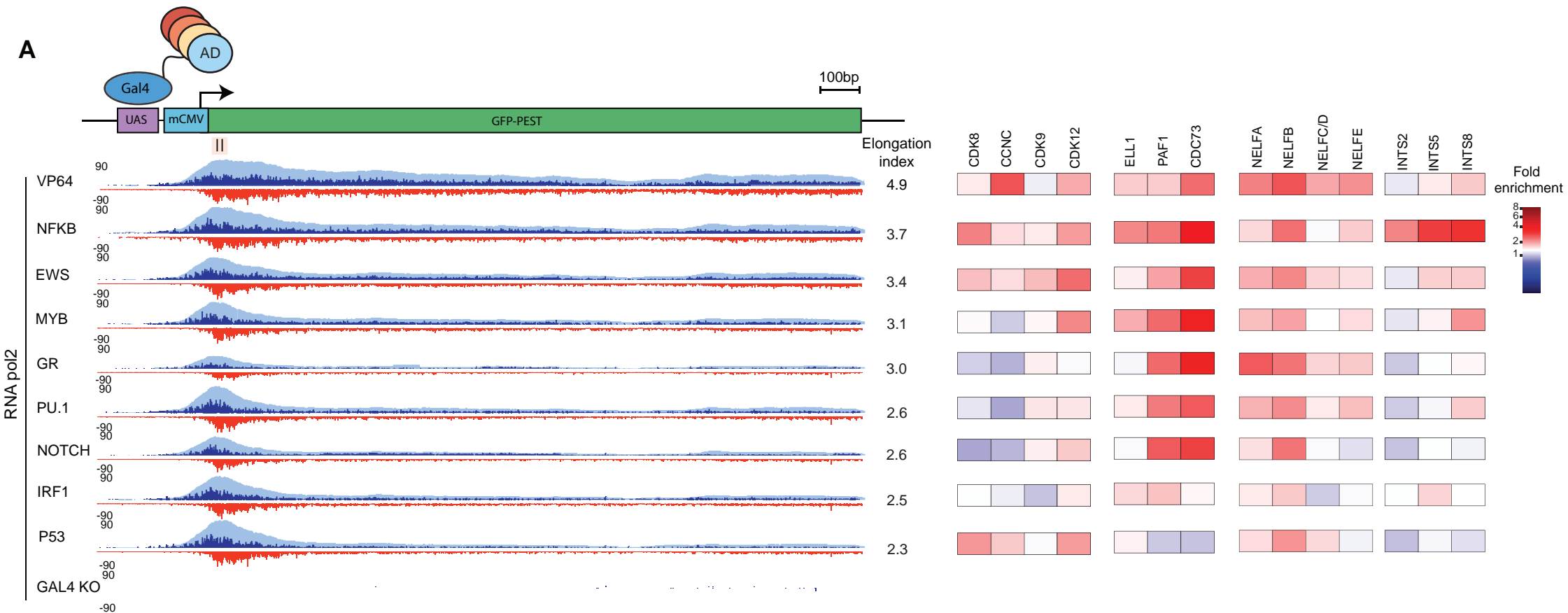
532 Representative gating strategy used to identify GFP positive cells throughout the manuscript.  
533 Live cells are identified by FSC-A and SSC-A, single cells identified by FSC-A and FSC-H  
534 and GFP positive cells gated relative to a negative control population.

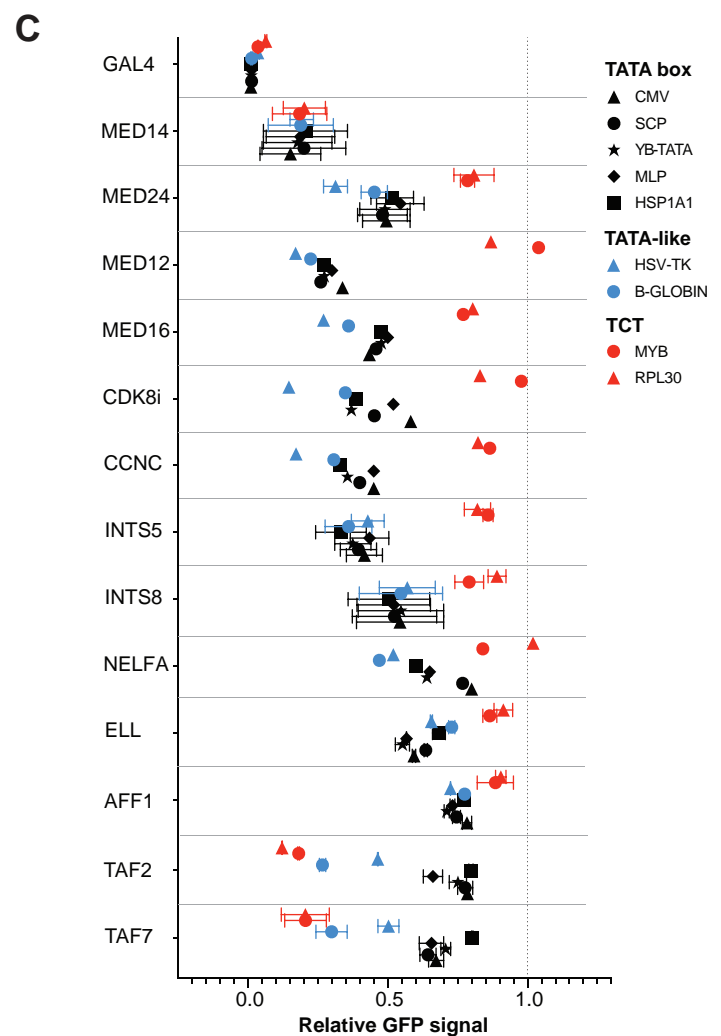
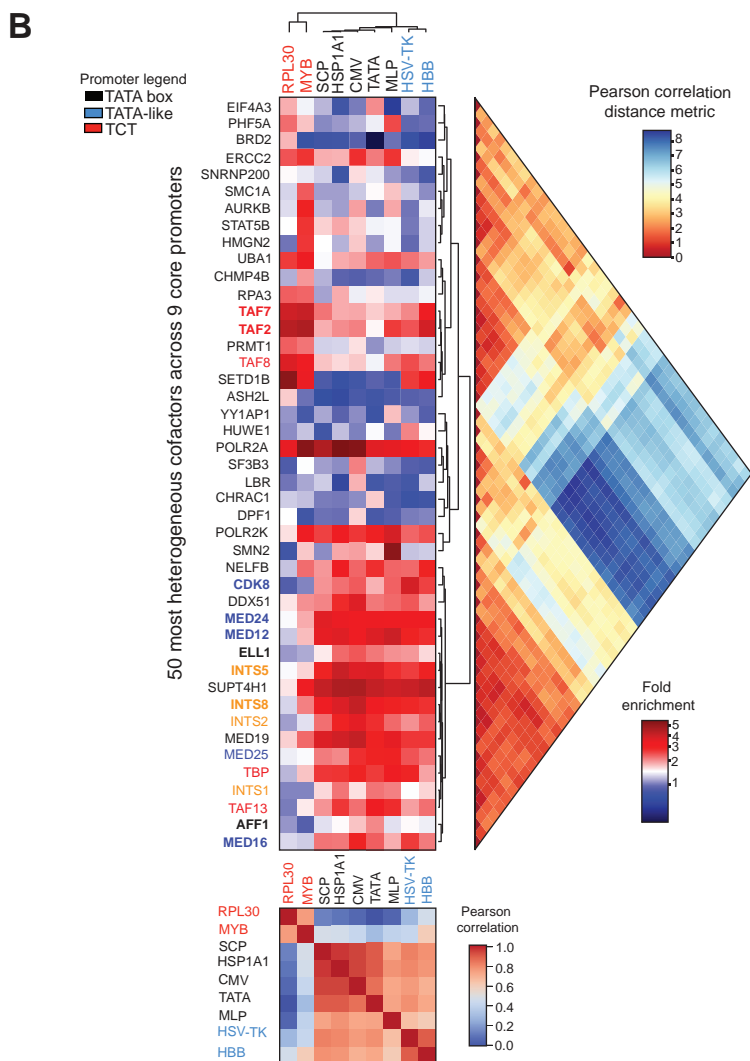
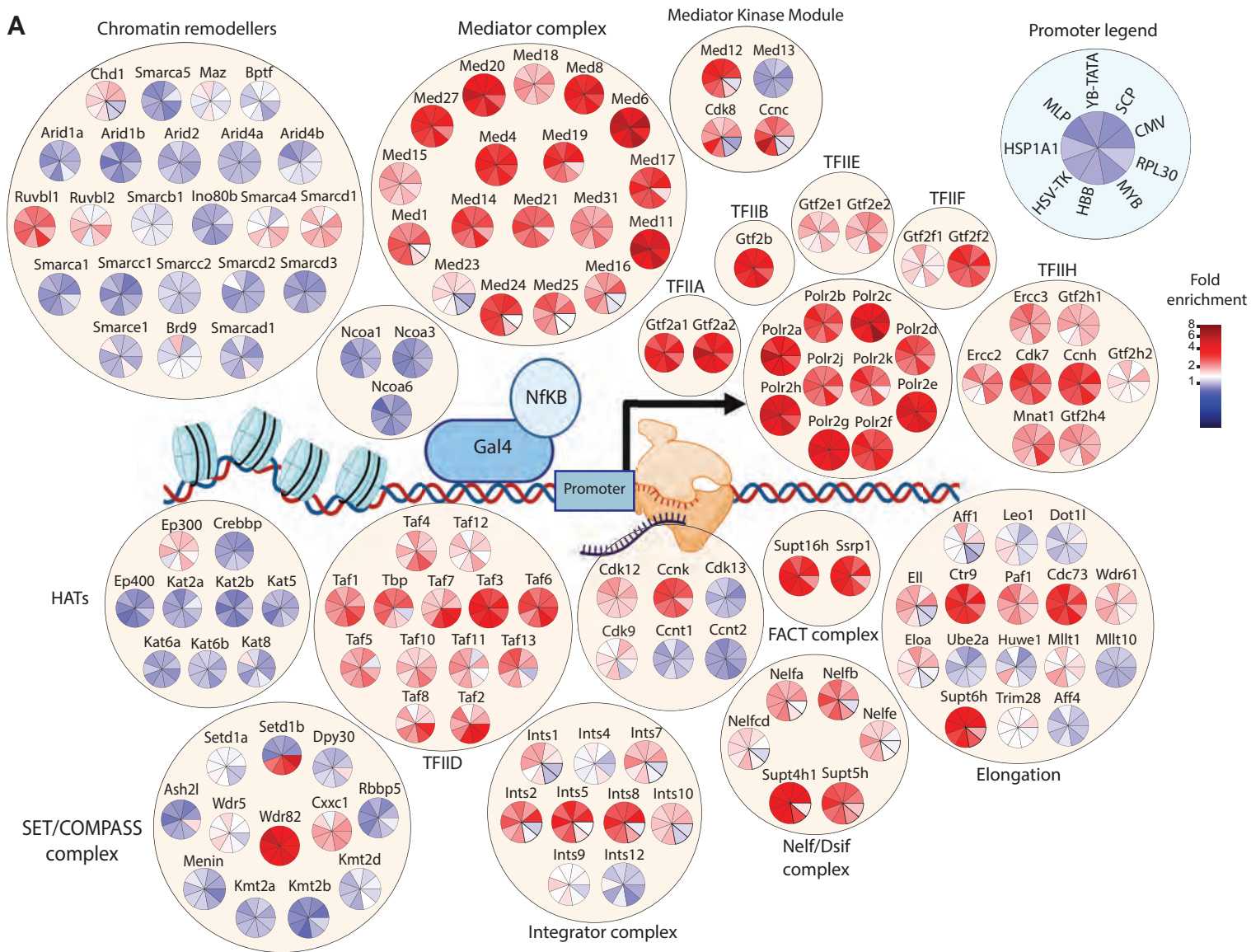
535

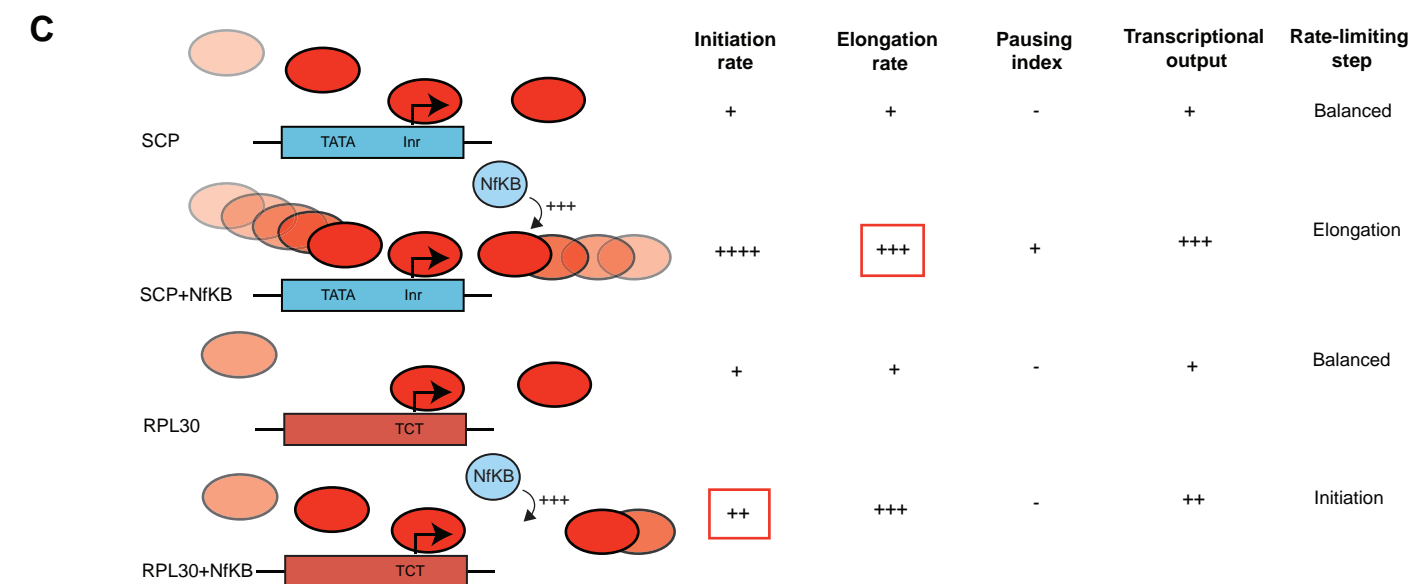
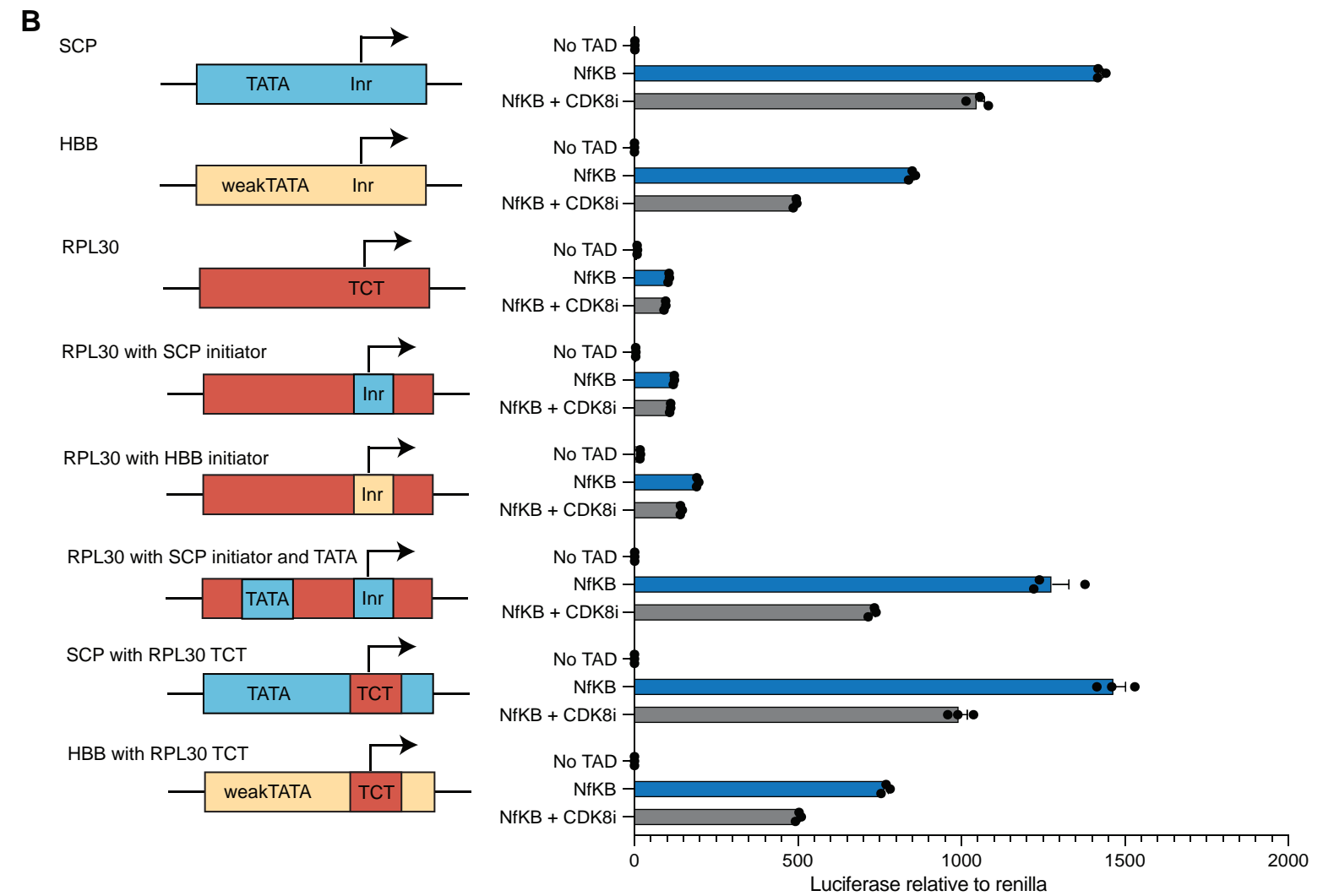
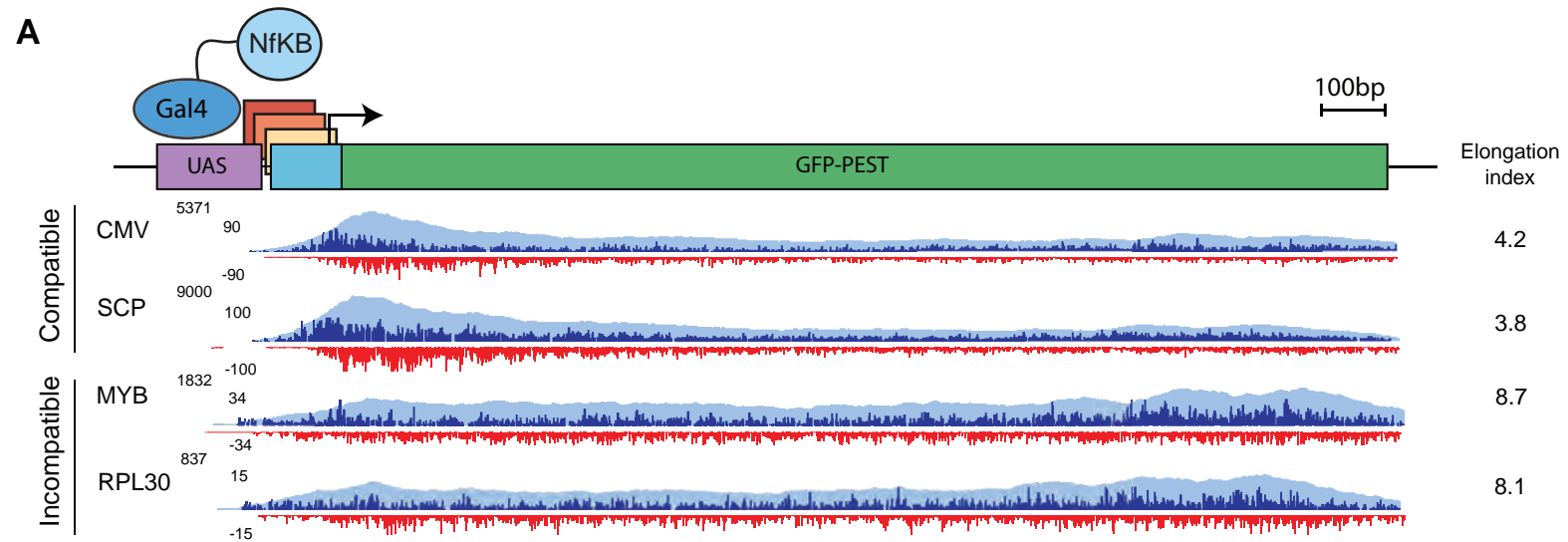




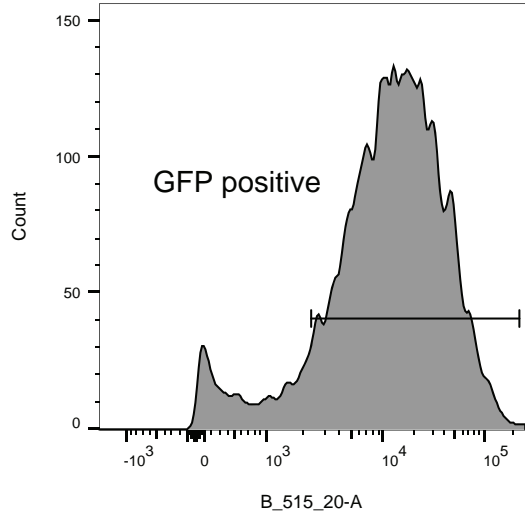
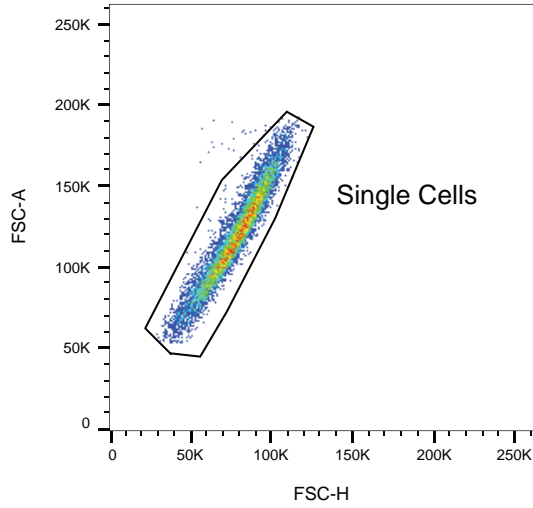
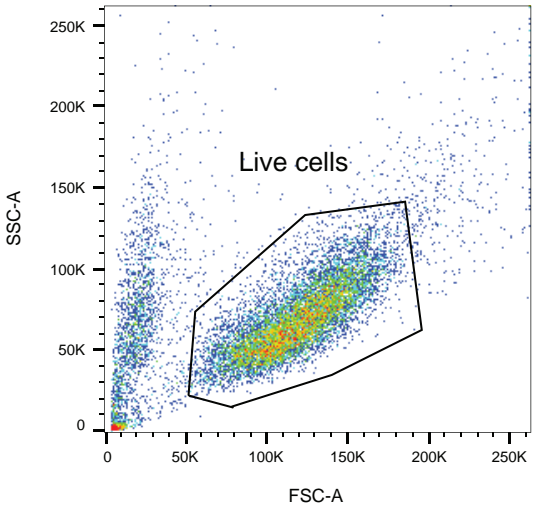








# Representative FACS gating



551 **References**

- 552 1. Lambert, S. A. *et al.* The Human Transcription Factors. *Cell* **172**, 650–665 (2018).  
 553 2. Ptashne, M. & Gann, A. Transcriptional activation by recruitment. *Nature* **386**, 569–  
 554 577 (1997).  
 555 3. Roeder, R. G. Transcriptional regulation and the role of diverse coactivators in animal  
 556 cells. *FEBS Lett* **579**, 909–915 (2005).  
 557 4. Ferrie, J. J., Karr, J. P., Tjian, R. & Darzacq, X. “Structure”-function relationships in  
 558 eukaryotic transcription factors: The role of intrinsically disordered regions in gene  
 559 regulation. *Mol Cell* 1–15 (2022) doi:10.1016/j.molcel.2022.09.021.  
 560 5. Reiter, F., Wienerroither, S. & Stark, A. Combinatorial function of transcription  
 561 factors and cofactors. *Curr Opin Genet Dev* **43**, 73–81 (2017).  
 562 6. Levine, M., Cattoglio, C. & Tjian, R. Looping Back to Leap Forward: Transcription  
 563 Enters a New Era. *Cell* **157**, 13–25 (2014).  
 564 7. Haberle, V. *et al.* Transcriptional cofactors display specificity for distinct types of core  
 565 promoters. *Nature* **570**, 122–126 (2019).  
 566 8. Neumayr, C. *et al.* Differential cofactor dependencies define distinct types of human  
 567 enhancers. *Nature* **606**, 406–413 (2022).  
 568 9. Stampfel, G. *et al.* Transcriptional regulators form diverse groups with context-  
 569 dependent regulatory functions. *Nature* **528**, 147–151 (2015).  
 570 10. Zabidi, M. A. *et al.* Enhancer-core-promoter specificity separates developmental and  
 571 housekeeping gene regulation. *Nature* **518**, 556–559 (2015).  
 572 11. Alerasool, N., Leng, H., Lin, Z.-Y., Gingras, A.-C. & Taipale, M. Identification and  
 573 functional characterization of transcriptional activators in human cells. *Mol Cell* **82**,  
 574 677-695.e7 (2022).  
 575 12. Nemčko, F. & Stark, A. Proteome-scale identification of transcriptional activators in  
 576 human cells. *Mol Cell* **82**, 497–499 (2022).  
 577 13. Donczew, R., Warfield, L., Pacheco, D., Erijman, A. & Hahn, S. Two roles for the  
 578 yeast transcription coactivator SAGA and a set of genes redundantly regulated by  
 579 TFIID and SAGA. *Elife* **9**, 1–27 (2020).  
 580 14. Bergman, D. T. *et al.* Compatibility rules of human enhancer and promoter sequences.  
 581 *Nature* **106**, 1–22 (2022).  
 582 15. Martinez-Ara, M., Comoglio, F., van Arensbergen, J. & van Steensel, B. Systematic  
 583 analysis of intrinsic enhancer-promoter compatibility in the mouse genome. *Mol Cell*  
 584 (2022) doi:10.1016/j.molcel.2022.04.009.  
 585 16. Arensbergen, J. Van, Steensel, B. Van & Bussemaker, H. J. In search of the  
 586 determinants of enhancer – promoter interaction specificity. *Trends Cell Biol* **24**, 695–  
 587 702 (2014).  
 588 17. Galouzis, C. C. & Furlong, E. E. M. Regulating specificity in enhancer-promoter  
 589 communication. *Curr Opin Cell Biol* **75**, 102065 (2022).  
 590 18. Kim, S. & Wysocka, J. Deciphering the multi-scale, quantitative cis-regulatory code.  
 591 *Molecular Cell* vol. 83 373–392 Preprint at  
 592 <https://doi.org/10.1016/j.molcel.2022.12.032> (2023).  
 593 19. Schmid-Burgk, J. L., Höning, K., Ebert, T. S. & Hornung, V. CRISPaint allows  
 594 modular base-specific gene tagging using a ligase-4-dependent mechanism. *Nat*  
 595 *Commun* **7**, 12338 (2016).  
 596 20. Pattabiraman, D. R. *et al.* Interaction of c-Myb with p300 is required for the induction  
 597 of acute myeloid leukemia (AML) by human AML oncogenes. *Blood* **123**, 2682–2690  
 598 (2014).  
 599 21. Vojnic, E. *et al.* Structure and VP16 binding of the Mediator Med25 activator  
 600 interaction domain. *Nat Struct Mol Biol* **18**, 404–409 (2011).

- 601 22. Mittler, G. *et al.* A novel docking site on Mediator is critical for activation by VP16 in  
602 mammalian cells. *EMBO Journal* **22**, 6494–6504 (2003).
- 603 23. Yang, F., DeBeaumont, R., Zhou, S. & Näär, A. M. The activator-recruited  
604 cofactor/Mediator coactivation subunit ARC92 is a functionally important target of the  
605 VP16 transcriptional activator. *Proc Natl Acad Sci U S A* **101**, 2339–2344 (2004).
- 606 24. Sandberg, M. L. *et al.* c-Myb and p300 regulate hematopoietic stem cell proliferation  
607 and differentiation. *Dev Cell* **8**, 153–166 (2005).
- 608 25. Xu, Y. *et al.* A TFIID-SAGA Perturbation that Targets MYB and Suppresses Acute  
609 Myeloid Leukemia. *Cancer Cell* **33**, 13-28.e8 (2018).
- 610 26. Donner, A. J., Szostek, S., Hoover, J. M. & Espinosa, J. M. CDK8 Is a Stimulus-  
611 Specific Positive Coregulator of p53 Target Genes. *Mol Cell* **27**, 121–133 (2007).
- 612 27. Chung, C. Y. *et al.* Cbx8 Acts Non-canonically with Wdr5 to Promote Mammary  
613 Tumorigenesis. *Cell Rep* **16**, 472–486 (2016).
- 614 28. Zheng, H. *et al.* Identification of Integrator-PP2A complex (INTAC), an RNA  
615 polymerase II phosphatase. *Science (1979)* **370**, (2020).
- 616 29. El Khattabi, L. *et al.* A Pliable Mediator Acts as a Functional Rather Than an  
617 Architectural Bridge between Promoters and Enhancers. *Cell* **178**, 1145–1158 (2019).
- 618 30. Abdella, R. *et al.* Structure of the human Mediator-bound transcription preinitiation  
619 complex. *Science (1979)* **372**, 52–56 (2021).
- 620 31. Jaeger, M. G. *et al.* Selective Mediator dependence of cell-type-specifying  
621 transcription. *Nat Genet* 825299 (2020) doi:10.1038/s41588-020-0635-0.
- 622 32. Warfield, L., Donczew, R., Mahendrawada, L. & Hahn, S. Yeast Mediator facilitates  
623 transcription initiation at most promoters via a Tail-independent mechanism. *Mol Cell*  
624 **82**, 4033-4048.e7 (2022).
- 625 33. Nabet, B. *et al.* The dTAG system for immediate and target-specific protein  
626 degradation. *Nat Chem Biol* **14**, 431–441 (2018).
- 627 34. Shao, W. & Zeitlinger, J. Paused RNA polymerase II inhibits new transcriptional  
628 initiation. *Nat Genet* **49**, 1045–1051 (2017).
- 629 35. Aoi, Y. *et al.* NELF Regulates a Promoter-Proximal Step Distinct from RNA Pol II  
630 Pause-Release. *Mol Cell* **78**, 261-274.e5 (2020).
- 631 36. Steinparzer, I. *et al.* Transcriptional Responses to IFN- $\gamma$  Require Mediator Kinase-  
632 Dependent Pause Release and Mechanistically Distinct CDK8 and CDK19 Functions.  
633 *Mol Cell* **76**, 485-499.e8 (2019).
- 634 37. Leach, K. M. *et al.* Characterization of the human  $\beta$ -globin downstream promoter  
635 region. *Nucleic Acids Res* **31**, 1292–1301 (2003).
- 636 38. Stewart, J. J., Fischbeck, J. A., Chen, X. & Stargell, L. A. Non-optimal TATA  
637 elements exhibit diverse mechanistic consequences. *Journal of Biological Chemistry*  
638 **281**, 22665–22673 (2006).
- 639 39. Stewart, J. J. & Stargell, L. A. The Stability of the TFIIA-TBP-DNA Complex Is  
640 Dependent on the Sequence of the TATAAA Element. *Journal of Biological*  
641 *Chemistry* **276**, 30078–30084 (2001).
- 642 40. Smale, S. T. & Kadonaga, J. T. The RNA Polymerase II Core Promoter. *Annu Rev*  
643 *Biochem* **72**, 449–479 (2003).
- 644 41. Kadonaga, J. T. Perspectives on the RNA polymerase II core promoter. *Wiley*  
645 *Interdiscip Rev Dev Biol* **1**, 40–51 (2012).
- 646 42. Morachis, J. M., Murawsky, C. M. & Emerson, B. M. Regulation of the p53  
647 transcriptional response by structurally diverse core promoters. *Genes Dev* **24**, 135–  
648 147 (2010).

- 649 43. Kwak, H., Fuda, N. J., Core, L. J. & Lis, J. T. Precise Maps of RNA Polymerase  
650 Reveal How Promoters Direct Initiation and Pausing. *Science (1979)* **339**, 950–953  
651 (2013).
- 652 44. Gilchrist, D. A. *et al.* Pausing of RNA polymerase II disrupts DNA-specified  
653 nucleosome organization to enable precise gene regulation. *Cell* **143**, 540–551 (2010).
- 654 45. Core, L. & Adelman, K. Promoter-proximal pausing of RNA polymerase II: A nexus  
655 of gene regulation. *Genes Dev* **33**, 960–982 (2019).
- 656 46. Parry, T. J. *et al.* The TCT motif, a key component of an RNA polymerase II  
657 transcription system for the translational machinery. *Genes Dev* **24**, 2013–2018 (2010).
- 658 47. Patel, A. B. *et al.* Structure of human TFIID and mechanism of TBP loading onto  
659 promoter DNA. *Science (1979)* **362**, eaau8872 (2018).
- 660 48. Petrenko, N., Jin, Y., Dong, L., Wong, K. H. & Struhl, K. Requirements for RNA  
661 polymerase II preinitiation complex formation in vivo. *Elife* **8**, 1–19 (2019).
- 662 49. Louder, R. K. *et al.* Structure of promoter-bound TFIID and model of human pre-  
663 initiation complex assembly. *Nature* (2016) doi:10.1038/nature17394.
- 664 50. Petrenko, N. & Struhl, K. Comparison of transcriptional initiation by rna polymerase ii  
665 across eukaryotic species. *Elife* **10**, 1–23 (2021).
- 666 51. Hoopes, B. C., LeBlanc, J. F. & Hawley, D. K. Contributions of the TATA box  
667 sequence to rate-limiting steps in transcription initiation by RNA polymerase II. *J Mol*  
668 *Biol* **277**, 1015–1031 (1998).
- 669 52. Yean, D. & Gralla, J. Transcription reinitiation rate: a special role for the TATA box.  
670 *Mol Cell Biol* **17**, 3809–3816 (1997).
- 671 53. Serebreni, L. *et al.* Functionally distinct promoter classes initiate transcription via  
672 different mechanisms reflected in focused versus dispersed initiation patterns. *EMBO J*  
673 **42**, (2023).
- 674 54. Wang, Y. L. *et al.* TRF2, but not TBP, mediates the transcription of ribosomal protein  
675 genes. *Genes Dev* **28**, 1550–1555 (2014).
- 676 55. Klumpe, H. E. *et al.* The context-dependent, combinatorial logic of BMP signaling.  
677 *Cell Syst* **13**, 388–407.e10 (2022).
- 678 56. Su, C. J. *et al.* Ligand-receptor promiscuity enables cellular addressing. *Cell Syst* **13**,  
679 408–425.e12 (2022).
- 680 57. Klumpe, H. E., Garcia-Ojalvo, J., Elowitz, M. B. & Antebi, Y. E. The computational  
681 capabilities of many-to-many protein interaction networks. *Cell Systems* vol. 14 430–  
682 446 Preprint at <https://doi.org/10.1016/j.cels.2023.05.001> (2023).
- 683 58. Danko, C. G. *et al.* Signaling Pathways Differentially Affect RNA Polymerase II  
684 Initiation, Pausing, and Elongation Rate in Cells. *Mol Cell* **50**, 212–222 (2013).
- 685 59. Blau, J. *et al.* Three functional classes of transcriptional activation domain. *Mol Cell*  
686 *Biol* **16**, 2044–2055 (1996).
- 687 60. Harden, T. T., Vincent, B. J. & DePace, A. H. Transcriptional activators in the early  
688 *Drosophila* embryo perform different kinetic roles. *Cell Syst* **14**, 258–272 (2023).
- 689 61. Herschlag, D. & Johnson, F. B. Synergism in transcriptional activation: a kinetic view.  
690 *Genes Dev* **7**, 173–179 (1993).
- 691 62. Martinez-Corral, R. *et al.* Transcriptional kinetic synergy: A complex landscape  
692 revealed by integrating modeling and synthetic biology. *Cell Syst* **14**, 324–339 (2023).
- 693 63. Scholes, C., DePace, A. H. & Sánchez, Á. Combinatorial Gene Regulation through  
694 Kinetic Control of the Transcription Cycle. *Cell Syst* **4**, 97–108.e9 (2017).
- 695 64. Dudnyk, K., Shi, C. & Zhou, J. Sequence basis of transcription initiation in human  
696 genome. *bioRxiv* (2023) doi:10.1101/2023.06.27.546584.

- 697 65. Li, X. C., Fuqua, T., van Breugel, M. E. & Crocker, J. Mutational scans reveal  
698 differential evolvability of *Drosophila* promoters and enhancers. *Philosophical*  
699 *Transactions of the Royal Society B: Biological Sciences* **378**, (2023).
- 700 66. Sahu, B. *et al.* Sequence determinants of human gene regulatory elements. *Nat Genet*  
701 **54**, 283–294 (2022).
- 702 67. Yang, C., Bolotin, E., Jiang, T., Sladek, F. M. & Martinez, E. Prevalence of the  
703 initiator over the TATA box in human and yeast genes and identification of DNA  
704 motifs enriched in human TATA-less core promoters. *Gene* **389**, 52–65 (2007).
- 705
- 706

## 707 **Methods**

### 708 **Cell culture**

709 A clonal K562 Cas9 cell line was generated previously to ensure high efficiency CRISPR  
710 editing<sup>68</sup>. K562 cells were cultured in RPMI-1640 supplemented with 20% FCS, streptomycin  
711 (100ug/ml), penicillin (100 units/ml) and Glutamax, under standard culture conditions (5%  
712 CO<sub>2</sub>, 37°C). HEK293ET cells were grown in DMEM supplemented with 10% FCS,  
713 streptomycin (100ug/ml), penicillin (100 units/ml) and Glutamax, under standard culture  
714 conditions (5% CO<sub>2</sub>, 37°C). All cell lines were subjected to regular mycoplasma testing and  
715 underwent short tandem repeat (STR) profiling.

716

### 717 **Lentivirus production and transduction**

718 Lentivirus was prepared by transfecting HEK293ET cells with plasmid:pVSV-G:psPAX2  
719 plasmids in a 3:2:1 ratio using PEI reagent. The viral supernatant was collected 48-72hrs  
720 following transfection, filtered through a 0.45 µm filter and added to cells.

721

### 722 **Drug treatment**

723 Senexin A (CDK8i) (Selleckchem) was dosed at 10uM. GAL4-GR cells were dosed with 1uM  
724 Dexamethasone (Sigma) to induce GR activity. Recombinant human TNF-α (Peprotech)  
725 treatment was performed for 6hrs at 25ng/ml. For acute dTAG degradation experiments, cells  
726 were dosed with dTAG-V1 (Tocris Biosciences) at 500nM for 4hrs. For GFP half-life analysis  
727 of the reporter system, cells were treated with triptolide (10uM)

728

### 729 **Flow cytometry analyses**

730 Flow cytometry analyses were performed on the LSRFortessa X-20 flow cytometer (BD  
731 Biosciences). Data were analysed with FlowJo v10 software (Tree Star). Cell sorting was  
732 performed on the FACSARIA or Fusion 5 flow sorter (BD Biosciences).

733

### 734 **Cloning of screening system**

735 pKLV-U6gRNA(BbsI)-Puro<sup>2</sup>ABFP vector was used as the base vector for cloning the lentiviral  
736 GAL4-AD vector. The entire gRNA, Puromycin and BFP regions of the plasmid were removed  
737 and replaced by the GAL4-DBD together with an IgA linker through standard cut and paste  
738 cloning. The EF1a, IRES and mCherry were then introduced sequentially. The vector was  
739 designed for simple cut and paste replacement of the AD region downstream of the GAL4-

740 DBD with alternative ADs. ADs of interested were amplified by PCR from cDNA expression  
741 vectors obtained from Addgene. Primers used for amplification and the final AD sequences are  
742 listed in Supplementary Table 2 and 6.

743

744 The base for the reporter construct was obtained from Addgene (#79199). The original vector  
745 is a lentiviral vector that includes the 5xUAS upstream of a minimal CMV promoter.  
746 Downstream of this promoter, Turbo-GFP-PEST was subcloned from another Addgene vector  
747 (#67180). To produce different promoter reporters, promoter regions were obtained from  
748 previous publications or from the eukaryotic promoter database (Supplementary Table 2). For  
749 endogenous promoters, a region was selected to capture a 100bp window around the centre of  
750 the CAGE signal reported on the Eukaryotic Promoter Database. Oligos corresponding to these  
751 regions were synthesized by IDT, annealed and cloned into the 5xUAS-mCMV-Turbo-GFP-  
752 PEST construct, replacing the mCMV promoter (Supplementary Table 2).

753

#### 754 **Generation of GAL4-AD and promoter reporter cell lines**

755 For AD screens, the lentiviral 5xUAS mCMV Turbo-GFP-PEST reporter was introduced into  
756 clonal K562-Cas9-Blasticidine cell line using high titre virus to achieve a high MOI. High MOI  
757 infection is necessary to minimise locus specific effects and to ensure robust detection of GFP  
758 signal upon activation by lower potency ADs. Into this reporter line, each of the GAL4-AD  
759 constructs were introduced at a high MOI (~90-100% of cells infected) by lentiviral integration.  
760 For promoter screens, the lentiviral 5xUAS Turbo-GFP-PEST reporter with variable promoters  
761 were integrated into a clonal K562-Cas9-Blasticidine cell line using high titre virus to achieve  
762 a high MOI. For all cell lines, GFP positive cells were sorted until a pure and stable GFP  
763 population was obtained.

764

#### 765 **sgRNA design and cloning**

766 sgRNAs were designed using the IDT CRISPR design tool or were obtained from the  
767 sequences of guides in the pooled guide library. sgRNAs were cloned into the pKLV-  
768 U6gRNA(BbsI)-Puro<sub>2A</sub>BFP vector using standard golden gate cloning.

769

#### 770 **sgRNA and primer sequences**

771 The sequences for sgRNA sequences and relevant primer sequences are included in  
772 Supplementary Table 6.

773

774 **Validation and quantification of screen hits**

775 All experiments validating and quantifying the effect of cofactor knockout were performed by  
776 quantifying the mean fluorescence intensity (M.F.I. or average fluorescence signal) of the GFP  
777 reporter at day 5 after infection with the relevant sgRNA. The relative GFP signal was  
778 calculated by dividing average GFP signal in the AD line infected with an sgRNA of interest  
779 by the same AD line infected with a control sgRNA targeting a safe genomic locus (safe guide).  
780 A number of examples of FACS plots used to calculate the change in GFP signal are provided  
781 in Extended Data Fig. 5. Each AD line was infected with the same batch of virus in parallel to  
782 minimise technical variation between the quantification. Cofactors of interest were validated  
783 with at least 2 sgRNAs and at least 2 biological replicates.

784

785 **HDR mediated AAVS knock-in**

786 The 5xUAS, mCMV promoter and Turbo-GFP-PEST were cloned by Gibson assembly into  
787 the pMK232 (CMV-OsTIR1-Puro), which contained homology arms for the AAVS locus. The  
788 sgRNA targeting the AAVS was introduced into the pX330-mCherry vector, which contains  
789 both Cas9 and the gRNA. The AAVS-reporter repair template and the pX330-Cas9-AAVS  
790 gRNA vector was electroporated into K562 cells using the Neon Transfection system (Thermo  
791 Fischer) with settings optimised for K562 cells. Single cell clones were sorted 5 days after  
792 transfection and grown out for 2 weeks to obtain sufficient cells for analysis. AAVS knock-in  
793 clones were identified by In-Out PCR and Sanger sequencing.

794

795 **Guide library design, generation and cloning**

796 To assess the requirement of transcriptional regulators, a bespoke library of gRNAs that targets  
797 over 1137 known chromatin and transcriptional regulators was designed (Supplementary Table  
798 3). The library was designed through a combination of searches for genes containing domains  
799 enriched in transcriptional regulators and manual curation. Each gene was targeted with 6  
800 independent gRNAs. As controls, the library also contains a large number of guides targeting  
801 safe regions and guides that do not target any genomic locus. The total library contains 7239  
802 gRNAs. The oligo pool was synthesized by CustomArray (Genescript). The sgRNA pool was  
803 PCR amplified and pot cloned into the pKLV-U6gRNA(BbsI)-Puro2ABFP vector using  
804 standard cut and paste cloning. The ligated product was electroporated into Electrocompetent  
805 cells (Lucigen) and grown in liquid culture overnight at 37 degrees before being extracted by  
806 Maxiprep. Low skewing of the plasmid was confirmed by sequencing of the cloned plasmid

807 pool. The library had a skew ratio of 4.35 (counts for top 10% of guides divided by counts for  
808 bottom 10% of guides). A skew ratio below 10 is considered acceptable<sup>69</sup>.

809

### 810 **Comparative CRISPR screens**

811 Prior to beginning the screens, reporter cell lines were sorted to obtain a pure GFP positive  
812 population. Sufficient cells were used to maintain 1000-fold representation at all stages of the  
813 screening process. The cells were transduced with an appropriate volume of viral supernatant  
814 to ensure only a single guide was present in most cells (MOI < 0.3, mean of 0.21,  
815 Supplementary Table 7). At day 5, 6 and 7 after guide library infection, at least 1 million guide  
816 positive (BFP positive), GFP negative cells (< 25% of the mean fluorescence intensity of the  
817 entire population) were sorted (refer to Supplementary Note 1 for FACS plots and further  
818 details). This translates to approximately 1000-fold representation of the library. Guide positive  
819 cells (at least 10 million cells) were also sorted as a library control at each time point to provide  
820 a library control reference to calculate enrichment (>1000-fold representation). Cells were  
821 pelleted after sorting and stored at -80°C until genomic DNA extraction was performed. Four  
822 of the GAL4-AD cell lines from the comparative CRISPR screens were also maintained until  
823 day 14 after guide infection to test which genes are required for cell growth. These four AD  
824 lines were used as independent replicates for the dropout analysis.

825

826 Genomic DNA was extracted using Monarch® Genomic DNA purification kit (New England  
827 Biolabs), according to the manufacturer's instructions. PCR was conducted to maintain guide  
828 representation, using Q5® High Fidelity DNA Polymerase (New England Biolabs). PCR was  
829 performed through a one-step PCR with 28 cycles. 500ng of template was added to each PCR.  
830 One step PCR helps to avoid excessive amplification, by minimising sample processing. PCR  
831 was optimised to ensure it stays within the exponential phase. Depending on the gDNA  
832 concentration from the extraction, approximately 10-20 PCR reactions were performed per  
833 screen sample and between 30-50 PCRs per library control. PCR products were pooled and  
834 sequenced on the NextSeq500 using 75bp single-end chemistry. The samples were sequenced  
835 with the following summary statistics: Min =  $3.86 \times 10^6$  reads, Q1 =  $6.24 \times 10^6$  reads, Q2=  
836  $7.37 \times 10^6$  reads, Q3 =  $8.51 \times 10^6$  reads, Max =  $12 \times 10^6$  reads.

837

### 838 **Analysis of comparative CRISPR screens**

839 The sequence reads were trimmed to remove the constant portion of the sgRNA sequences with  
840 cutadapt v4.3<sup>70</sup>, then mapped to the reference sgRNA library with Bowtie2<sup>71</sup>. After filtering to  
841 remove multi-mapping reads, the read counts were computed for each sgRNA. After obtaining  
842 guide counts for all samples, a series of processing steps were performed to calculate mean  
843 fold enrichment values for each gene in each screen (see Supplementary Note 1 for further  
844 details). Firstly, guides that were very lowly represented (below 2.5<sup>th</sup> percentile) were filtered  
845 from the analysis, since their low representation caused extreme fold change values<sup>72,73</sup> (see  
846 Supplementary Note 1 for further details). The counts were then normalised to sequencing  
847 depth before calculating the fold enrichment for each guide by dividing the counts for each  
848 gene in the screen samples by the counts in the library control. This resulted in a total of 18  
849 individual fold enrichments for each gene (6 guides, 3 timepoints). To remove outliers, we  
850 filtered any guides that had a fold enrichment below 0.1 or greater than 10 (see Supplementary  
851 Note 1 for further details). To improve quantification, further outliers were removed by filtering  
852 guides that were more than 4-fold away from the mean fold change value. The filtering steps  
853 applied to the data are benchmarked using two highly correlated replicates of the GAL4-NF-  
854  $\kappa$ B screen ( $r=0.92$ , Pearson) (Supplementary Note 1).

855

856 Using this filtered guide list, we calculated a final fold enrichment score for each gene in each  
857 screen. In order to calculate what fold enrichment score should be considered statistically  
858 significant, a permutation test was performed for each screen (Supplementary Note 1). The  
859 permutation test shows what fold change distribution would be expected if you randomly  
860 sampled fold enrichment scores from guides in the data. Specifically, 6 guides were randomly  
861 sampled from each timepoint providing a vector of 18 values. The mean fold enrichment was  
862 calculated across these 18 values. Random sampling was performed 10000 times to produce a  
863 random sampling distribution. Genes that had an average fold enrichment above the 95<sup>th</sup>  
864 percentile of this random distribution, as well as at least 1/3<sup>rd</sup> of the guides (6/18) above the  
865 95<sup>th</sup> percentile of this distribution, were considered significant.

866

867 To identify heterogeneous regulators, the coefficient of variation was calculated for each gene.  
868 To produce the heatmaps displayed in Fig. 2 and Fig. 5, the top 50 most heterogeneous  
869 cofactors were then bi-clustered based on their Pearson correlation distance. SPC24, SPC25  
870 and NUF2 were filtered from the variability analysis as the function in regulating genome  
871 ploidy has been previously demonstrated to result in spurious variability across screens<sup>74</sup>.

872 Two relevant regulators of transcription, *CCNC* and *SETDIA* were not represented in the  
873 library. To calculate fold enrichment scores for these genes, we performed independent KO  
874 experiments using at least 3 sgRNAs and calculated the reduction in GFP signal as described  
875 above. The fold reduction in GFP signal for these genes is displayed as the fold enrichment  
876 score in Figure 1, 3 and 5.

877

878 To define which genes affected cell growth, MAGeCK v0.5.6 analysis was performed using  
879 the D14 timepoint from 4 of the AD screens, comparing them to the plasmid as the D0  
880 reference<sup>75</sup>. Any genes with an adjusted p-value below 0.05 were considered significant.

881

### 882 **ZFP-VP64 piggyBac reporter screen**

883 A replicate screen was performed using an alternative integration method and alternative DNA  
884 binding domain to demonstrate the broad relevance and reproducibility of our findings. In order  
885 to perform this screen, a construct in which VP64-AD is recruited through an artificial ZFP  
886 protein<sup>76</sup> was developed (37ZFP, Addgene #176627). To generate the DNA binding-AD  
887 construct, the GAL4-VP64 vector was cut and the GAL4-DBD was replaced by the ZFP DNA  
888 binding domain. A fully insulated PiggyBac reporter construct was also developed. This  
889 reporter construct contains the A1 insulator<sup>77</sup> upstream and downstream of a GFP-PEST  
890 reporter. GFP-PEST is activated by a minimal CMV promoter with 6 upstream binding sites  
891 for 37ZFP-VP64. The reporter construct was cloned by a combination of Gibson assembly and  
892 standard cut and paste cloning. The binding sites for 37ZFP were obtained by PCR from  
893 Addgene vector #176627.

894

895 Upon successful cloning of both the reporter and ZFP-AD constructs, a reporter line was  
896 generated by piggyBac-mediated integration of the insulated ZFP-reporter construct. 1 million  
897 Cas9-K562 cells were transfected with 1ug of the reporter and 250ng of HyBase transposase<sup>78</sup>  
898 using the Lonza 4D nucleofection system. Transfected cells were then infected with the ZFP-  
899 VP64 construct by lentiviral integration at high MOI (~90-100% of cells infected). GFP  
900 positive cells were then isolated by FACS sorting. The screen was performed and analysed as  
901 described above, in order to enable direct comparison of the results. Guides targeting *FKBP1A*  
902 and *FKBP1C* were excluded from the analysis as they directly target the ZFP sequence.

903

### 904 **Cofactor KO CHIP-seq and RNA-seq experimental design**

905 sgRNAs targeting *MED12*, *MED14*, *MED16*, *MED24*, *MED25*, *CDK8* and *CCNC* were  
906 lentivirally introduced into a K562-Cas9 clone. Cells were grown for 4 days after infection at  
907 which timepoint they were harvested for ChIP-seq. For INTS5 RNA-seq and ChIP-seq,  
908 sgRNAs targeting INTS5 were introduced into a K562-Cas9 clone. Cells were grown for 4  
909 days post guide infection and treated with PBS or TNF- $\alpha$  for 6hrs before being harvested for  
910 ChIP-seq or RNA-seq.

911

### 912 **Cloning & Generation of dTAG knock-in cell lines**

913 The dTAG degen (FKBP12<sup>F36V</sup>) was selectively knocked-in into the N-termini of *MED12*,  
914 *MED14* and *MED25*. Cloning of knock-in plasmids and the subsequent generation of knock-  
915 in cells lines were conducted as previously described<sup>33,79</sup>. Briefly, the hU6-PITCh-gRNA  
916 cassette from pX330S-2-PITCh (Addgene, #63670) was subcloned into pX330A-1x2  
917 (Addgene, # 58766) via BsaI digestion to create an all-in-one CRISPR-Cas9 vector labelled  
918 pX330-A+S. sgRNAs against target loci were ligated into pX330-A+S via BpiI digestion and  
919 golden-gate assembly. Donor vectors were constructed by using PCR to add 20bp  
920 microhomology sequences against target loci to pCRIS-PITChv2-Puro-dTAG (Addgene,  
921 #91793). 750ng each of the paired gRNA (px330-A+S) and donor vectors (pCRIS-PITChv2)  
922 were electroporated into  $3 \times 10^5$  K562 cells in Buffer R using the Neon™ Transfection System  
923 10uL kit (Thermo Fisher). Cells were allowed to recover for 48 hours, followed by 5-7 days of  
924 puromycin selection (2ug/mL). Single cell clones were isolated via FACS sorting into 96-wells  
925 and allowed to expand. Genomic DNA was isolated using DirectPCR Lysis Reagent® (Viagen  
926 Biotech) according to manufacturer's instructions and directly used as input for genotyping  
927 PCRs. Clones demonstrating homozygous knock-in were further validated by sanger  
928 sequencing of the homozygous knock-in gel extracted product, as well as further validated by  
929 immunoblot analysis. Supplementary Table 6 lists dTAG cloning and PCR oligo sequences.

930

### 931 **Chromatin immunoprecipitation (ChIP)**

932 For each ChIP, at least 20 million cells were crosslinked for 15 mins with 1% formaldehyde.  
933 Crosslinked material was sonicated to approximately 200-1000bp using the Covaris  
934 Ultrasonicator S2. Sonicated material was incubated overnight with each antibody in IP buffer  
935 (10mM Tris-HCl pH8, 1% Triton X-100, 0.1% sodium deoxycholate, 90mM NaCl), then  
936 incubated for 3hrs with 50ul of either Protein A or Protein G Dynabeads (Thermo Fisher).  
937 Antibody bound beads were washed twice with low salt wash buffer (20mM Tris-HCl pH8,

938 2mM EDTA, 1% Triton X-100, 0.1% SDS, 150mM NaCl) and once with high salt wash buffer  
939 (20mM Tris-HCl pH8, 2mM EDTA, 1% Triton X-100, 0.1% SDS, 500mM NaCl) and once  
940 with TE, before the ChIP material was eluted and de-crosslinked overnight at 65 degrees in  
941 elution buffer (1% SDS, 100mM NaHCO<sub>3</sub>). DNA was purified using Qiagen Minelute  
942 columns. All ChIP antibodies were used at ~10ug per IP. Sequencing libraries were prepared  
943 using the ThruPLEX® DNA-seq kit (Takara Bio). Libraries were size selected between 200-  
944 500bps and sequenced on the NextSeq500 using the 75bp single-end chemistry. The following  
945 antibodies were used for ChIP: Mouse anti-RNA polymerase II antibody clone CTD4H8 (6ul)  
946 (Merck Millipore, 05-623), Rabbit anti-NF-kB p65 antibody clone D14E12 (10ul) (Cell  
947 Signalling, 8242), mouse anti-GAL4-DBD antibody clone RK5C1 (10uL) (sc-510). For  
948 quantification of occupancy on the GAL4-reporter construct, ChIP-qPCR was performed using  
949 primers specific to the promoter of the GAL4-reporter construct and compared to a gene desert  
950 negative control region.

951

#### 952 **ChIP-seq analysis**

953 Reads were aligned to the human genome (GRCh38) with Bowtie2<sup>71</sup>. Duplicate reads and reads  
954 mapping to blacklist regions or mitochondria were removed. ChIP-seq coverage across  
955 selected genomic regions was calculated with BEDtools v2.31.0<sup>80</sup>. To define which genes are  
956 Mediator dependent, the 10000 genes with the most RNA pol II signal across the gene were  
957 isolated. From this list, genes with at least 30% reduction in total RNA pol II signal in the  
958 MED14 KO were defined as Mediator dependent (1020 genes). For each KO sample, we then  
959 calculated the change in RNA Pol II signal by comparison to the SAFE guide control. For the  
960 mediator dTAG degron ChIP-seq analysis, correlation plots were performed on the top 10000  
961 genes by RNA Pol II signal.

962

#### 963 **ChIP-nexus**

964 ChIP-nexus was performed as described previously<sup>34,81,82</sup>. Briefly, the immunoprecipitation  
965 and washes were performed using the same conditions as the ChIP protocol. Upon completion  
966 of these steps, the DNA was end-repaired, A-tailed, adaptors ligated, exonuclease treated,  
967 circularized on Dynabeads as described previously<sup>34,81,82</sup>. DNA was then eluted from the beads,  
968 and PCR was performed to produce sequencing ready libraries. For ChIP-nexus performed on  
969 the different GAL4-AD lines, DNA was sequenced on the NextSeq500 using the 75bp single-  
970 end chemistry. For ChIP-nexus on the different promoter lines, DNA was sequenced on the

971 NextSeq500 using 75bp single-end chemistry, which was configured to produce paired-end  
972 37bp reads.

973

#### 974 **ChIP-nexus data analysis**

975 ChIP-nexus analysis was performed as previously described<sup>81</sup>. Specifically, reads that passed  
976 the Illumina quality filter were filtered for the presence of a fixed barcode. The fixed barcode  
977 was used to demultiplex the samples, before being filtered from the reads by Cutadapt v4.3<sup>70</sup>.  
978 The random barcode on each read was retained to enable UMI based quantification. Any  
979 remaining adapter sequences were trimmed, and reads were removed if they were less than  
980 22bp in length. Reads were then aligned using Bowtie2<sup>71</sup> to a human genome (GRCh38) that  
981 was modified to contain an additional chromosome with the relevant reporter construct  
982 sequence. Duplicate reads were removed, and each sample was converted into two bigwig files,  
983 one with strand specific information and one that aggregates the reads from both strands. The  
984 sequence coverage across the reporter construct was then visualised using IGV. To enable  
985 better visualisation of the disproportionate effect of CDK8i on elongation (Figure 4B), CDK8i  
986 samples are scaled to the height of the DMSO samples. The scale reflects the number of reads  
987 in the DMSO sample.

988

#### 989 **RNA-seq**

990 RNA was extracted using the Qiagen RNeasy kit. RNA concentration was quantified with a  
991 NanoDrop spectrophotometer (Thermo Scientific). Libraries were prepared using a plate based  
992 in-house library prep method based on DRUG-seq<sup>83</sup>. The method results in 3' RNA-seq  
993 libraries containing a UMI and a well ID on read 1, and the unique transcript information on  
994 read 2. Libraries were sequenced on the NextSeq500 using the 75bp single end chemistry, run  
995 with paired-end settings. 25bps was allocated for the Read1 and 50bps for Read2.

996

#### 997 **RNA-seq analysis**

998 Fastq files were demultiplexed and mapped to the human genome (hg19) using STARsolo  
999 v2.7.9a<sup>84</sup>. Downstream processing of the output counts matrix was then performed in R. Using  
1000 the Seurat package<sup>85</sup>, the raw counts matrix was transformed and then subject to differential  
1001 gene expression analysis using DESeq2 v3.18<sup>86</sup>. Genes were classified as differentially  
1002 expressed if they had an absolute fold change above 1.5 and a p-value <0.05. TNF target genes  
1003 were defined as genes with a fold increase greater than 1.5 with a p-value < 0.05 and displayed  
1004 a p65 binding defined by MACS2 v2.2.7 within 10kb of the gene.

## 1005 **SLAM-seq**

1006 SLAM-seq was performed as previously described with minor modifications<sup>87</sup>. Briefly, a total  
1007 of 10<sup>7</sup> K562 cells were treated with dTAGV<sup>-1</sup> (Tocris) as described above for a total of 4 hours.  
1008 In the final hour of treatment, cells were labelled with 200uM of 4-thioridine (4sU; Cayman  
1009 Chemical) to capture nascent mRNA transcripts. RNA extraction was performed using TRIzol  
1010 (Ambion) following the manufacturer's instructions, with the addition of 1mM DTT to the  
1011 isopropanol precipitation and ethanol wash steps. Total RNA was eluted in nuclease-free H<sub>2</sub>O  
1012 containing 0.1mM DTT. 10ug of total RNA was treated with fresh 10mM iodoacetamide  
1013 (Pierce) in reaction buffer containing 50mM Tris, pH 8.0 and 50% DMSO at 50°C for 15  
1014 minutes, light-protected and shaking at 1000rpm. The alkylation reaction was quenched with  
1015 20mM of fresh DTT, followed by adding 1ug of unlabelled Drosophila S2 RNA. Total RNA  
1016 was cleaned up using the RNeasy MinElute Cleanup Kit (Qiagen) and DNase treated. Libraries  
1017 were prepared using 500ng of material using the QuantSeq 3' mRNA-Seq Library Prep Kit  
1018 FWD (Lexogen; V1 kit with single 6nt i7 indexes) according to the standard manufacturer's  
1019 protocol. Sequencing of cDNA libraries was performed on the Illumina NextSeq2000 with  
1020 100bp single-end configuration. SLAM-seq was performed in biological triplicate.

1021

## 1022 **SLAM-seq analysis**

1023 Quality assessment was performed on sequenced reads using FastQC v0.11.6 and adapters  
1024 were trimmed using TrimGalore v0.6.6 and Cutadapt v4.3<sup>70</sup>. Read alignment to HG38  
1025 reference genome, read filtering, SNP calling and masking, and feature calling were performed  
1026 with SlamDunk v0.2.4<sup>88</sup>. Reads containing at least 2 T>C conversions were retained as nascent  
1027 transcripts. edgeR v3.38.1<sup>89</sup> was used to perform TMM normalisation, before performing  
1028 differential expression analysis with limma voom v3.52.1<sup>90</sup>. Genes defined as down-regulated  
1029 were those with a negative fold change value and an adjusted p-value < 0.05.

1030

## 1031 **GAL4-AD protein expression levels and stability**

1032 As commercially available GAL4 antibodies performed unreliably in western blot, it was  
1033 necessary to introduce an epitope tag to the GAL4-AD constructs. The DBD region of each  
1034 GAL4-AD construct was replaced by a 3xFLAG tagged GAL4-DBD synthesized by IDT.  
1035 FLAG-GAL4-ADs constructs were introduced at a high MOI into K562-Cas9 cells containing  
1036 the 5xUAS mCMV GFP-PEST reporter to confirm that their transactivation capacity was not  
1037 impacted by the addition of the FLAG tag. Cells were sorted based on the same relative levels  
1038 of GAL4-AD expression as the original GAL4-AD lines used for the screens. This was

1039 achieved by direct comparison of the expression level of the IRES mCherry in the original AD  
1040 cell lines and the newly derived AD cell lines. To assess protein expression and stability, one  
1041 million of each of the FLAG-GAL4-AD cell lines were treated with either DMSO or  
1042 cycloheximide (100uM) for 24hrs before being harvested for western blot.

1043

#### 1044 **Immunoblot**

1045 Cells were lysed in RIPA lysis buffer (50mM Tris (pH 7.4), 150mM NaCl, 1mM EDTA, 1%  
1046 Triton X-100, 0.5% sodium deoxycholate, 0.5% SDS supplemented with protease and  
1047 phosphatase inhibitors (Roche)) and protein concentration was determined using a BCA  
1048 protein assay kit (Pierce). Normalised concentrations of lysate were reduced and denatured for  
1049 5 min at 95°C in Laemmli buffer containing 10% beta-mercaptoethanol and subsequently  
1050 electrophoresed on 4–15% precast polyacrylamide gels (Mini-PROTEAN® TGX; Bio-Rad)  
1051 under denaturing conditions. Proteins were wet transferred onto PVDF using the Mini Trans-  
1052 Blot Electrophoretic Transfer Cell System (Bio-Rad) at 100V (400mA) for 60 min at 4°C.  
1053 Membranes were blocked for 1 hour at room temperature in Intercept® Blocking Buffer (LI-  
1054 COR) and subsequently probed with the following primary antibodies diluted at 1:1000 in  
1055 blocking buffer supplemented with 0.1% Tween-20 overnight at 4°C on a roller: anti-HA-TAG  
1056 (Cell Signaling, #2367), anti-MED12 (Bethyl Laboratories, #A300-774A), anti-MED14  
1057 (Abcam; #ab72141), anti-MED25 (Abcam, #ab221741), anti-MYC (Abcam, #ab32072), anti-  
1058 alpha-tubulin (Cell Signaling Technology; #3873), mouse anti-FLAG M2 (Sigma, #F3165),  
1059 rabbit anti-LAMIN-B1 clone D4Q4Z (Cell Signaling, #12586). After washing, membranes  
1060 were probed with the appropriate IRDye-conjugated secondary antibodies (LI-COR, 926-  
1061 68071, 926-32210) diluted at 1:10,000 for 1 hour at room temperature. Membranes were  
1062 scanned using an Odyssey ® Infrared Imaging System (LI-COR).

1063

#### 1064 **Luciferase assays**

1065 To generate the reporter constructs for the luciferase assays, promoters of interest were cloned  
1066 into the pGL4.35 (luc2p/9xgal4uas/hygro) luciferase construct (Promega, E1370) downstream  
1067 of the 9xUAS site. Luciferase constructs were introduced into HEK293T cells by transient  
1068 transfection using PEI. The luciferase construct of interest was co-transfected with or without  
1069 the relevant GAL4-AD and the pRL Renilla control (Promega, E2261). Cells were harvested  
1070 48hrs after transfection. Luciferase signal and Renilla signal were analysed using the Dual-  
1071 Luciferase reporter system (Promega, E1910) using the Cytation 3 plate-reader (BioTek).

1072

1073 **Statistics and reproducibility**

1074 No statistical method was used to predetermine sample size. No data were excluded from the  
1075 analyses. Experiments were not randomized. The investigators were not blinded to the  
1076 allocation during experiments and outcome assessment.

1077

1078 **Data availability**

1079 All high-throughput sequencing data relevant to this study have been deposited in the NCBI  
1080 Gene Expression Omnibus under primary accession code: GSE198944. All of the relevant  
1081 source data has been provided with the manuscript.

1082

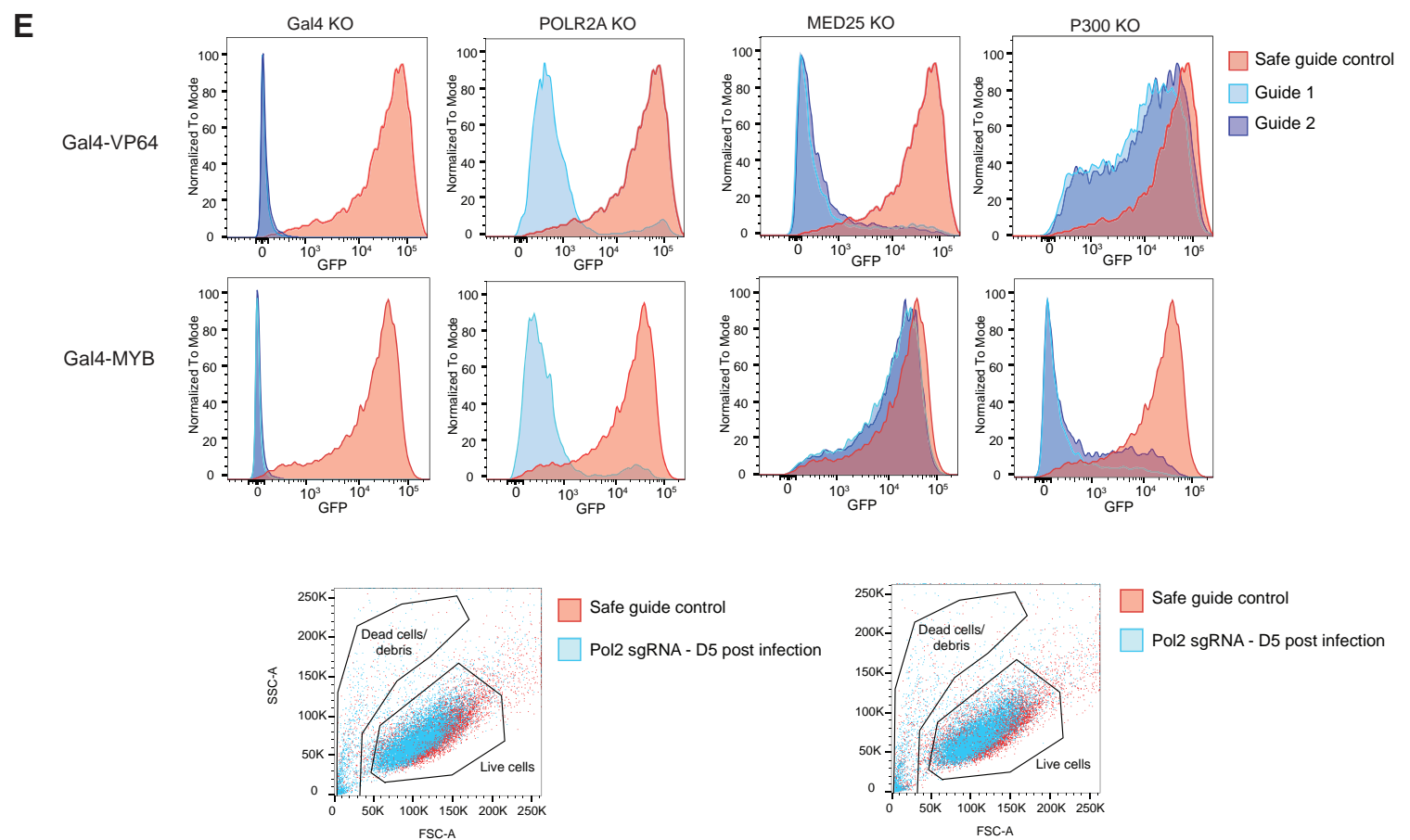
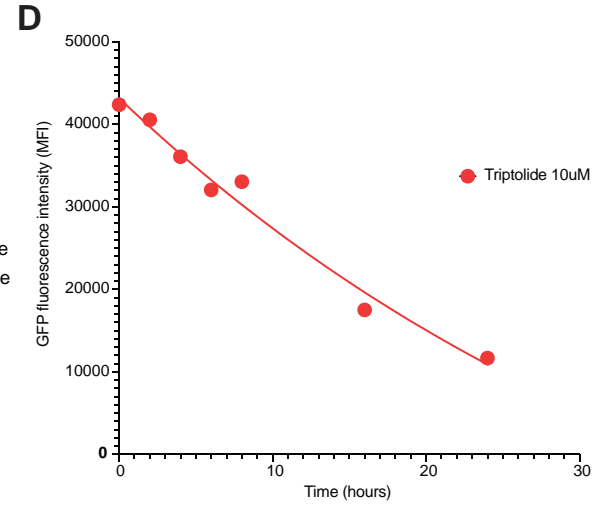
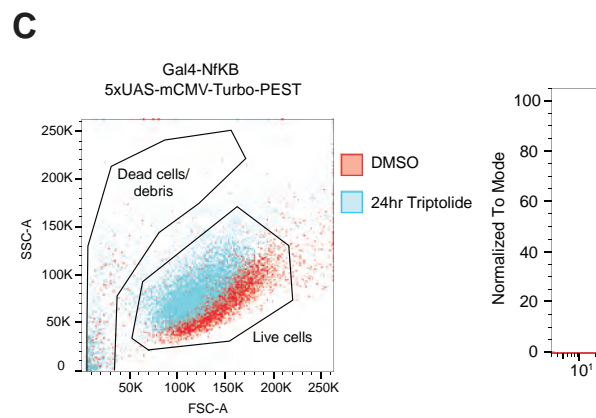
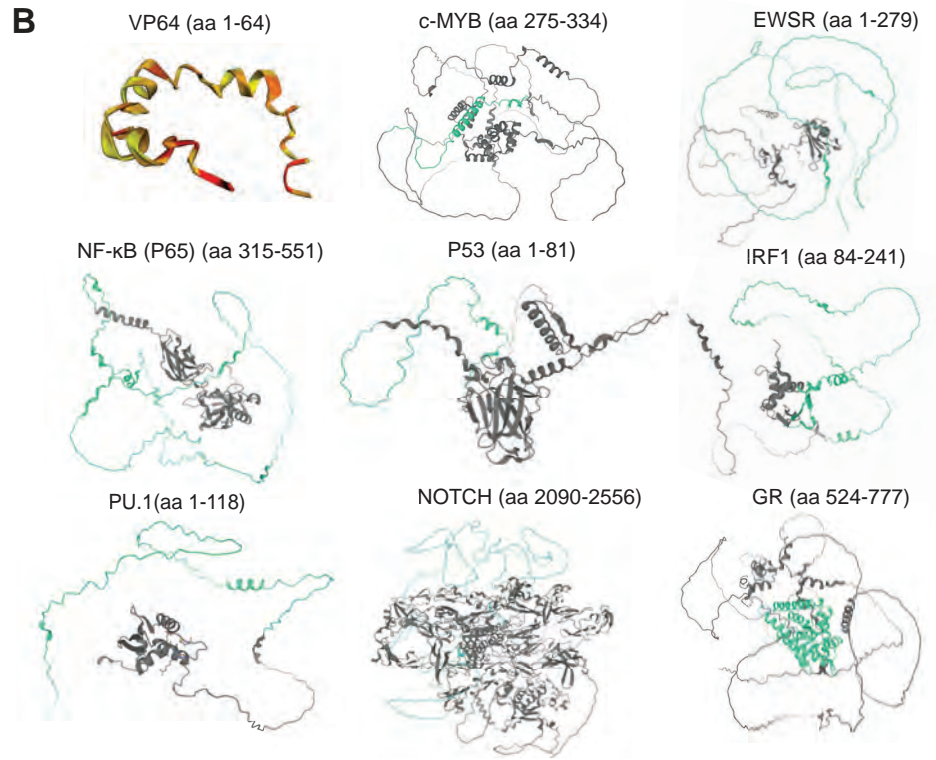
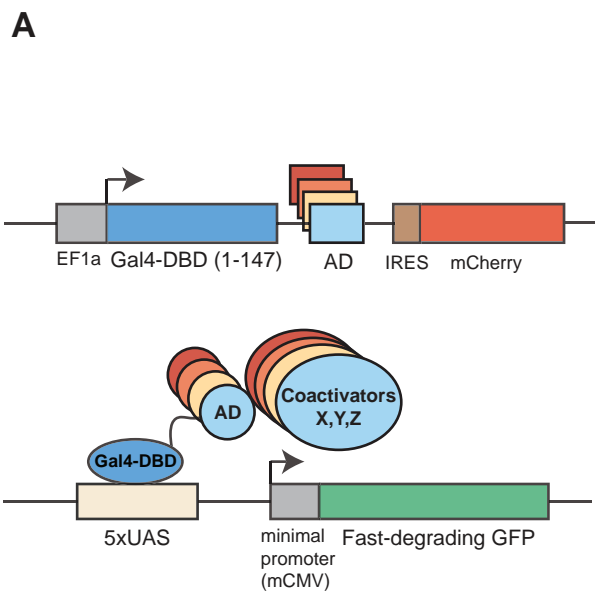
1083 **Code availability**

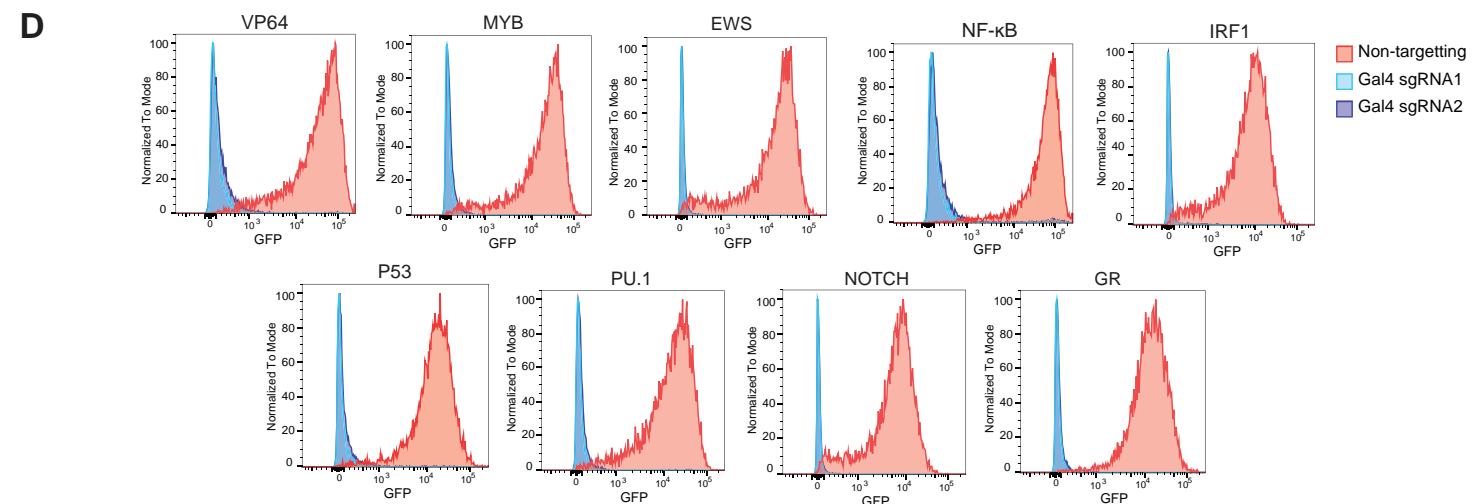
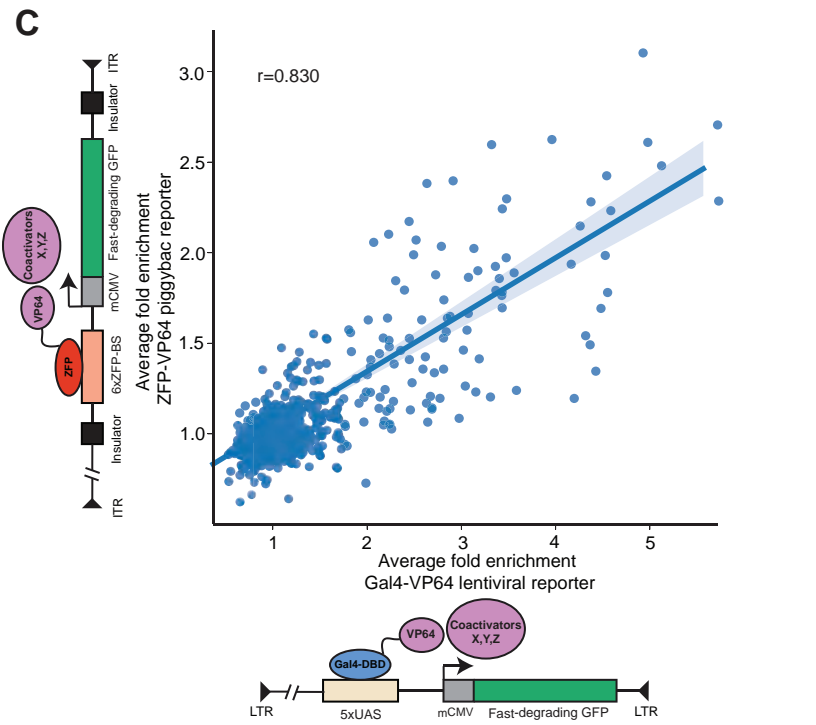
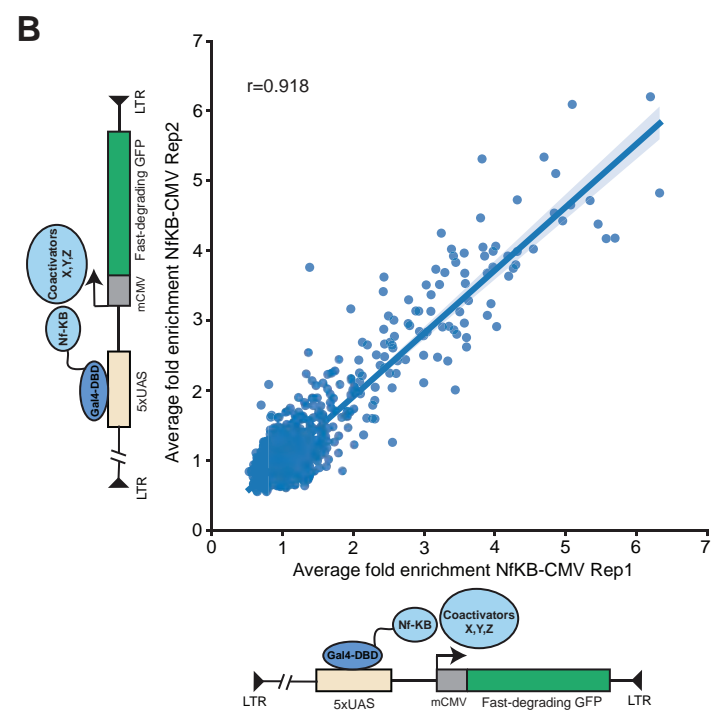
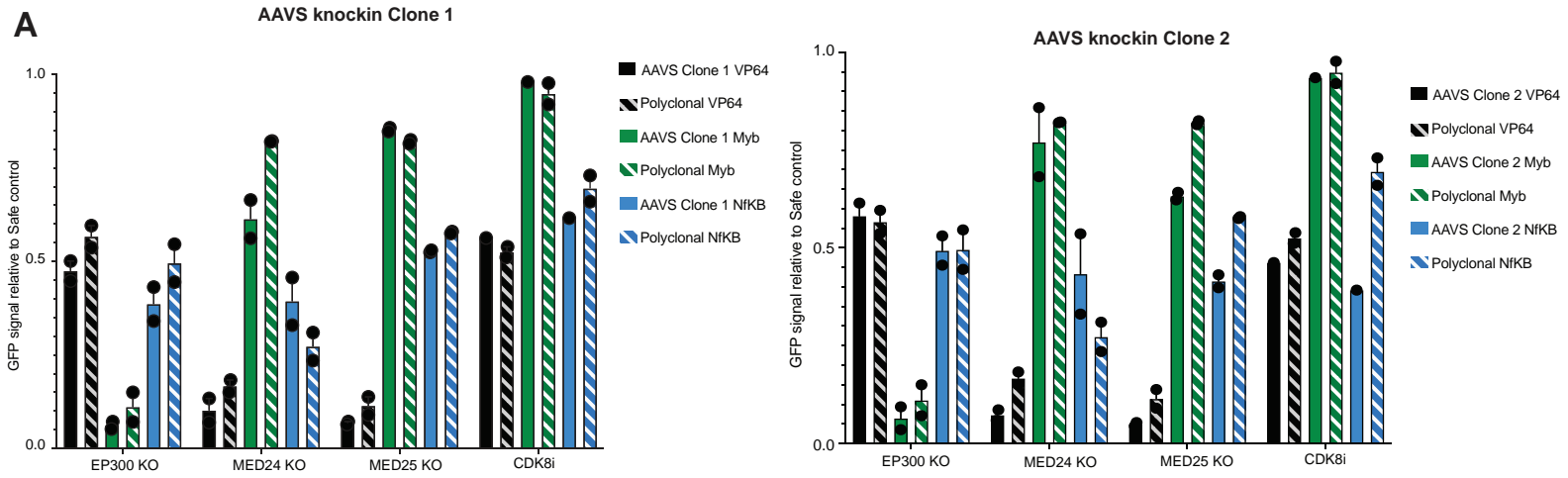
1084 The manuscript does not include any custom code beyond implementation of pre-existing  
1085 publicly available software packages. All computational analysis can be reproduced from the  
1086 descriptions provided in the methods using the listed publicly available software.

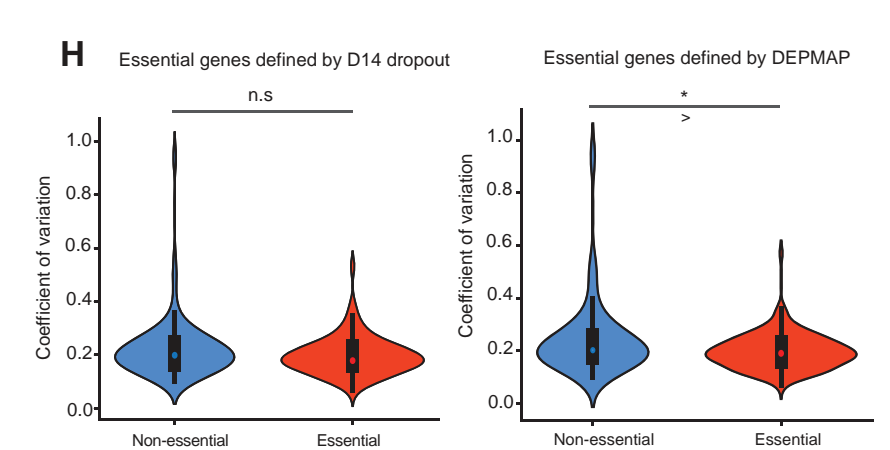
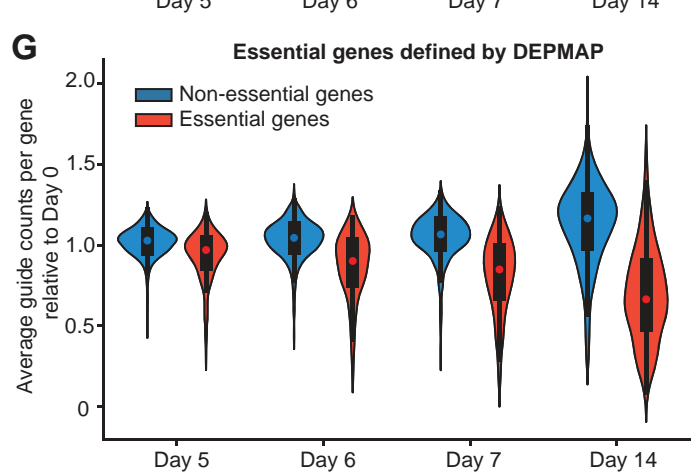
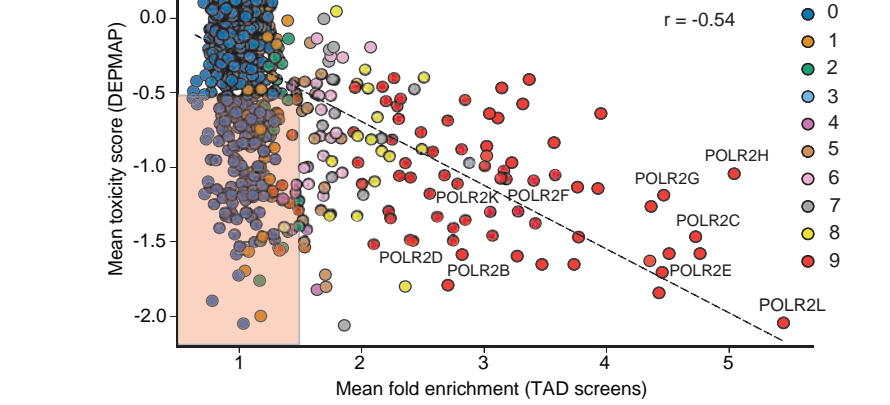
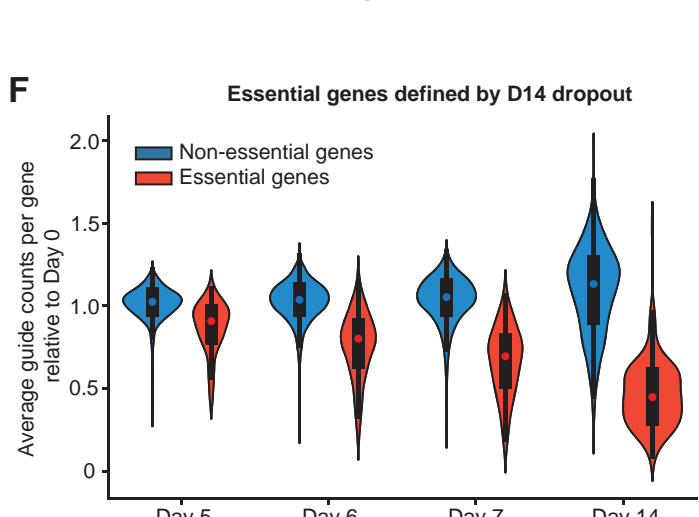
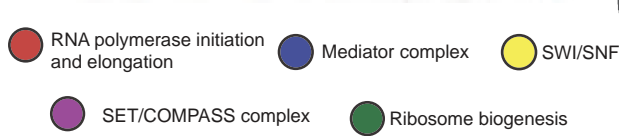
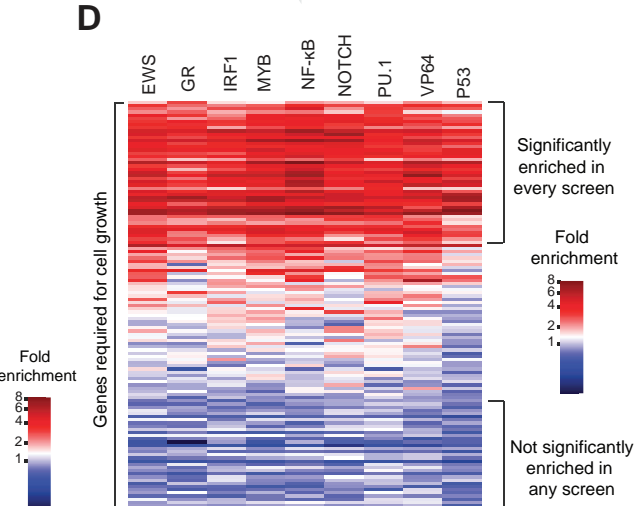
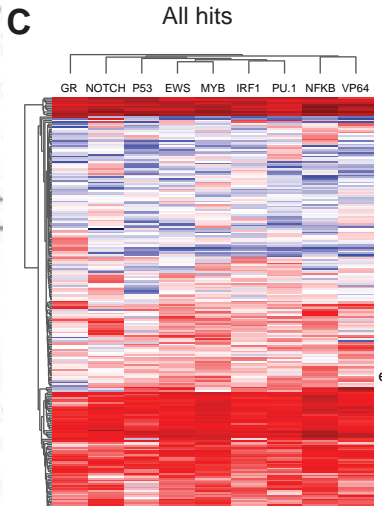
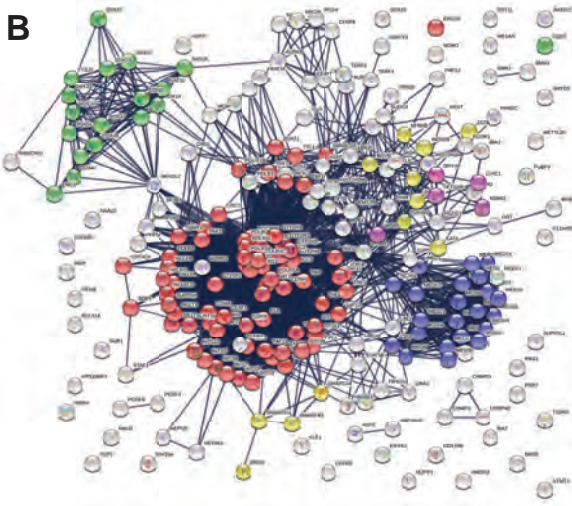
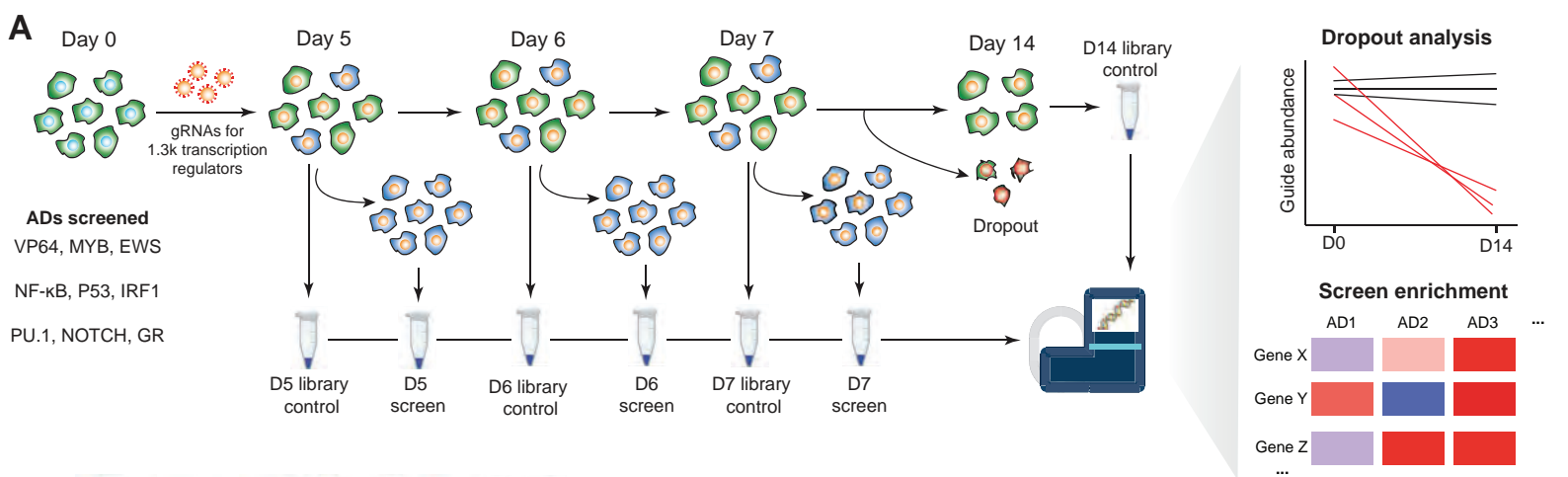
1087 **Methods-only References**

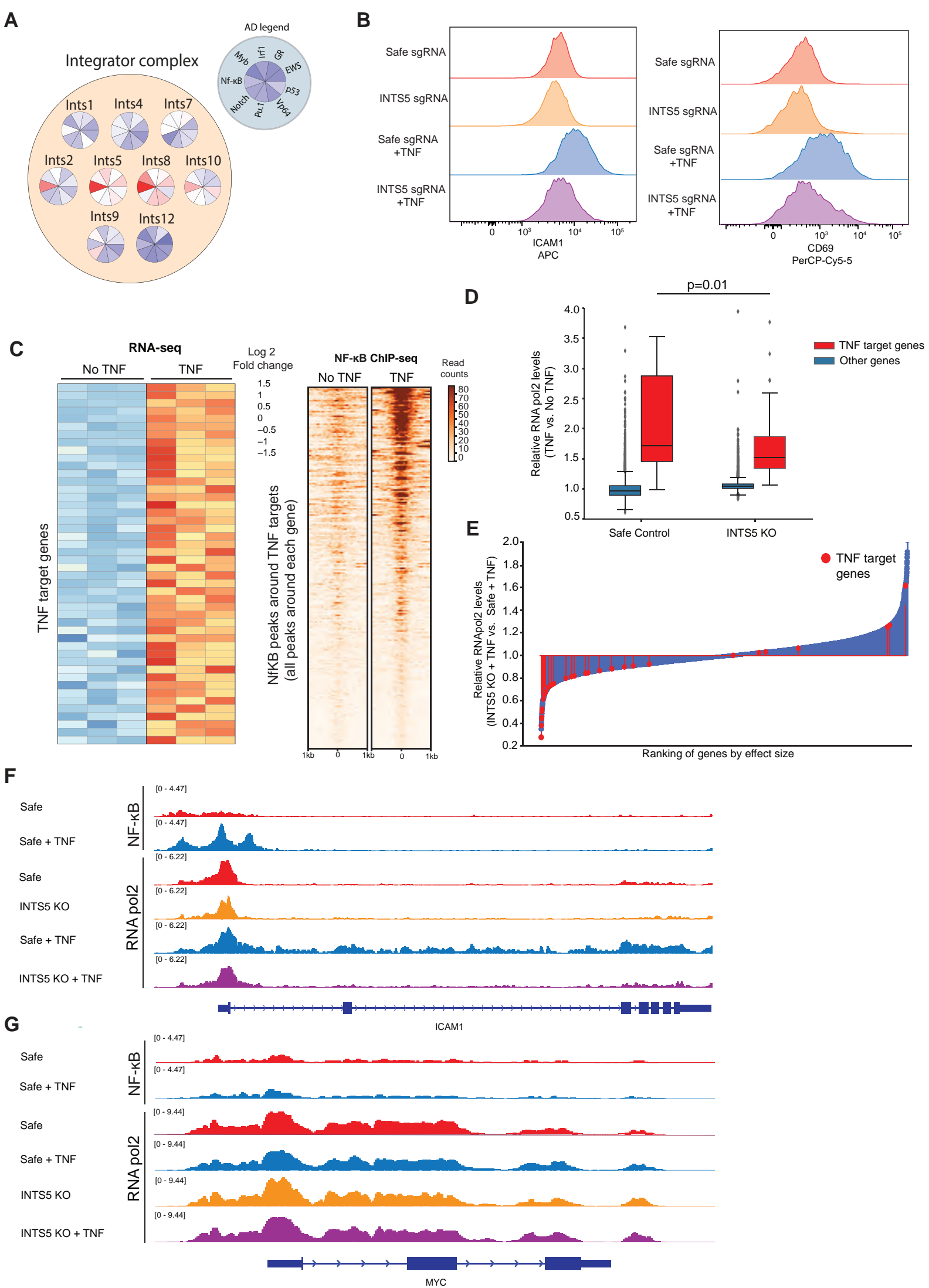
- 1088 68. Burr, M. L. *et al.* An Evolutionarily Conserved Function of Polycomb Silences the  
1089 MHC Class I Antigen Presentation Pathway and Enables Immune Evasion in Cancer. *Cancer*  
1090 *Cell* 1–17 (2019) doi:10.1016/j.ccell.2019.08.008.
- 1091 69. Joung, J. *et al.* Genome-scale CRISPR-Cas9 knockout and transcriptional activation  
1092 screening. *Nat Protoc* **12**, 828–863 (2017).
- 1093 70. Martin, M. Cutadapt removes adapter sequences from high-throughput sequencing  
1094 reads. *EMBnet J* **17**, 10 (2011).
- 1095 71. Langmead, B. & Salzberg, S. L. Fast gapped-read alignment with Bowtie 2. *Nat*  
1096 *Methods* **9**, 357–359 (2012).
- 1097 72. Michlits, G. *et al.* CRISPR-UMI: Single-cell lineage tracing of pooled CRISPR-Cas9  
1098 screens. *Nat Methods* **14**, 1191–1197 (2017).
- 1099 73. Parnas, O. *et al.* A Genome-wide CRISPR Screen in Primary Immune Cells to Dissect  
1100 Regulatory Networks. *Cell* **162**, 675–686 (2015).
- 1101 74. Replogle, J. M. *et al.* Mapping information-rich genotype-phenotype landscapes with  
1102 genome-scale Perturb-seq. *Cell* **185**, 2559-2575.e28 (2022).
- 1103 75. Li, W. *et al.* MAGeCK enables robust identification of essential genes from genome-  
1104 scale CRISPR/Cas9 knockout screens. *Genome Biol* **15**, 554 (2014).
- 1105 76. Zhu, R., del Rio-Salgado, J. M., Garcia-Ojalvo, J. & Elowitz, M. B. Synthetic  
1106 multistability in mammalian cells. *Science (1979)* **375**, (2022).
- 1107 77. Liu, M. *et al.* Genomic discovery of potent chromatin insulators for human gene  
1108 therapy. *Nat Biotechnol* **33**, 198–203 (2015).
- 1109 78. Yusa, K., Zhou, L., Li, M. A., Bradley, A. & Craig, N. L. A hyperactive piggyBac  
1110 transposase for mammalian applications. *Proc Natl Acad Sci U S A* **108**, 1531–1536 (2011).
- 1111 79. Sakuma, T., Nakade, S., Sakane, Y., Suzuki, K. I. T. & Yamamoto, T. MMEJ-  
1112 Assisted gene knock-in using TALENs and CRISPR-Cas9 with the PITCh systems. *Nat*  
1113 *Protoc* **11**, 118–133 (2016).
- 1114 80. Quinlan, A. R. & Hall, I. M. BEDTools: A flexible suite of utilities for comparing  
1115 genomic features. *Bioinformatics* **26**, 841–842 (2010).
- 1116 81. He, Q., Johnston, J. & Zeitlinger, J. ChIP-nexus enables improved detection of in vivo  
1117 transcription factor binding footprints. *Nat Biotechnol* **33**, 395–401 (2015).
- 1118 82. Shao, W., Alcantara, S. G. M. & Zeitlinger, J. Reporter-Chip-nexus reveals strong  
1119 contribution of the drosophila initiator sequence to RNA polymerase pausing. *Elife* **8**, 1–25  
1120 (2019).
- 1121 83. Ye, C. *et al.* DRUG-seq for miniaturized high-throughput transcriptome profiling in  
1122 drug discovery. *Nat Commun* **9**, 1–9 (2018).
- 1123 84. Kaminow, B., Yunusov, D., Dobin, A. & Spring, C. STARsolo : accurate , fast and  
1124 versatile mapping / quantification of single-cell and single-nucleus RNA-seq data. 1–35  
1125 (2021) doi:10.1101/2021.05.05.442755.
- 1126 85. Hao, Y. *et al.* Integrated analysis of multimodal single-cell data. *Cell* **184**, 3573-  
1127 3587.e29 (2021).
- 1128 86. Love, M. I., Huber, W. & Anders, S. Moderated estimation of fold change and  
1129 dispersion for RNA-seq data with DESeq2. *Genome Biol* **15**, 1–21 (2014).
- 1130 87. Herzog, V. A. *et al.* Thiol-linked alkylation of RNA to assess expression dynamics.  
1131 *Nat Methods* **14**, 1198–1204 (2017).
- 1132 88. Neumann, T. *et al.* Quantification of experimentally induced nucleotide conversions  
1133 in high-throughput sequencing datasets. *BMC Bioinformatics* **20**, (2019).
- 1134 89. Robinson, M. D., McCarthy, D. J. & Smyth, G. K. edgeR: A Bioconductor package  
1135 for differential expression analysis of digital gene expression data. *Bioinformatics* **26**, 139–  
1136 140 (2009).

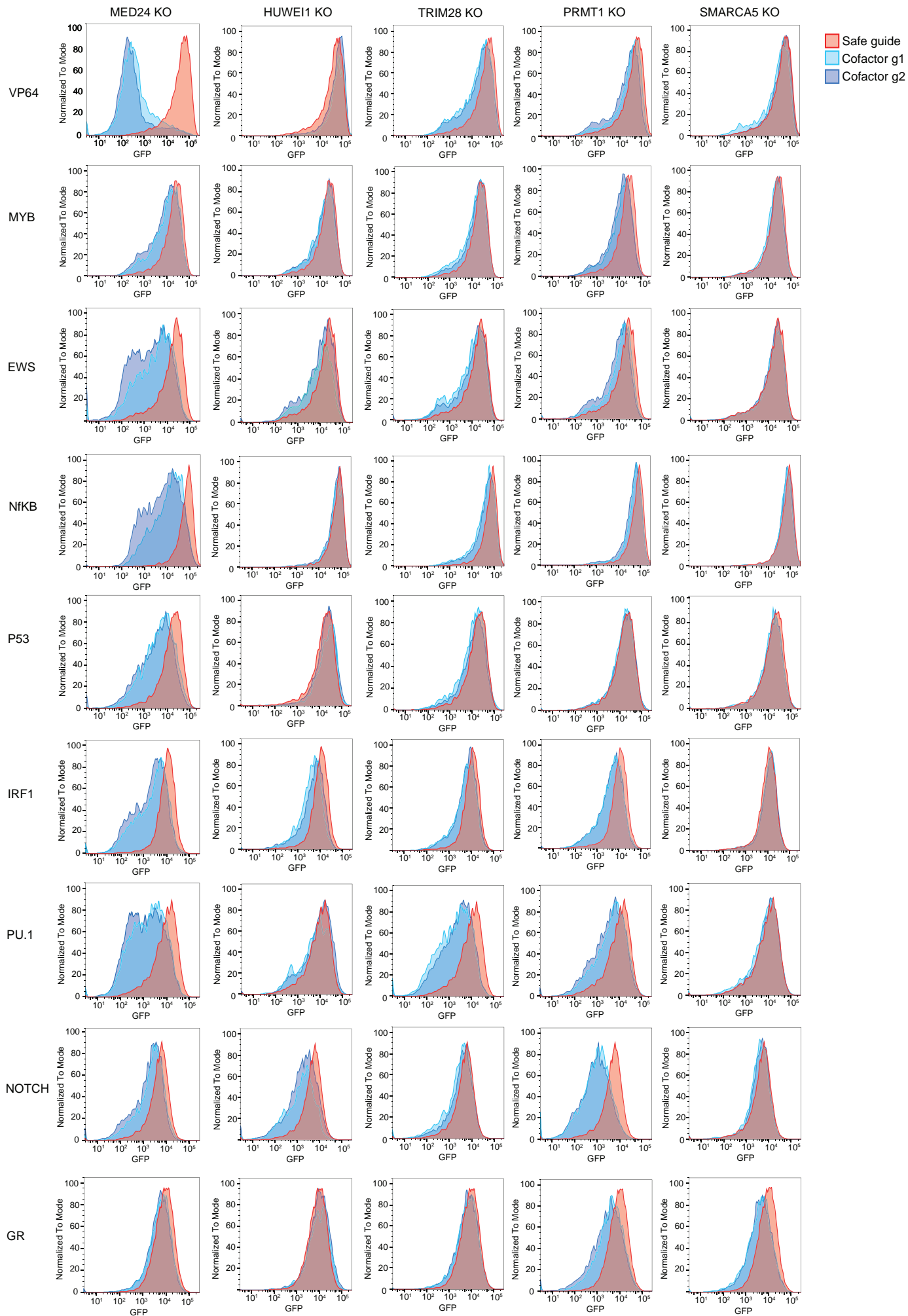
1137 90. Law, C. W., Chen, Y., Shi, W. & Smyth, G. K. *Voom: Precision Weights Unlock*  
1138 *Linear Model Analysis Tools for RNA-Seq Read Counts*. *Genome Biology* vol. 15  
1139 <http://genomebiology.com/2014/15/2/R29> (2014).

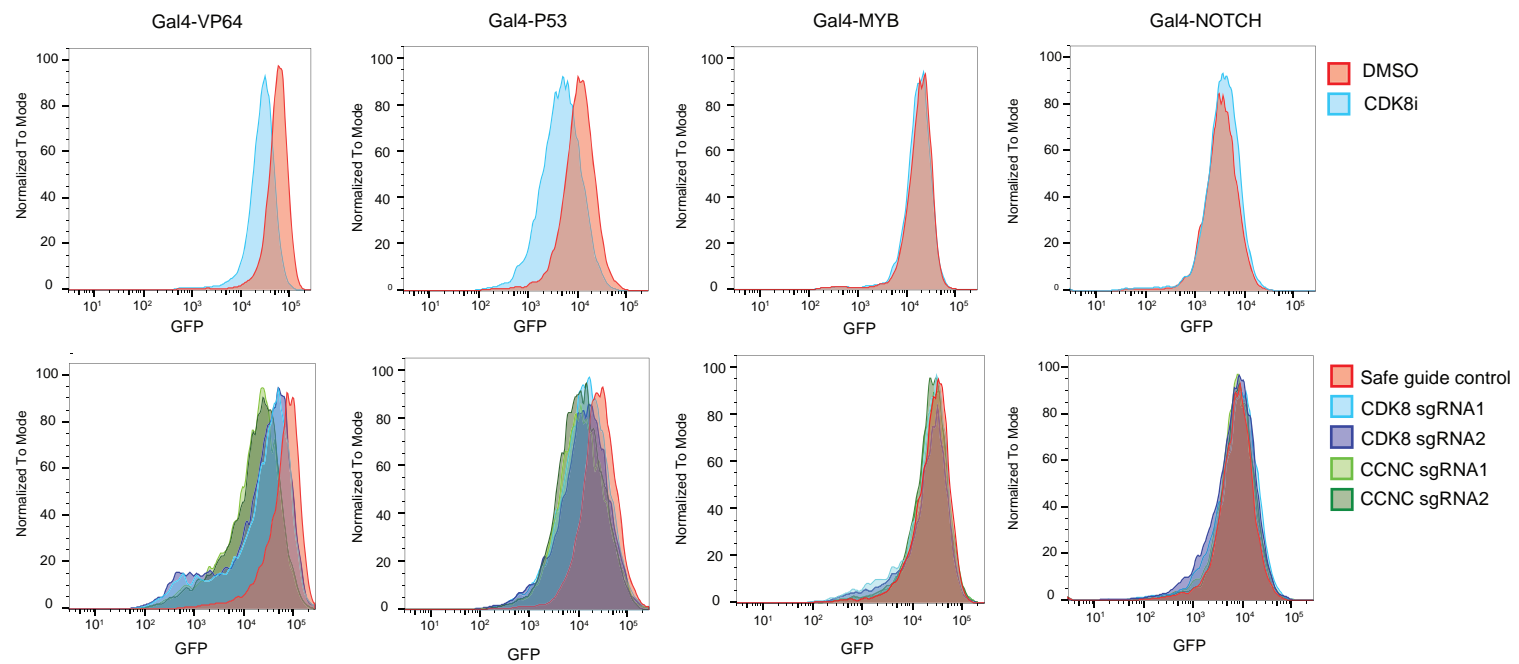
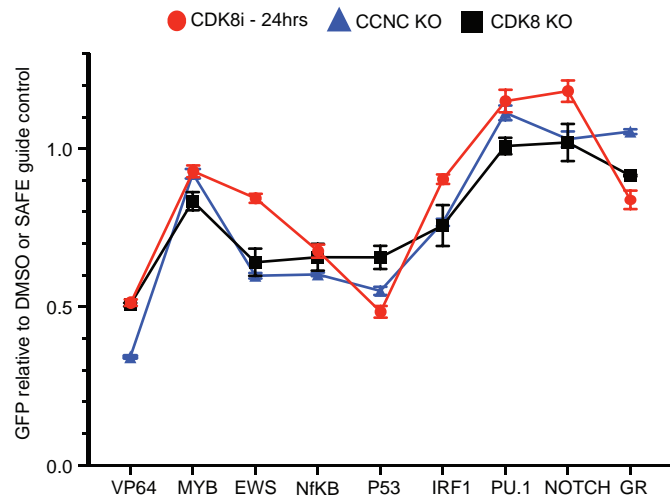
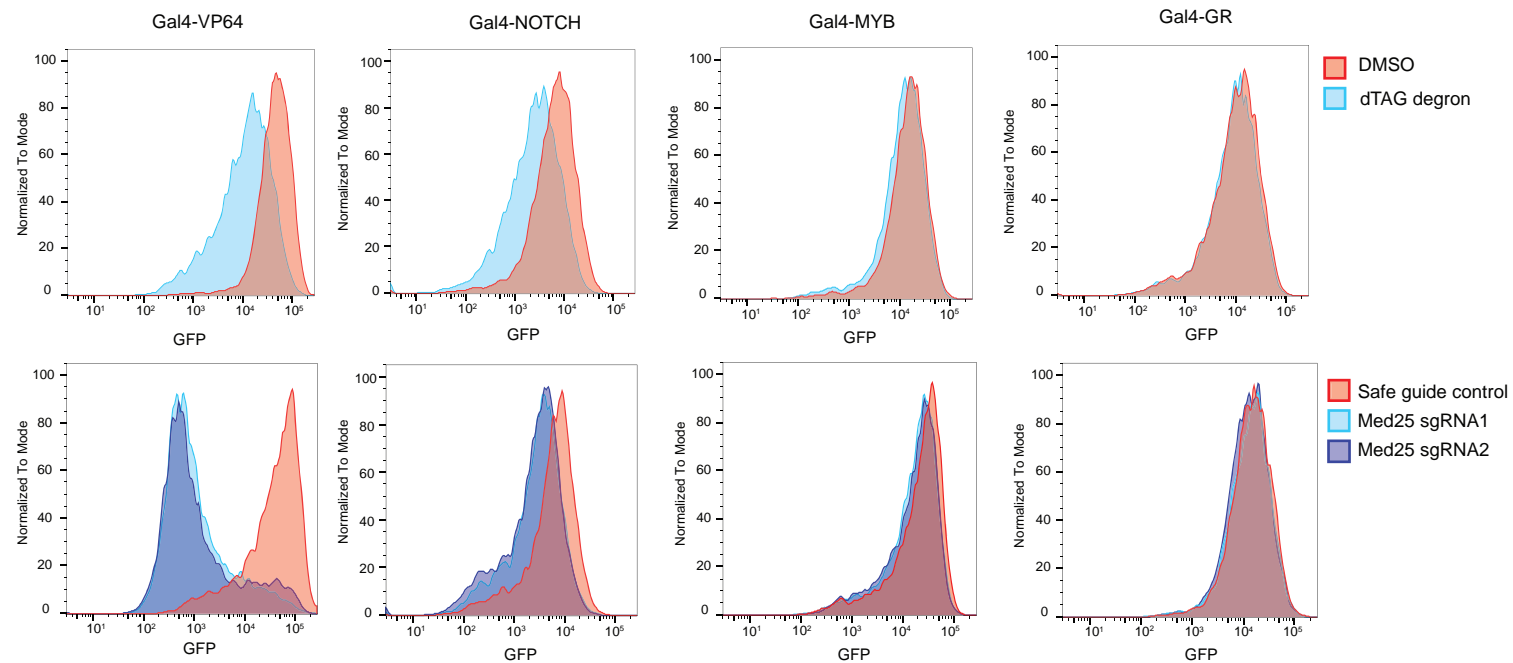
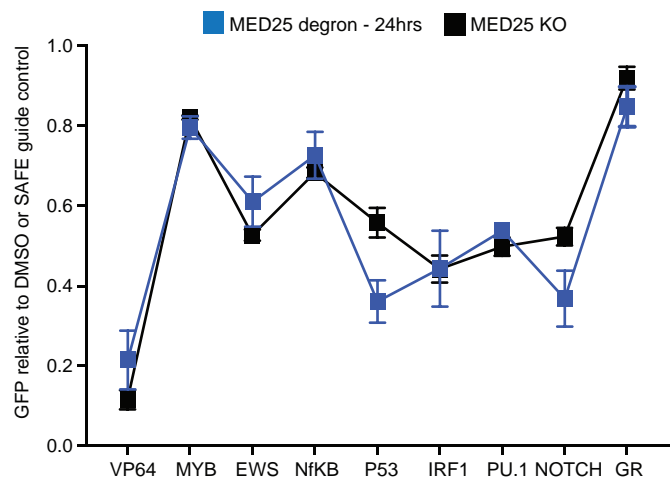


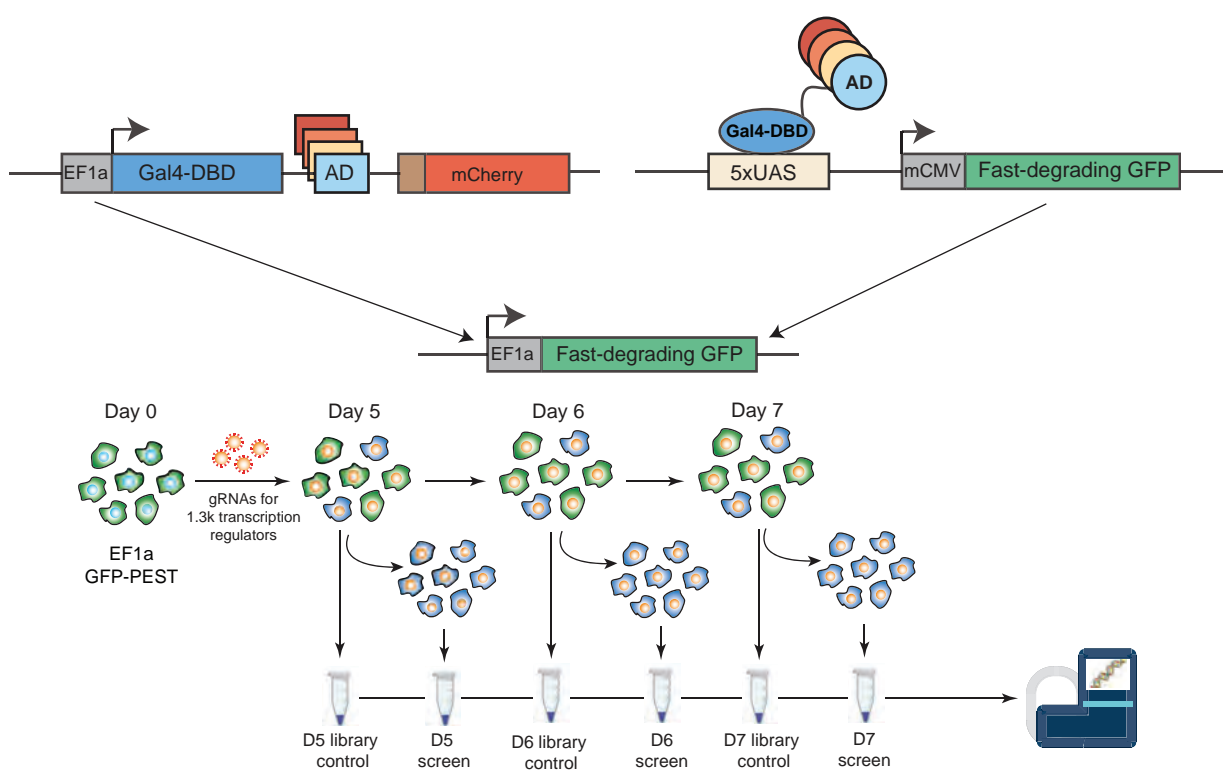




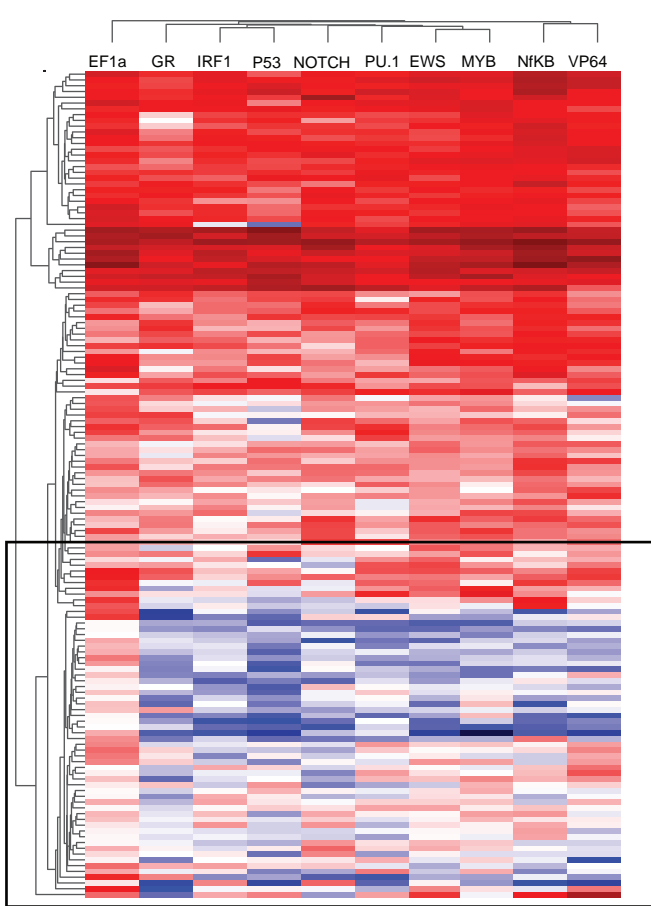




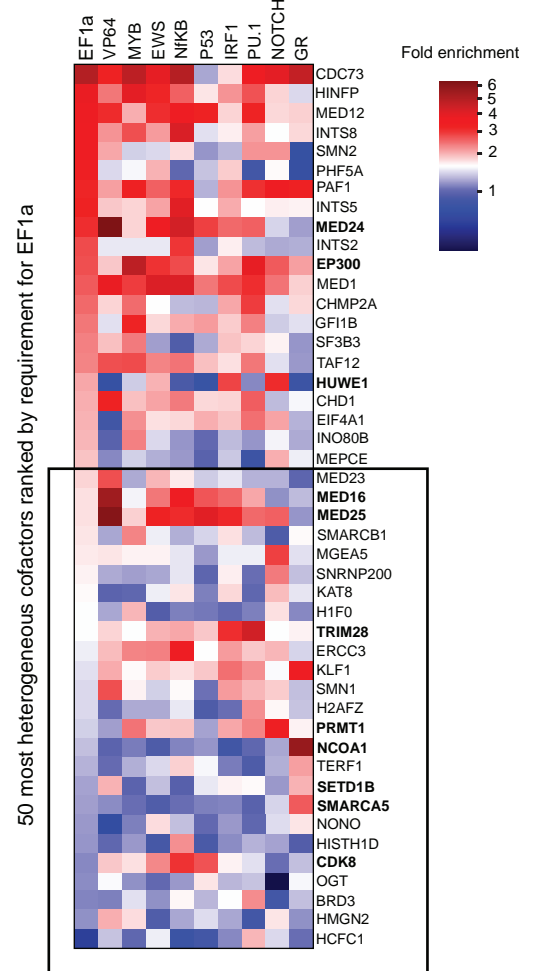
**A****B**

**A****B**

All hits required for EF1a expression

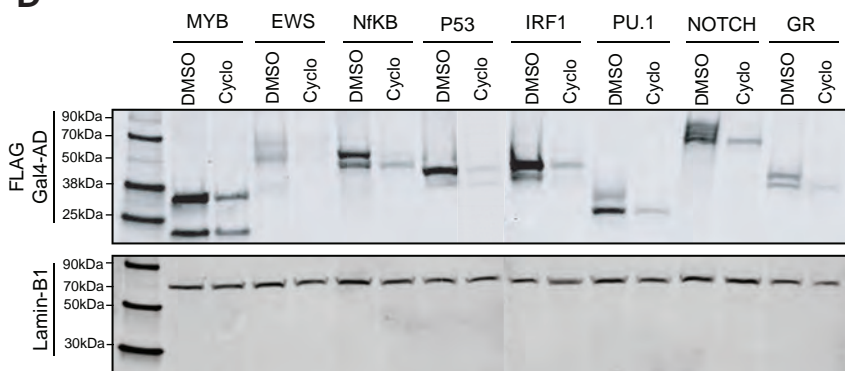
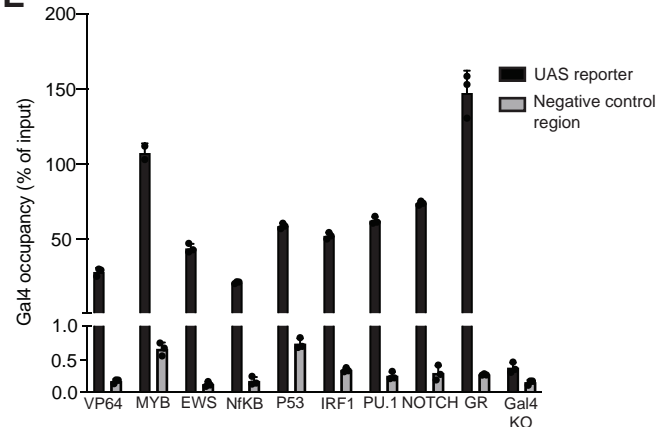


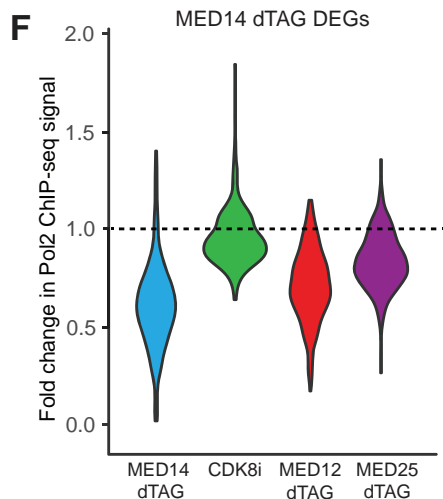
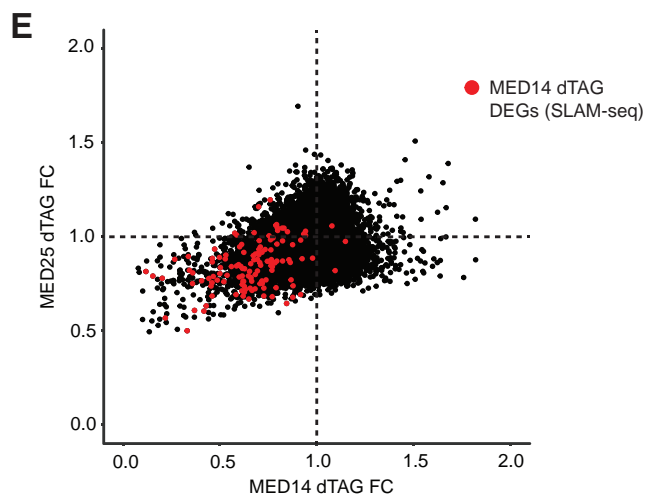
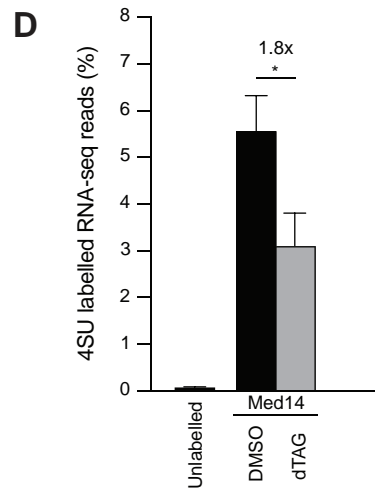
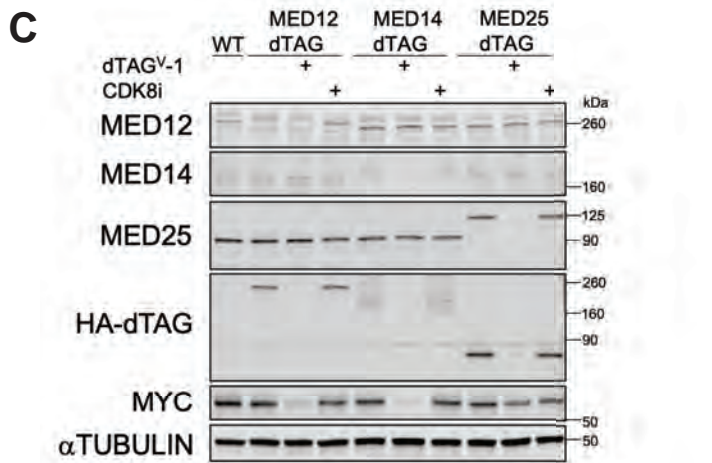
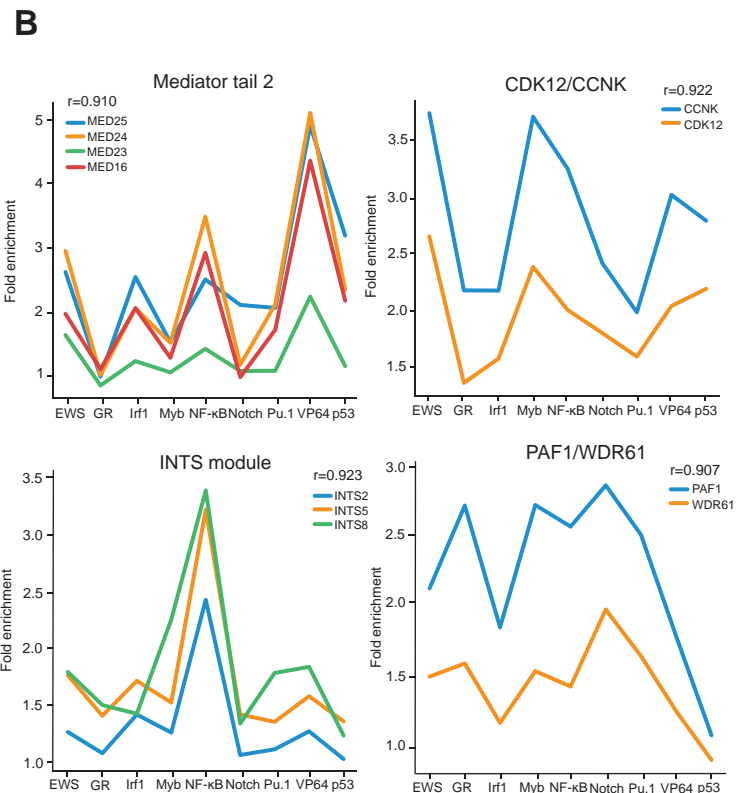
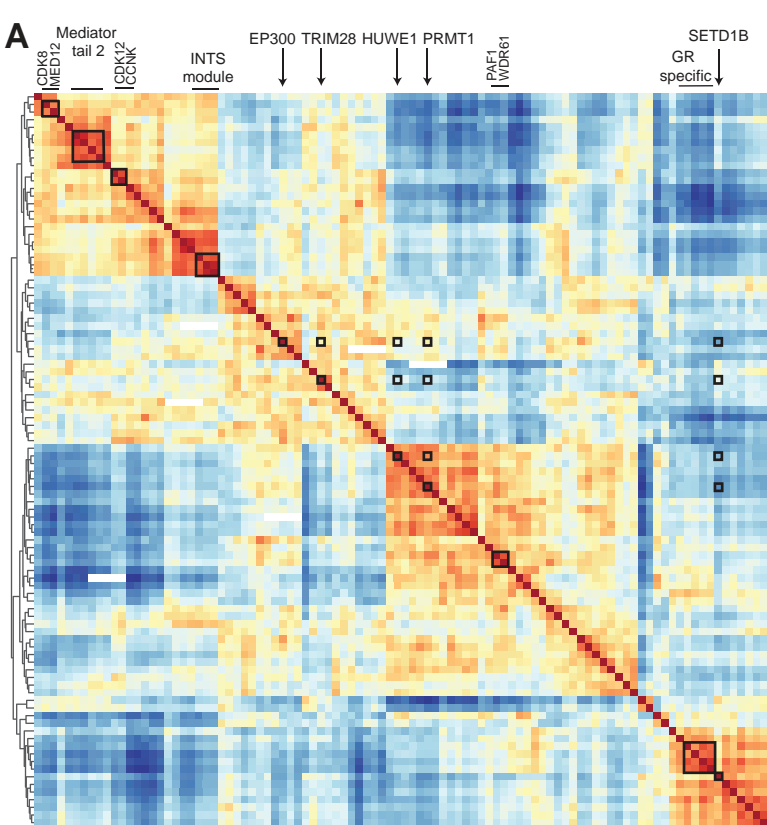
Many EF1a dependent genes are not required for all ADs and no clear simple pattern of certain ADs requiring the same factors as EF1a

**C**

A number of the top heterogeneously required cofactors are **not** required by EF1a.

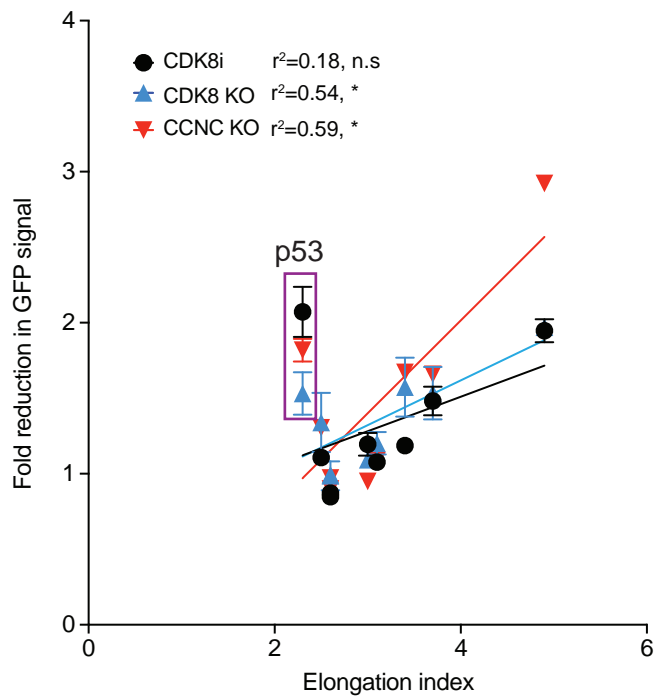
Those that are, do **not** display a simple pattern that would indicate their heterogeneity is caused by indirect effects

**D****E**

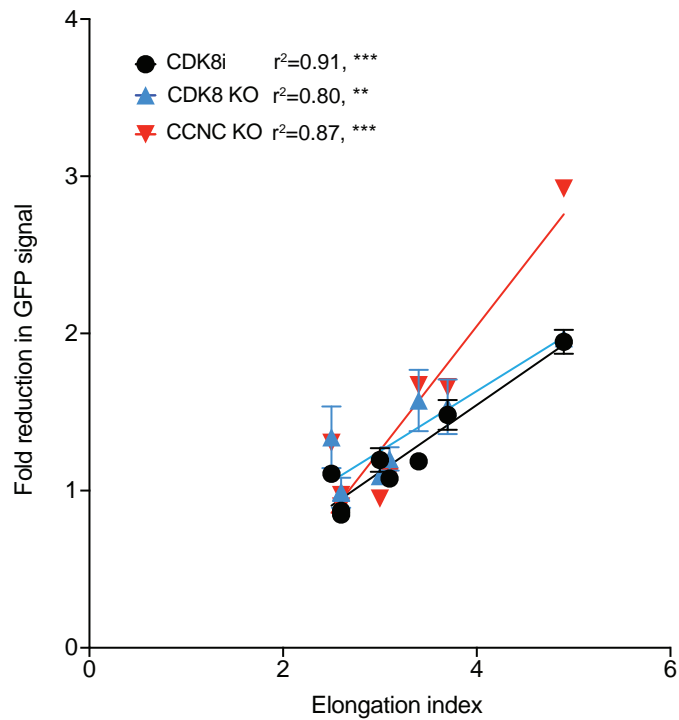


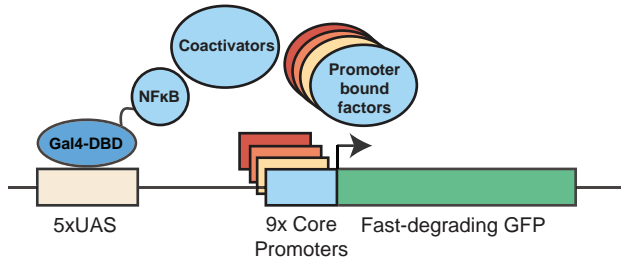
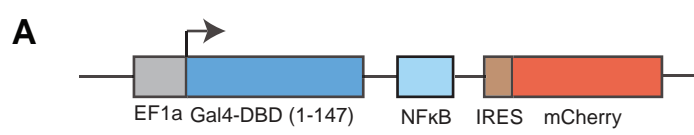
**A**

Including p53

**B**

Excluding p53





**B**

**TATA box promoters**

mCMV TAGGCGTGTACGGTGGGAGGCCTATATAAGCAGAGCTCGTTTAGTGAACCGTCAGATCGCCTGGAGACGCCATCCACGCTGTTTTGACCTCCATAGAAGACACCGGGACCGATCCAGC

SCP TAGGTCTATATAAGCAGAGCTCGTTTAGTGAACCGTCAGATCGCCTGGAGACGTCGAGCCGAGTGGTTGTGCCTCCATAGAA

YB-TATA TCTAGAGGGTATATAATGGGGCCA

MLP TGGGGCTATAAAAGGGGGTGGGGCGCGTTTCCTCACTCTTCCGCATCGCTGTCTGCGAGGGCCAGCTGTTGGGGTGA

HSP1A1 TGAAAAGGCGGGTCTCCGTGACGACTTATAAAGCCCGAGGGCAAGCGGTCCGGATAACGGCTAGCCTGAGGAGCTGCTGC

TSS

**TATA-like / weak TATA promoters**

HSV-TK CGCATATTAAGGTGACGCGTGTGGCCTCGAACACCGAGCGACCCTGCAGCGACCCGCTTAA

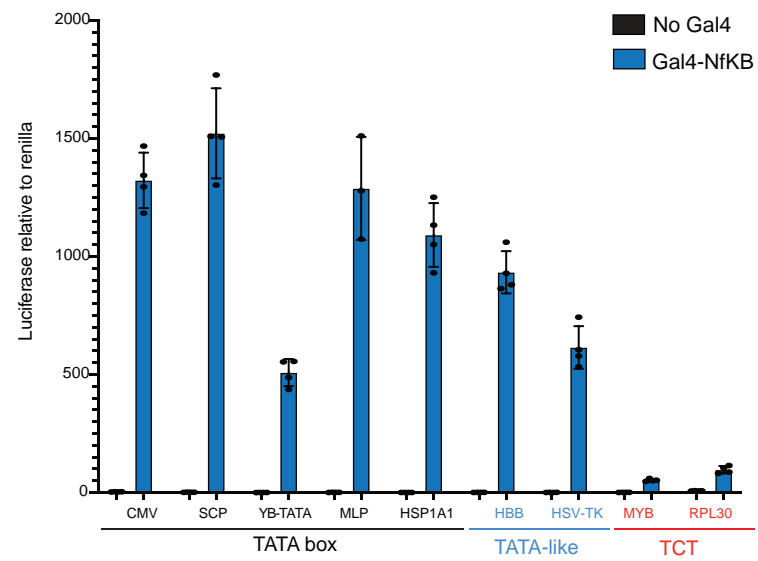
HBB TCCCGGGCTGGGCATAAAAGTCAGGGCAGAGCCATCTATTGCTTACATTGCTTCT

**TCT promoters**

MYB ATCAACCTGTTTCCCTCCTCCTTCTCCTCCTCCTCGTGACCTCCTCCTCCTTCTTCTCCTGAGAAACTTCGCCCCAGCGGTGCGGAGCGCCGCTGCGCAGCCGGGGAG

RPL30 CCGTCCCGCAGTCCGGCTCTGCCGTGAAGAGCTTTCATTGTGGGAGTCTTTCTTCTCCTGTTCCCGGCCATCTTAG

**C**

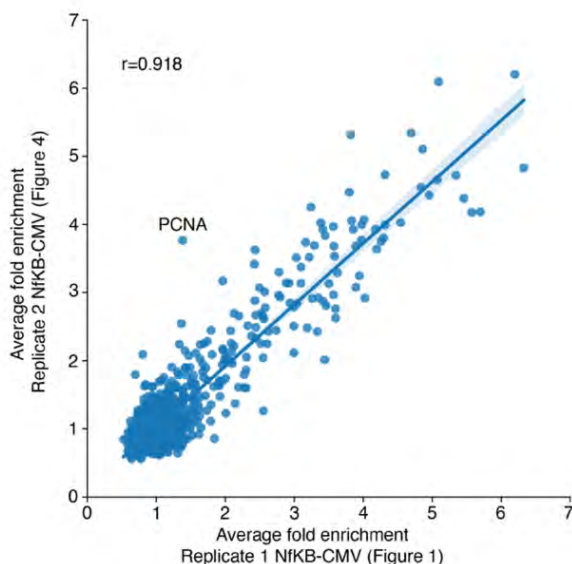


## Supplementary Note 1 – designing and analysing comparative CRISPR screens

Our manuscript pioneers the use of comparative CRISPR screens. Most prior studies that have used CRISPR screens have been designed with the intention of identifying individual hits that regulate a specific phenotype of interest<sup>1</sup>. These hits are then validated and studied in further detail. For that purpose, it is not necessary to obtain a highly quantitative measure of the degree of enrichment of individual genes, as the hits do not need to be compared across different screening conditions. Here, our goal was to *compare across* screens to obtain more general insights into the specificity of transactivation domains and core promoters. We hoped to use the screens not only to identify important cofactors, but to provide insights into their degree of requirement across different conditions. This requires a relatively reproducible and precise measure of guide enrichment.

Since most CRISPR screens are not designed to obtain quantitative information, the analysis tools currently available are not designed to handle multiple timepoints, or to compare enrichment values across screens. As a result, it was necessary for us to develop bespoke screen design and analysis methods that would provide the most accurate quantitative information. In this Supplementary Note, we discuss the rationale and provide justification for the screen design and analyses steps we performed. We also demonstrate how the inclusion of certain filters in the analyses improve the reproducibility of the data.

Throughout, we benchmark our analysis approach by using two independent biological replicates performed on GAL4-NfKB activating the minimal CMV promoter. Upon processing the data according to our pipeline, the two replicates have a very high degree of correlation ( $r=0.918$ , Pearson), demonstrating that our design and analysis pipeline produces highly reproducible data.



**Supplementary Note Fig. 1)** Correlation between the fold enrichment scores in the two replicates of the GAL4-NfKB mCMV screens.  $r$  = Pearson correlation. PCNA is outlined as the only major outlier. Error bands reflect 95% confidence interval of Pearson correlation.

### Demonstrating the importance of filtering outliers for accurate quantification of the screen data

In the analysis of CRISPR screen data, fold enrichment values are calculated for each guide in the library by dividing the number of counts in the screen sample by the number of counts in

the matched library control. Our library contains 6 different guides targeting each gene and we isolated samples at 3 timepoints (D5, D6 and D7 after guide library infection). This resulted in a total of 18 guide enrichment values for each gene in each screen. These 18 enrichment values were averaged, resulting in a single fold enrichment value per gene per screen.

Upon initial inspection of the raw data, we noticed single sgRNAs targeting a gene with fold enrichment values of up to 500-fold, when other independent sgRNAs against the same gene were not enriched. These are examples of outliers potentially caused by random sampling variation, or due to random overamplification in the PCR step, which is an issue that has been previously reported in CRISPR screens<sup>2</sup>. Inclusion of these guides in the analysis would obscure the calculation of an accurate fold enrichment value. Consequently, we realised that some filtering of the guides would be necessary to remove outliers.

The following filtering steps were applied during the processing of the data:

- 1) Removal of guides with low guide counts in the plasmid pool (lowest 2.5% of guides)
- 2) Removal of guides that have a fold enrichment value below 0.1 or above 10-fold
- 3) Removal of guides that have a fold enrichment value that  $> 4$ -fold from the mean fold enrichment value (mean of 18 values – i.e., all 6 sgRNA's for a particular gene assessed at D5, D6, D7)

We demonstrate how each of these steps helped to improve the quality of the data below.

#### ***Removal of lowly represented guides:***

To reduce the prevalence of outlier guides, we initially removed guides with low counts, which is a common processing step in CRISPR screens<sup>3</sup>. Low representation can cause sampling error in the dataset resulting in erratic fold change values. Prior studies remove the bottom 5% of guides<sup>3</sup>, however due to our low skew ratio (4.38) and our desire to retain as many guides as possible, we decided to only remove the bottom 2.5% of guides.

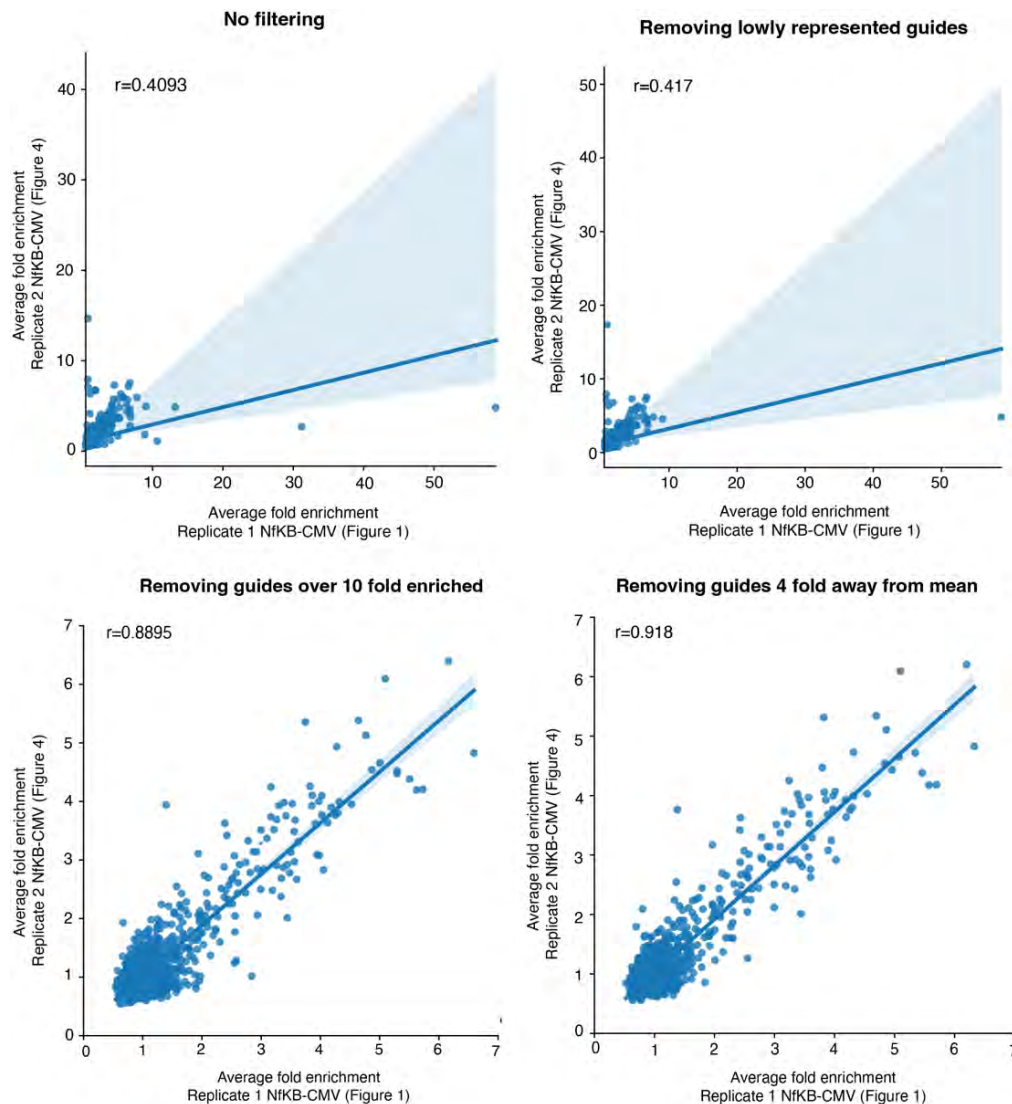
#### ***Filtering guides with fold enrichment below 0.1 or above 10:***

Even upon removal of these lowly represented guides, we still observed guides with unrealistic, high fold enrichment values that were not correlated between biological replicates (Supplementary Note Fig. 2, top right). These guides interfere with an accurate calculation of fold enrichment values. Therefore, we reasoned that further filtering was necessary. In order to set appropriate thresholds for filtering outlier guides from the screen data, we leveraged our two biological replicates of the GAL4-NfKB mCMV screen. We noted that none of the sgRNAs with fold enrichment values above 10 were correlated between the two replicates suggesting that a score above 10 is very unlikely to reflect a real enrichment score (Supplementary Note Fig. 2, top right). Therefore, we filtered any guides with a fold enrichment value above 10. We also reasoned that a depletion of 10-fold was just as likely to be due to sampling error as an enrichment above 10, so as not to bias the data in a specific direction, we also removed guides with a fold enrichment below 0.1. This filter dramatically improved the reproducibility between the replicates (Supplementary Note Fig. 2, bottom left).

#### ***Filtering guides with fold enrichment value $> 4$ -fold from the mean:***

The final filter we applied, removed guides that were four-fold away from the mean fold change calculated from the 18 individual enrichment values (i.e., all 6 sgRNAs for a particular gene assessed at D5, D6, D7). This filter was applied because we noted that some target genes were being classified as significant due to a single outlier guide (enrichment value  $< 10$  and  $> 0.1$ ) that caused the fold enrichment for that gene to increase beyond the significance cut-off.

Introduction of this filter clearly reduces the dispersion of the data (observable by the reduced spread of the values around a fold change of 1). This filter also increased the Pearson correlation between replicates from  $r=0.890$  to  $r=0.918$  (Supplementary Note Fig. 2, bottom right).



**Supplementary Note Fig. 2)** Correlation plot of fold enrichment scores of all genes in the library across two replicates of GAL4-NfKB mCMV screen with different guide filtering applied. (Top Left) No filter applied. (Top Right) Removing bottom 2.5% represented guides in the plasmid pool. (Bottom left) removing guides with a fold enrichment over 10-fold. (Bottom right) removing guides with a fold enrichment more than 4-fold away from the mean value of all 18 guides.  $r$ =Pearson correlation. Error bands reflect 95% confidence interval of Pearson correlation.

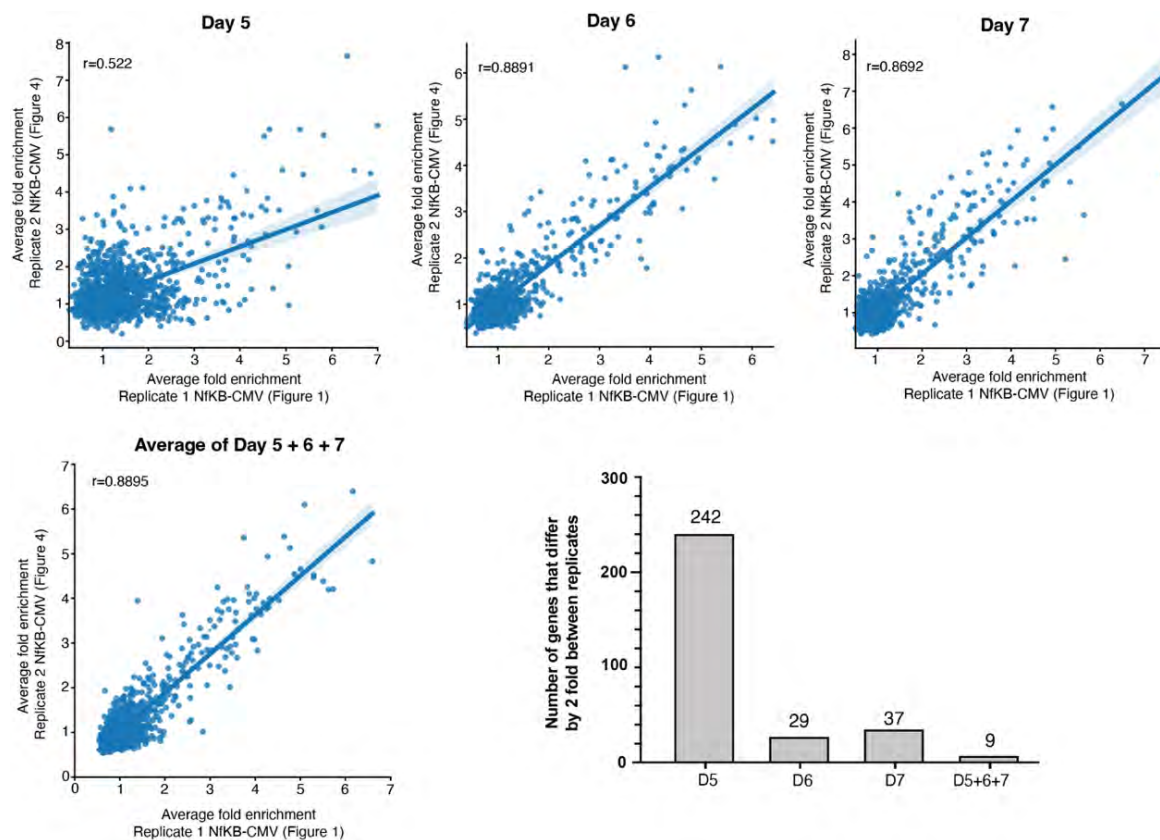
The three filters we applied to the raw guide values were the only methods of post-processing performed on the raw data prior to the calculation of a fold enrichment value. By using the biological replicates of the same screen, we can see that each of these filtering steps increased the reproducibility and were necessary to obtain an accurate fold enrichment value.

### Demonstrating the importance of using multiple timepoints

Based on our prior experience with CRISPR screens<sup>4-9</sup>, we reasoned that it would be necessary to include multiple timepoints as part of our screen design to reduce the potential effects of sampling error, by increasing the number of sampling events per guide. Since our screens were

performed at a relatively early timepoint, we also reasoned that using multiple timepoints would help to minimise overlooking guides that work with different kinetics. Once again, we can compare the results from the two independent biological replicates, to assess how aggregating across the three timepoints (D5, D6 and D7 post guide infection) helped to improve the reproducibility of the results.

To assess how aggregating the timepoints impacts the data, we can compare the correlation between individual timepoints from our two biological replicates, with the correlation when all three timepoints are aggregated. We found that the day 5 timepoint has greater variability between the two biological replicates, than the day 6 and day 7 timepoint (Supplementary Note Fig. 3), which suggests that while day 5 provides a window into the earliest changes that occur after gene knockout, these early changes are more prone to variability likely due to kinetic differences in sgRNA integration, expression and editing efficiency. At day 6 and day 7, the enrichments are far more consistent across the two biological replicates (Supplementary Note Fig. 3). However, aggregating the data across all three timepoints produces the highest correlation between the two biological replicates (Supplementary Note Fig. 3).



**Supplementary Note Fig. 3)** Correlation between two NfκB CMV biological replicates at each of the screen timepoints, as well as the data aggregated across the 3 timepoints. Each dot represents the fold enrichment of the 6 guides that target each gene, other than the aggregated plot, which represents the average of all 18 datapoints. R = Pearson correlation. (Bottom left) Bar plot shows the number of genes that differ in fold enrichment values by at least 2-fold between the two biological replicates at each timepoint and in the aggregated data. Error bands reflect 95% confidence interval of Pearson correlation.

To further reinforce the value of aggregating the three timepoints, we calculated how many genes display at least a 2-fold difference in enrichment values between the two biological

replicates. This analysis demonstrates that aggregating the data dramatically reduces the number of genes with a greater than 2-fold difference between replicates (Supplementary Note Fig. 3, Bottom Right). Only 9 genes display a difference of at least 2-fold between the two biological replicates when the data is aggregated. This reflects a greater than 3-fold improvement over the most reproducible individual timepoint (day 6). Overall, by aggregating across three timepoints, we can both capture the earliest consequences of gene knockout, while improving the reproducibility of the screens.

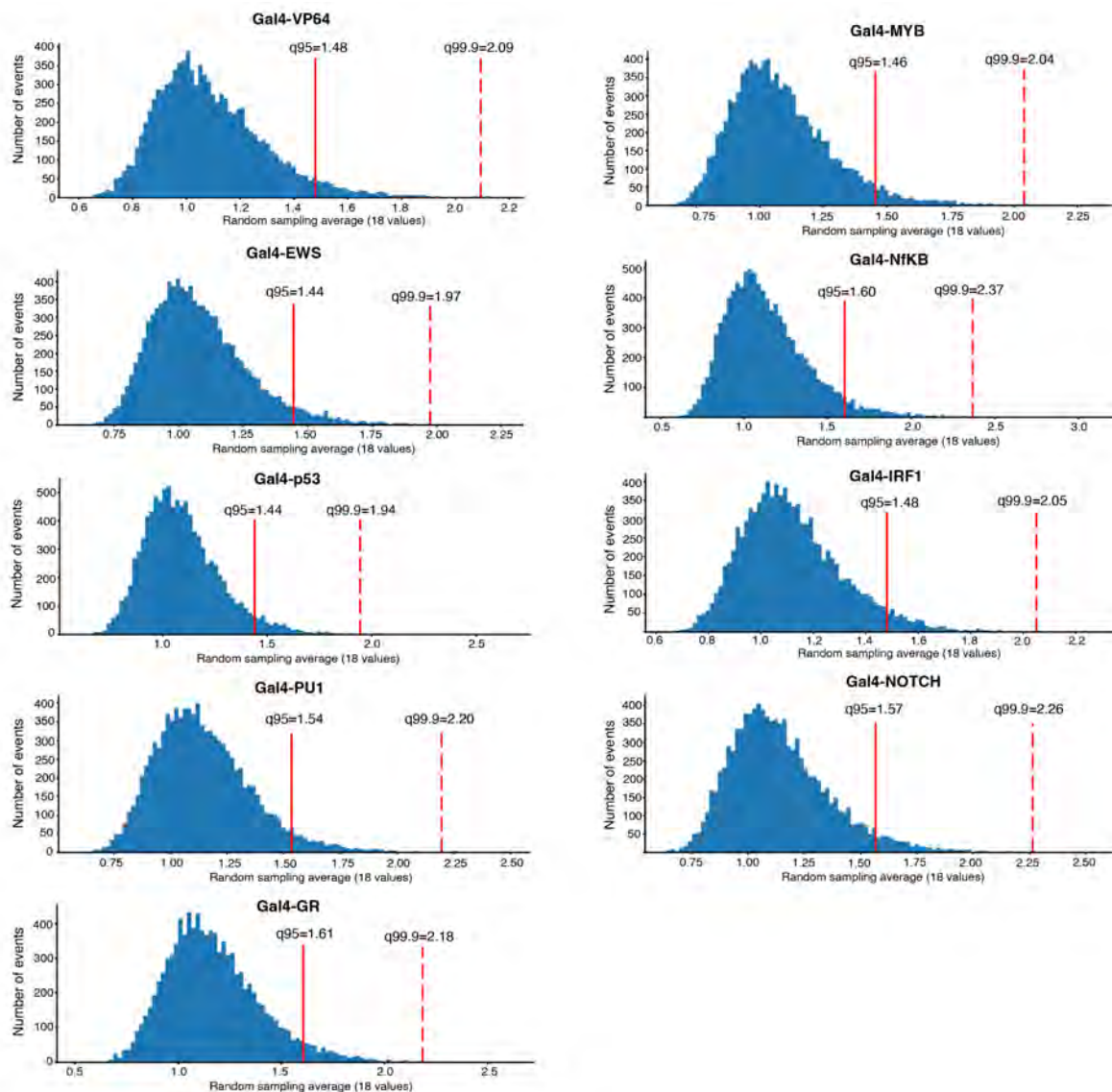
### **Permutation test approach to calculate an empirical p-value for each gene**

The majority of the data presented throughout the manuscript uses the fold enrichment score to represent the requirement for a particular cofactor. For the most part, we avoided categorizing the data unnecessarily, as cofactor requirement appears to exist on a spectrum and is therefore not a categorical variable. However, for some of the analyses, it was helpful to define which genes were statistically significantly enriched in each screen. It is important to point out that classification as a hit based on statistical significance does not have any impact on the calculation of the fold enrichment score.

In order to calculate which genes should be considered significantly enriched in each screen, we used permutation testing to calculate empirical p-values. Permutation testing works by randomly sampling from the data to obtain an empirical distribution of the values. We obtained this distribution by randomly sampling 18-fold enrichment values (6 from each timepoint) from the 7240 guides in the library. Sampling was performed 10000 times on the data that had been pre-filtered to remove outliers (using the above methods). An independent permutation test was performed for each screen to ensure that we were accounting for screen specific differences in the distribution of values. The cut-off to categorize a gene as statistically significant was a fold enrichment score above the 95<sup>th</sup> percentile of this random sampling distribution, which equates to an empirical p value < 0.05. The 95<sup>th</sup> percentile of the random distribution was similar across all of the AD screens suggesting that the distribution of guide values was very similar across all of the screens.

The values that correspond to the 95<sup>th</sup> percentile of this random sampling distribution are provided in a table below:

<b>AD screen</b>	<b>Enrichment score for p&lt;0.05</b>
GAL4-VP64	1.48
GAL4-MYB	1.46
GAL4-EWS	1.44
GAL4-NfKB	1.60
GAL4-P53	1.44
GAL4-IRF1	1.48
GAL4-PU1	1.54
GAL4-Notch	1.57
GAL4-GR	1.61



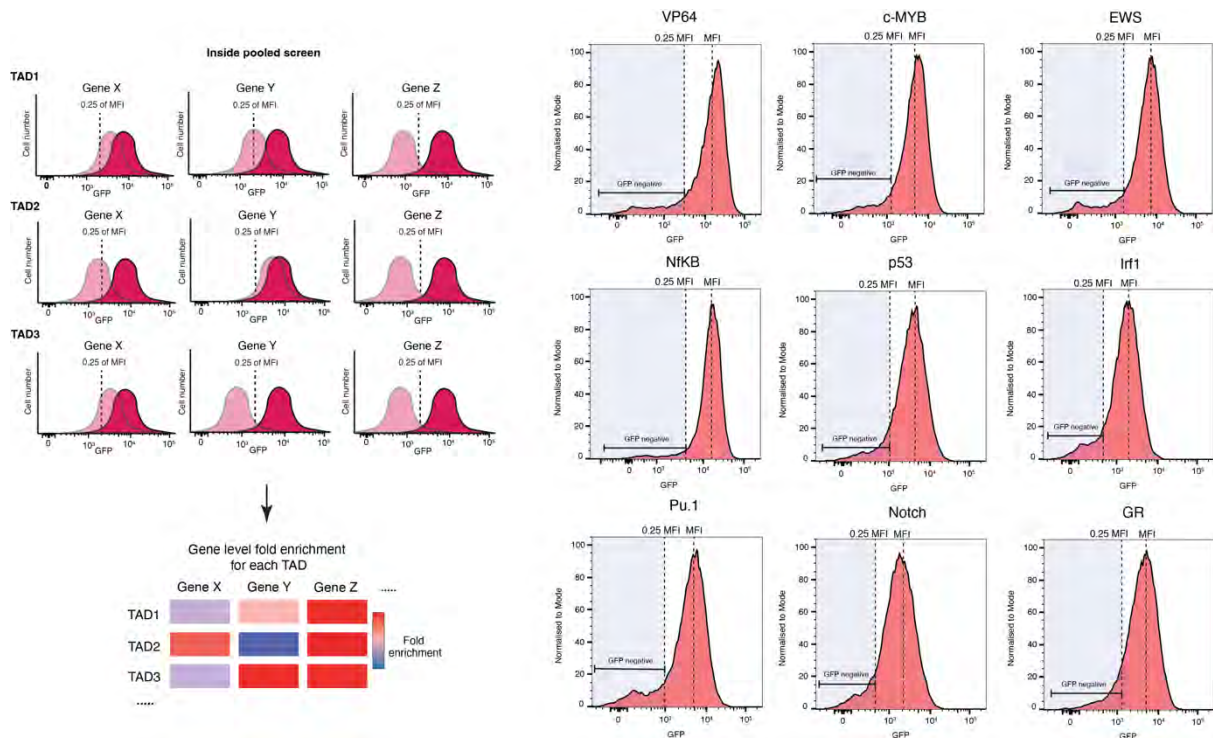
**Supplementary Note Fig. 4)** Random sampling distributions obtained from permutation test performed on each screen. Solid red line reflects the 95<sup>th</sup> percentile of the distribution which corresponds to an empirical p-value < 0.05. The dashed red line reflects the 99.9<sup>th</sup> percentile, which corresponds to an empirical p-value < 0.001.

To provide extra stringency to what is classified as a hit, we also reasoned that genuine hits should have multiple guides enriched. Therefore, we applied an additional cut-off for significance that at least 1/3<sup>rd</sup> of the guide values (6 out of 18 values) should display a fold enrichment score above the 95<sup>th</sup> percentile. This cut-off did not have a dramatic effect on the number of genes classified as hits, but did further increase the stringency of the data, by reducing the impact of certain individual guides.

### Obtaining quantitative information from CRISPR screen data

As stated above our ambition for the comparative CRISPR screens was to obtain relatively quantitative data about the degree of requirement for different cofactors across a range of ADs and core promoters. Generally, CRISPR screens are considered to provide a binary output i.e., a gene is either identified as required or not. This is largely due to the design of the screens and the gates used to isolate cells displaying a particular phenotype. For our screens, as demonstrated above and throughout the manuscript, we were able to achieve relatively accurate

and sensitive quantification of the transcriptional effects of different cofactors. This was achieved by setting the gates for isolating cells at an intermediate distance (0.25 of the Mean Fluorescence Intensity (M.F.I) from the initial normal distribution of GFP expression (Supplementary Note Fig. 5). By setting the gate at an intermediate distance, we were able to isolate a different number of cells in the GFP-negative gate depending on the degree of effect on transcription (Supplementary Note Fig. 5, left). Setting the gate too close to the MFI of the unperturbed cells would result in genes with large effects on transcription having similar enrichment to genes with low effect sizes. Setting the gate too far from the main population of would result in genes with smaller effect sizes not being identified, reducing the sensitivity of the screens.



**Supplementary Note Fig. 5)** (Left) Schematic demonstrating the logic of the gating strategy that enables quantitative data to be obtained from a single gated-CRISPR screen. (Right) FACS gating strategy applied to each of the samples in the AD-screens. M.F.I = mean fluorescence intensity (i.e., average GFP signal).

Various pieces of evidence suggest that our screens resulted in quantitative data. The high degree of correlation in fold enrichment values (Extended Data Fig. 2B), correlation between the degree of requirement and specificity of the cofactors (Fig. 2A) support the quantitative nature of the screens. Likewise, our co-dependency analysis identified highly concordant patterns of requirement across different subunits in the same complex, which would not have been observable if the screen data was not highly quantitative (Extended Data Fig. 8B). Our validation experiments also demonstrate that there is a high degree of concordance between the fold enrichments identified in the screen and the fold change in transcription in our validation experiments (Fig. 2C-D). Altogether, these data demonstrate that our gating approach was capable of obtaining quantitative data from CRISPR screens. The accuracy and reproducibility of the quantification is likely the result of the many design and analyses choices detailed above.

## Supplementary Note References

1. Michlits, G. *et al.* CRISPR-UMI: Single-cell lineage tracing of pooled CRISPR-Cas9 screens. *Nat Methods* **14**, 1191–1197 (2017).
2. Parnas, O. *et al.* A Genome-wide CRISPR Screen in Primary Immune Cells to Dissect Regulatory Networks. *Cell* **162**, 675–686 (2015).
3. Burr, M. L. *et al.* CMTM6 maintains the expression of PD-L1 and regulates anti-Tumour immunity. *Nature* **549**, 101–105 (2017).
4. Sparbier, C. E. *et al.* Targeting Menin disrupts the KMT2A/B and polycomb balance to paradoxically activate bivalent genes. *Nat Cell Biol* (2023) doi:10.1038/s41556-022-01056-x.
5. Burr, M. L. *et al.* An Evolutionarily Conserved Function of Polycomb Silences the MHC Class I Antigen Presentation Pathway and Enables Immune Evasion in Cancer. *Cancer Cell* 1–17 (2019) doi:10.1016/j.ccell.2019.08.008.
6. Bell, C. C. *et al.* Targeting enhancer switching overcomes non-genetic drug resistance in acute myeloid leukaemia. *Nat Commun* **10**, 2723 (2019).
7. MacPherson, L. *et al.* HBO1 is required for the maintenance of leukaemia stem cells. *Nature* **577**, 266–270 (2020).
8. Gilan, O. *et al.* CRISPR–ChIP reveals selective regulation of H3K79me2 by Menin in MLL leukemia. *Nat Struct Mol Biol* (2023) doi:10.1038/s41594-023-01087-4.